THESIS FOR THE DEGREE OF DOCTOR OF PHILOSOPHY

Spectroscopy of Stable and Radioactive Negative Ions

ANNIE RINGVALL MOBERG

Department of Physics
UNIVERSITY OF GOTHENBURG
Gothenburg, Sweden 2023

Annie Ringvall Moberg

isbn 978-91-8069-227-4 (print)
isbn 978-91-8069-228-1 (pdf)
Available at: http://hdl.handle.net/2077/75503

Department of Physics
University of Gothenburg
se-412 96 Göteborg, Sweden
Telephone +46 31 772 10 00

Printed by Stema AB, Borås, 2023

Typeset in XeLaTeX with Times Ten and Akzidenz-Grotesk

“A wizard is never late, nor is he early. He arrives precisely when he means to.”

- Gandalf, *The Fellowship of the Ring* by J.R.R. Tolkien

Abstract

Negative ions are unique quantum systems which are of fundamental interest within the field of atomic physics due to the importance of the electron correlation in their creation, stability, and existence. Properties of these ions, such as the electron affinity, i.e. the binding energy of the additional electron (EA), are of importance for example within theoretical calculations, astrophysics, medical applications, antimatter studies, and accelerator mass spectrometry.

This work aims to improve the understanding of negative ions and electron correlation by measuring previously not, or less precisely, known binding energies and lifetimes of both stable and radioactive negative ions by using laser photodetachment spectroscopy. In order to achieve this, several technical developments were carried out and their feasibility was demonstrated. The measurements were performed at several different facilities: ISOLDE at CERN, the Gothenburg University Negative Ion and Laser LAboratory (GUNILLA), the Double ElectroStatic Ion Ring ExpEriment (DESIREE).

The results of this thesis can be divided into different categories, the first being the determinations of the EAs of 128-iodine of $3.059\,052(38)$ eV and of 211-astatine to be $2.415\,78(7)$ eV, marking the first ever measurements of EAs of radioactive isotopes, and thereby paving the way to future EA measurements of other elements of the periodic table.

Second, high precision measurements of the EAs of cesium and rubidium have been performed at GUNILLA, utilizing a new technique: state selected detection of the residual atom in the photodetachment processes. The measured EAs were determined to be $471.5987(6)$ meV for cesium and $485.898(4)$ meV for rubidium, which are both improvements of previously determined values. This measurement technique can, if combined with the radioactive beam technique at CERN, be applied to study francium.

Third, the radiative lifetimes of the excited states in rhodium have been investigated at the DESIREE facility. In addition to the two previously known bound states, a highly mixed bound state and an autodetaching state were observed. By measuring radiative lifetimes of negative ions, theoretical models within this field can be benchmarked.

Fourth, the molecular dissociation process within the Radio-Frequency Quadrupole cooler and buncher (RFQcb), ISCOOL, at ISOLDE, CERN, has been investigated to determine the efficiency of producing atomic beams from molecular beams.

Finally, a new non-radioactive mass separator beamline has been designed, built and commissioned at ISOLDE, CERN. This new facility will be dedicated to ion source developments, beam optics and beam manipulation studies aiming to improve ion beam quality and the performance of target-ion sources during on-line operation at the ISOLDE facility.

Keywords: Atomic Physics, ISOLDE, CERN, Electron Correlation, Electron Affinity, Photodetachment, Negative Ions, Anions, Radioisotopes, Laser Photodetachment Spectroscopy, Resonance Ionization, Neutral Particle Detection, Wigner Threshold Law, Molecular Dissociation, RFQcb, DESIREE, Radiative Lifetimes.

List of Publications

This thesis consists of an introductory text and the following papers:

I **"Laser photodetachment of radioactive 128 I Laser photodetachment of radioactive"**

Sebastian Rothe[1,2,3], Julia Sundberg[1,2], Jakob Welander[2], Katerina Chrysalidis[1,4], Thomas Day Goodacre[1,3], Valentin Fedosseev[1], Spyridon Fiotakis[1], Oliver Forstner[5], Reinhard Heinke[4], Karl Johnston[1], Tobias Kron[4], Ulli Köster[6], Yuan Liu[7], Bruce Marsh[1], Annie Ringvall-Moberg[1,2], Ralf Erik Rossel[1,4], Christoph Seiffert[1], Dominik Studer[4], Klaus Wendt[4] and Dag Hanstorp[2].

[1] Engineering Department, CERN, Geneva, Switzerland
[2] Department of Physics, Gothenburg University, Gothenburg, Sweden
[3] School of Physics and Astronomy, The University of Manchester, Manchester, UK
[4] Institut für Physik, Johannes Gutenberg-Universität, Mainz, Germany
[5] Friedrich Schiller Universität, Jena, Germany
[6] Institut Laue-Langevin (ILL), Grenoble, France
[7] Physics Division, Oak Ridge National Laboratory (ORNL), Oak Ridge, Tennessee, USA

Published by: *Journal of Physics G: Nuclear and Particle Physics*, 44, p. 104003, 2017, DOI: 10.1088/1361-6471/aa80aa.

II **"The electron affinity of astatine"**

David Leimbach[1,2,3], Julia Karls[2], Yangyang Guo[4], Rizwan Ahmed[5], Jochen Ballof[1,6], Lars Bengtsson[2], Ferran Boix Pamies[1], Anastasia Borschevsky[4], Katerina Chrysalidis[1,3], Ephraim Eliav[11], Dmitry Fedorov[7], Valentin Fedosseev[1], Oliver Forstner[8,9], Nicolas Galland[10], Ronald Fernando Garcia Ruiz[1], Camilo Granados[1], Reinhard Heinke[3], Karl Johnston[1], Agota Koszorus[1], Ulli Köster[13], Moa K. Kristiansson[14], Yuan Liu[15], Bruce Marsh[1], Pavel Molkanov[7], Lukáš F. Pašteka[12], Joao Pedro Ramos[1], Eric Renault[10], Mikael Reponen[16], Annie Ringvall-Moberg[1,2], Ralf Erik Rossel[1], Dominik Studer[3], Adam Vernon[17], Jessica Warbinek[2,3], Jakob Welander[2], Klaus Wendt[3], Shane Wilkins[1], Dag Hanstorp[2] and Sebastian Rothe[1]

[1] Engineering Department, CERN, Geneva, Switzerland
[2] Department of Physics, Gothenburg University, Gothenburg, Sweden
[3] Institut für Physik, Johannes Gutenberg-Universität, Mainz, Germany

[4] Van Swinderen Institute for Particle Physics and Gravity, University of Groningen, Groningen, The Netherlands
[5] National Centre for Physics (NCP), Islamabad, Pakistan
[6] Institut für Kernchemie, Johannes Gutenberg-Universität, Mainz, Germany
[7] Petersburg Nuclear Physics Institute - NRC KI, Gatchina, Russia
[8] Institut für Optik und Quantenelektronik, Friedrich-Schiller-Universität Jena, Germany
[9] Helmholtz-Institut Jena, Jena, Germany
[10] CEISAM, Université de Nantes, CNRS, Nantes, France
[11] School of Chemistry, Tel Aviv University, Tel Aviv, Israel
[12] Department of Physical and Theoretical Chemistry & Laboratory for Advanced Materials, Faculty of Natural Sciences, Comenius University, Bratislava, Slovakia
[13] Institut Laue-Langevin (ILL), Grenoble, France
[14] Department of Physics, Stockholm University, Stockholm, Sweden
[15] Physics Division, Oak Ridge National Laboratory, Oak Ridge, Tennessee, USA
[16] Department of Physics, University of Jyväskylä, Jyväskylä, Finland
[17] School of Physics and Astronomy, The University of Manchester, Manchester, UK

Published by: *Nature Communications*, 11, pp. 1–9, 2020, DOI: 10.1038/s41467-020-17599-2.

III **"Upgrades of the GANDALPH photodetachment detector towards the determination of the electron affinity of astatine"**

D. Leimbach[1,2,3] S. Rothe[1], L. Bengtsson[2], A. Ringvall-Moberg[1,2], J. Sundberg[1,2], K. Wendt[3], D. Hanstorp[2],

[1]CERN, Esplanade des Particules 1, 1211 Geneva, Switzerland
[2]Department of Physics, University of Gothenburg, SE-412 96 Gothenburg, Sweden
[3]Institut für Physik, Johannes Gutenberg-Universität, Mainz, Germany

Published by: *Nuclear Instruments and Methods in Physics Research, Section B: Beam Interactions with Materials and Atoms*, 463, pp. 277–279, 2020, DOI: 10.1016/j.nimb.2019.05.015.

IV **"A high-resolution measurement of the electron affinity of cesium"**

José E. Navarro-Navarrete[1], Miranda Nichols[2], Annie Ringvall-Moberg[2], Jakob Welander[2], Di Lu[2], Moa K. Kristiansson[1] Gustav Eklund[1] Ruslan Chulkov[3,2] Vitali Zhaunerchyk[2] and D. Hanstorp[2].

[1]Department of Physics, Stockholm University, SE-106 91 Stockholm, Sweden
[2]Department of Physics, University of Gothenburg, SE-412 96, Gothenburg, Sweden
[3]Institute of Physics, National Academy of Science of Belarus, 220072 Minsk

Submitted to Physical Review A.

V **"The electron affinity of rubidium: A state selective measurement"**

Annie Ringvall-Moberg[1], Miranda Nichols[1], José E. Navarro-Navarrete[2], Uldis Bērziņš[3], Yazareth Peña Rodriguez[1,4], Di Lu[1], Viola D'mello[1], Rachel Poulose[1,5], Andrea Morales Rodríguez[1,4], Keerthana Ravi[1,5], Meera Ramachandran[1,5], Vitali Zhaunerchyk[1], D. Hanstorp[1] and David Leimbach[1]

[1]Department of Physics, University of Gothenburg, SE-412 96, Gothenburg, Sweden
[2]Department of Physics, Stockholm University, SE-106 91 Stockholm, Sweden
[3]Institute of Atomic Physics and Spectroscopy, University of Latvia, LV-1586 Riga, Latvia
[4]Facultad de Ciencias, Universidad Nacional Autonóma de México, Ciudad de México 04510, Mexico
[5]Cochin University of Science and Technology, Kerala 682022, India

In Manuscript.

VI **"Lifetimes of excited states in Rh-"**

J. Karls[1] S. Schiffmann[2,3] N. D. Gibson[4] M. Ji[5] M. K. Kristiansson[5] D. Leimbach[6,7] J. E. N. Navarrete[5] R. Ponce[4] A. Ringvall-Moberg[1,6] H. T. Schmidt[5] S. E. Spielman[4] C. W. Walter[4] T. Brage[2] D. Hanstorp[1]

[1]Department of Physics, University of Gothenburg, SE-412 96 Gothenburg, Sweden
[2]Division of Mathematical Physics, Department of Physics, Lund University, SE-22100 Lund, Sweden
[3] Spectroscopy, Quantum Chemistry and Atmospheric Remote Sensing

(SQUARES), CP160/09, Université libre de Bruxelles (ULB), B-1050 Bruxelles, Belgium
[4]Department of Physics and Astronomy, Denison University, Granville, Ohio 43023, USA
[5]Department of Physics, Stockholm University, AlbaNova, SE-106 91 Stockholm, Sweden
[6]CERN, 1211 Geneva, Switzerland
[7]Institut für Physik, Johannes Gutenberg-Universität, D-55 128 Mainz, Germany

In Manuscript.

VII **"Time-of-Flight study of molecular beams extracted from the ISOLDE RFQ cooler and buncher"**

A. Ringvall Moberg[1,2], S.Warren[1], C. Muñoz Pequeño[1], J. Cruikshank[1] T. Giles[1] and D. Hanstorp[2]

[1]CERN, Esplanade des Particules 1, 1211 Geneva, Switzerland
[2]Department of Physics, University of Gothenburg, SE-412 96 Gothenburg, Sweden

Published by: *Nuclear Instruments and Methods in Physics Research, Section B: Beam Interactions with Materials and Atoms*, 463, pp. 522–524, 2020, DOI: 10.1016/j.nimb.2019.03.014.

VIII **"A new fast time of flight detector for single ion counting to high flux radioactive beams at ISOLDE"**

S.Warren[1], T. Giles[1], C. M. Pequeno[1] and A. Ringvall-Moberg[1,2]

[1]CERN, Esplanade des Particules 1, 1211 Geneva, Switzerland
[2]Department of Physics, University of Gothenburg, SE-412 96 Gothenburg, Sweden

Published by: *Review of Scientific Instruments*, 90, p. 103313, 2019, DOI: 10.1063/1.5122715.

IX **"The Offline 2 facility at ISOLDE, CERN"**

Annie Ringvall Moberg[1,2] Stuart Warren[1], Mark Lloyd Bissell[1], Bernard Crepieux[1], Tim Giles[1], David Leimbach[1,2], Bruce Marsh[1], Carlos Muñoz Pequeño[1], Michael Owen[1], Yago. N. Vila Gracia[1], Shane G. Wilkins[1], Dag Hanstorp[1,2] and Sebastian Rothe

[1]CERN, Esplanade des Particules 1, 1211 Geneva, Switzerland
[2]Department of Physics, University of Gothenburg, SE-412 96 Gothenburg, Sweden

Available at the CERN Document Server `http://cds.cern.ch`.

X **"Offline 2, ISOLDE's target, laser and beams development facility"**

S.Warren[1], T. Giles[1], C. Muñoz Pequeño[1] and A. Ringvall Moberg[1,2]

[1]CERN, Esplanade des Particules 1, 1211 Geneva, Switzerland
[2]Department of Physics, University of Gothenburg, SE-412 96 Gothenburg, Sweden

Published by: *Nuclear Instruments and Methods in Physics Research, Section B: Beam Interactions with Materials and Atoms*, 463, pp. 115–118, 2020, DOI: `10.1016/j.nimb.2019.07.016`.

Specification of my contributions

I **"Laser photodetachment of radioactive 128 I Laser photodetachment of radioactive"**

I took part in preparatory work of the experimental apparatus, where Julia Karls and I designed and assembeled the GANDALPH beamline. I took part in the commissioning of the apparatus as well as the experiment, the data analysis and assisted in the final stages of the manuscript preparation.

II **"The electron affinity of astatine"**

I took part in upgrading the GANDALPH beamline and also in the preparatory phase, including target testing and commissioning of the upgraded version of GANDALPH. I also took part in the data taking and assisted in the final stages of the manuscript preparation.

III **"Upgrades of the GANDALPH photodetachment detector towards the determination of the electron affinity of astatine"**

I participated in the upgrading and commissioning of the GANDALPH spectrometer at ISOLDE, CERN. I also assisted in the final stages of the manuscript preparation.

IV **"A high-resolution measurement of the electron affinity of cesium"**

I participated in preparatory work and the experimental work at the GUNILLA facility during experimental runs. I am one of the four authors who wrote the draft of the manuscript.

V **"The electron affinity of rubidium: A state selective measurement"**

The experiment was coordinated by me and David Leimbach. We planned this work and were responsible for the preparatory work at the GUNILLA facility. I took part in the experimental data taking and the data analysis. I am one of the main authors who contributed to the manuscript.

VI **"Lifetimes of excited states in Rh-"**

I participated in the experiment and assisted in the final stages of the manuscript preparation.

VII **"Time-of-Flight study of molecular beams extracted from the ISOLDE RFQ cooler and buncher"**

I coordinated this experiment. I planned the work and was responsible for data taking. I analysed the data and was the main author responsible for

the manuscript. In this experiment I used the detector presented in Paper VIII.

VIII **"A new fast time of flight detector for single ion counting to high flux radioactive beams at ISOLDE"**

I participated in the planning and designing of the detector as well as the assembly, commissioning process and testing. I also assisted in the final stages of the manuscript preparation.

IX **"The Offline 2 facility at ISOLDE, CERN"**

I spent two years working full time on this project, participating in planning, designing and commissioning of the Offline 2 facility. I was one of the four full time members of the group, together with the project leader, a post-doctoral researcher and a mechanical engineer. I wrote most parts of the manuscript and coordinated the completion of the manuscript. I was also the main author responsible for the manuscript.

X **"Offline 2, ISOLDE's target, laser and beams development facility"**

This is the first report of the Offline 2 facility, which is described in more detail in Paper IX. My contribution to this work is mentioned in the declaration of Paper IX. Here, I also assisted in the final stages of the manuscript preparation.

Additional Publications

The following papers are not included in the thesis.

I **"A concept for the extraction of the most refractory elements at CERN-ISOLDE as carbonyl complex ions"**

Jochen, Ballof[1,2,8], Katerina Chrysalidis[1,5], Christoph Düllmann[2,3,4], Valentin Fedosseev[1], Eduardo Granados[1], David Leimbach[1,5], Bruce Marsh[1], Joao Pedro Ramos[1,6,9], Annie Ringvall-Moberg[1,7], Sebastian Rothe[1], Thierry Stora[1], Shane Wilkins[1], Alexander Yakushev[3,4,6]

[1] Accelerator Systems Department, CERN, Geneva, Switzerland
[2] Department of Chemistry - TRIGA Site, Johannes Gutenberg University, Mainz, Germany
[3] GSI Helmholtzzentrum für Schwerionenforschung, Darmstadt, Germany
[4] Helmholtz-Institut Mainz, Mainz, Germany
[5] Department of Physics, Johannes Gutenberg University, Mainz, Germany
[6] Laboratory of Powder Technology, École Polytechnique Fédérale de Lausanne (EPFL), Lausanne, Switzerland
[7] Department of Physics, University of Gothenburg, Gothenburg, Sweden
[8] present address: FRIB, 640 S. Shaw Lane, East Lansing, MI 48824, USA
[9] present address: SCK CEN, Boeretang 200, 2400 Mol, Belgium

Published by: *European Physical Journal A*, 58, pp. 1–18, 2022, DOI: 10.1140/epja/s10050-022-00739-1.

II **"First laser ions at the CERN-MEDICIS facility"**

Vadim Maratovich Gadelshin[1,2], Shane Wilkins[3], Valentin Nikolaevich Fedosseev[3], Ermanno Barbero[3], Vincent Barozier[3], Ana Paula Bernardes[3], Eric Chevallay[3], Thomas Elias Cocolios[4], Bernard Crepieux[3], Kristof Dockx[4], Matthias Eck[1], Pascale Fernier[1], Roberto Formento Cavaier[5], Ferid Haddad[6,7], Johannes Jakobi[1], Laura Lambert[3], Bruce Allan Marsh[3], Stefano Marzari[3], Joao Pedro Ramos[3,4], Annie Ringvall Moberg[3,8], Sebastian Rothe[3], Thierry Stora[3], Dominik Studer[1], Andres Vieitez Suarez[3], Felix Weber[1], Klaus Wendt[1]

[1] Institut f˙ur Physik, Johannes Gutenberg-Universität, 55128 Mainz, Germany
[2] Institute of Physics and Technology, Ural Federal University, 620002

Yekaterinburg, Russia
[3] EN Department, CERN, 1211 Geneva, Switzerland
[4] Instituut voor Kern- en Stralingsfysica, KU Leuven, 3001 Leuven, Belgium
[5] Advanced Accelerator Applications, A Novartis Company, 10010 Colleretto Giacosa/Ivrea, Italy
[6] GIP ARRONAX, Nantes, France
[7] SUBATECH, Nantes University, Nantes, France
[8] Gothenburg University, Gothenburg, Sweden

Published by: *Hyperfine Interactions*, 241, **pages**, 2020, DOI: 10.1007/s10751-020-01718-y.

Contents

CHAPTER 1

INTRODUCTION

The idea that matter consists of small particles which are indivisible dates back to ancient Greece [13]. Since then, research within atomic physics has come a long way. In 1897, Sir J. J. Thomson[1] discovered that cathode rays consist of small particles, later known as electrons[2], which are negatively charged and several orders of magnitude smaller in mass than atoms [15]. Thomson also proposed a model of the atomic structure, where he postulated that the atom consist of negatively charged particles distributed in a sphere of uniform positive charge [16]. In the early 1900s, Ernest Rutherford and his colleagues came to question the atomic model that Thompson had suggested a few years earlier while performing a scattering experiment when passing alpha particles through a thin gold foil [17]. Rutherford proposed a new model where he stated that the majority of the mass was assumed to be concentrated in the nucleus, with a diffuse electron cloud orbiting the center which was held together with the nucleus by the Coulomb attraction. But new questions arose from this model since its classical interpretation resulted in an instability of the atomic system[3]. To solve this problem, Niels Bohr proposed that bound electrons can only exist in separate, quantized orbitals at different, distinct energies and radii with respect to the nucleus. Bohr also introduced the possibility of electrons jumping between these orbitals which resulted in photonemission. By combining this with his atomic model, he was able to explain the emission spectrum

[1] Thomson was awarded a Nobel prize in 1906 for his work on conductivity of electricity in gases [14].

[2] The initial name that J. J. Thomson used the name *corpuscles* for these negatively charged particles *corpuscles* [15].

[3] In this model the electrons would fall into the nucleus as they orbited around it.

of hydrogen. The Bohr model was published in a series of papers in 1913 [18, 19, 20] and even though this model is very simplified it is, to this day, a frequently used atomic model for the general public. Following this work, Bohr was awarded the Nobel Prize in 1922. Around the same time as Bohr postulated his model of the atomic system, further discoveries were made by Max Planck, Albert Einstein [21], Werner Heisenberg and Bohr himself [18] in the field of quantum mechanics, where the behavior and properties of particles with microscopic sizes were described. This lead to a more fundamental understanding of atomic and molecular sized systems. The mathematical descriptions of these systems were formulated by Erwin Schrödinger [22] for non-relativistic cases, while Paul Dirac [23] developed the relativistic expression. With the exception of the hydrogen atom and other hydrogen-like systems, most atomic systems are quite complex, and cannot be described analytically. Hence approximations have to be applied in order to simplify the expressions. One commonly used approximation is the so-called mean-field approximation, where the electrons are treated as independent particles in a Coulomb field and hence the electromagnetic interactions between the electrons are replaced by an average or effective interaction which simplifies the many-body problem to an effective one-body problem [24].

These atomic and molecular systems can either be neutral in charge or have a positive or negative net charge. Negative ions were first observed in a gas-discharge by J. J. Thomson in 1913 [25]. However, the research field of negative ions did not take off until Wildt proposed that the opacity of the sun's photosphere could be explained by so-called photodetachment processes of negative hydrogen ions [26]. This would explain the difference between the apparent and actual temperature of our sun where the negatively charged hydrogen ions absorb and emit light in the outer atmosphere of the sun. The negative hydrogen ions provide a continuum opacity at wavelengths smaller than approximately 1650 nm due to the electron affinity of H^- being 0.75 eV [27]. Without hydrogen present, the ultraviolet radiation would be more dominant in the solar spectrum. This discovery lead to the first experimental photodetachment study, performed by Branscomb *et al.* in 1953, when they investigated photodetachment processes of H^- [28] and O^- [29].

Furthermore, negative ions are fundamentally different from positive ions. Positive ions can be created quite easily by taking a neutral atom and adding sufficient energy, in form of for example photons or in a collision, to remove one, or several, electrons. Negative ions on the other hand are created when an extra electron is bound to a neutral atom. However, unlike neutral or positive systems, there is no long range Coulomb

attraction, and negative ions can therefore only exist if all electrons in the system move in such way that they share the attractive force created by the nucleus. Hence, these systems are interesting when studying electron correlation theories and processes, as they cannot be described using more common theoretical approaches such as the so-called Hartree-Fock model [30] where each electron is assumed to move in an average potential created by all other electrons in the same system, and the treat the electron correlation as a perturbation to this mean field. However, this theoretical approach is not suitable for most negative ions as it cannot predict a stable negatively charged system. Therefore, other theoretical approximations, where the electron correlation is included into the model describing the negative ion, have to be applied. This makes negative ions very interesting systems when studying and developing new theoretical models and their ability to include direct correlation between the electrons. Experimentally, the properties and structure of these systems can be investigated by measuring the binding energy of the extra electron, which is called the electron affinity. The electron affinity of most of the stable elements have been measured with some precision, and can be found in publications by for example Hotop *et al.* [31, 32], Andersen *et al.* [33] and Ning *et al.* [34]. Comprehensive overviews of both theoretical and experimental studies of negative ions can be found in reviews by Massey [35], Pegg [36], and Andersen [37].

Experimental investigations of negative ions and their corresponding electron affinity can be performed using laser photodetachment threshold (LPT) spectroscopy [36], where a beam of negative ions is overlapped with a laser beam. If the energy of the photons is sufficiently high, the photon can be absorbed by the negative ion which will then eject the additional electron resulting in a neutral atom and a free electron. The electron affinity can be determined by measuring the cross section of the photodetachment process as a function of the photon energy. The electron affinity can also be determined using other techniques such as laser photodetachment electron spectroscopy, where an insight into amplitude and phase of the outgoing electronic waves can be investigated by studying the angular distribution of the detached electrons [38, 39] and also velocity map imaging [40] where photoelectrons, emitted with different kinetic energies in a three dimensional distribution and projected onto a two dimensional position sensitive detector. High precision measurements of the electron affinity can also be performed using photodetachment microscopy [41, 42, 43]. As of today, the most accurate electron affinity measurement of any element was performed on oxygen by M. Kristiansson *et al.* [44] at the DESIREE facility [45]. The photodetachment process of negative ions has

also been studied in external magnetic and electric fields in order to, for example, investigate the Landau structure together with Zeeman transitions by trapping the negative ions in a magnetic field in order to investigate their effect on the photodetachment cross section near the threshold [46, 47, 48].

Ions of both positive and negative charge can be studied at different ion beam facilities around the world. At the DESIREE facility [45] in Stockholm, Sweden, at AMO physics laboratory at RIKEN [49], Japan, and at CSR [50] at the Max Planck Institute in Heidelberg, Germany, ions are stored in electrostatic storage rings in order to perform, for example, lifetime measurements of excited negatively charged ions [51, 52]. Ions can also be studied using ion traps [53, 54] or single pass techniques (which is the main method used in this thesis[1]), where the ions just make one single pass through the experimental apparatus without being stored or trapped. When it comes to short-lived radioactive isotopes, it is necessary to study these at radioactive ion beam facilities such as ISOLDE [55], ISAC at TRIUMF (Vancouver, Canada) [56], RIKEN (Tokyo,Japan) [57, 58], IGISOL at the University of Jyväskylä (Jyväskylä, Finland) [59] and GSI [60] (Darmstadt, Germany). So far, only a few studies on radioactive negative ions have been conducted. The first study was the electron affinity measurement on the radioisotope ^{128}iodine [1], which is a part of this thesis. Further, recent measurements on radioactive elements such as thorium [61], praseodymium, neodymium and terbium [62], and also astatine [2], which also is a part of this thesis, have been performed.

The study of negative ions is important in many practical areas (not just from a theoretical point of view), particularly in an astrophysical context. Hydrocarbons, such as C_6H^-, have been observed in interstellar clouds [63], and negative ions are also believed to have an essential part in the formation of H_2 in the early universe [64, 65, 27]. Negative ions are also important when it comes to fusion reactors of the TOKAMAK-type, such as the International Thermonuclear Experimental Reactor (ITER) [66], where negative ions are used to heat the fusion plasma. Furthermore, the electron affinity, combined with the ionization potential, give fundamental information of the properties of an element such as its electronegativity [67]. This is important within medical physics, as some radioactive elements can be used within cancer treatments such as Targeted Alpha Therapy (TAT) [68, 69, 70] where accurate determination of the electron affinity provides valuable information for computational chemistry when trying to predict the chemical behavior of these elements. Positive ions can also be

[1]Except for the lifetime measurement of Rh^- which was conducted at the DESIREE facility.

used for cancer therapy, such as hadron therapy, where an external beam of energetic neutrons, protons or heavier positive ions can be used to irradiate the cancer cells. Compared to X-rays, this is less harmful to the rest of the human tissue as the energy loss of the particle beam is exhibited as a Bragg peak and hence delivers the maximum radiation dose at the location of the tumor. This minimizes the damage to surrounding, healthy tissue [71].

Over the past years, an interest of negative ions within the field of laser cooling has been developed [72]. Laser cooling of atoms has been known since 1980s and in 1997 Steven Chu, Claude Cohen-Tannoudji and William D. Phillips received the Nobel prize for the new technique. This allows for a detailed study of the atomic system by cooling the system so that the thermal motion can be neglected and hence also the Doppler broadening of the atomic lines [73, 74, 75]. To laser cool a system, a suitable atomic transition has to be present within the system but in the case of most negative ions, the bound excited states have the same parity as the ground state. Hence, they decay through magnetic dipole, electric quadruple, or higher order transitions which makes laser cooling impossible. However, there are some exceptions where the excited states have been observed to have opposite parity [61, 76, 77, 78, 79], one of them being lanthanum which is a promising candidate for laser cooling. By laser cooling the ions, higher precision measurements can be conducted as well as allowing the possibility of sympathetic cooling of antiprotons [80]. In sympathetic cooling of positive ions, laser cooled ions are trapped and used to cool another trapped ion species through Coulomb interaction between the two ion species. Thus, any positively charged ion or molecule can be cooled [81]. If positive ions were to be used instead, of negative ions, the antiprotons and the ions would annihilate. Hence, negative ions are required, in form of a buffer gas, in order to perform sympathetic cooling of the anti-protons. This technique would enable more efficient production of anti-hydrogen, which is of great interest when studying the symmetry of matter [82]. Furthermore, the antiProton Unstable Matter Annihilation (PUMA) experiment at CERN is aiming towards studying antimatter by using cooled negative ions trapped in an ion trap [83].

The work carried out within this thesis focuses on both experimental measurements and technical developments which can be used to study charged particles and it is based on the work in the appended publications. Paper I, II, IV, V and VI are related to photodetachment threshold measurements and lifetime determinations of negative ions, Paper III is a technical paper which describes the upgrade of the experimental apparatus used to perform the electron affinity measurement of astatine. Paper VIII de-

scribes the detector which was built and used in the molecular dissociation experiment described in Paper VII. Paper IX and X are technical papers describing a new ion beam laboratory. The thesis begins with a theoretical background to atomic physics and a brief introduction to molecules and continues with a chapter explaining the different ion beam facilities which have been essential to carry out the work presented in this thesis. A summary and description of the experiments, their results, as well as the corresponding discussions have all been combined in one chapter. Final chapter is a conclusion and outlook of this work.

CHAPTER 2

THEORY

2.1 Atomic Physics

In the early 1900s, the Danish physicist Niels Bohr published his ideas stating that classical mechanics was not the most accurate way to look at particles on a microscopic scale [18, 19, 20]. Instead, he laid the foundations of quantum mechanics, which opened up a new chapter in the field of physics. Later, Louis de Broglie realized that matter has wave-like properties [84] described by the de Broglie wavelength, $\lambda = h/p$, where p is the momentum of the particle and h is Planck's constant. From the fundamental research of de Broglie, the Austrian physicist Erwin Schrödinger postulated a partial differential equation which describes the dynamics of a quantum state in a quantum mechanical system [22].

In quantum mechanics, a system can be described by the time-dependent Schrödinger equation,

$$H\left|\Psi(t)\right\rangle = -i\hbar\frac{\partial}{\partial t}\left|\Psi(t)\right\rangle, \tag{2.1}$$

where H is the Hamiltonian, Ψ is the wavefunction, which is the mathematical description of the quantum state, $\hbar$ is the reduced Planck's constant [1], t is the time and, i is the imaginary unit.

2.1.1 Single-Electron Systems

The simplest atomic structure consists of a nucleus of charge Ze, where Z is the atomic number, and e is the elementary charge. The interaction be-

[1]The reduced Planck's constant is equivalent to $\frac{h}{2\pi}$.

tween the nucleus and electron can be described by the Coulomb potential,

$$V(r) = -\frac{Ze^2}{4\pi\epsilon_0 r}. \tag{2.2}$$

Here, ϵ_0 is the permittivity of vacuum and r is the distance between the two charges. This structure is equivalent to a hydrogen-like atom and is the simplest atomic structure which can be solved using the time-independent Schrödinger equation, $H|\Psi\rangle = E|\Psi\rangle$, where E is the energy of the system. Since the system consists of two masses, the reduced mass, $\mu = \frac{m_e m_p}{m_e + m_p}$, where m_e and m_p are the masses of the electron and proton, can be used to write the Hamiltonian,

$$H = -\frac{\hbar^2}{2\mu}\nabla^2 - \frac{Ze^2}{4\pi\epsilon_0 r}, \tag{2.3}$$

where ∇^2 is the Laplace operator. The simplified, time-independent, Schrödinger equation can thus be written as

$$H|\Psi\rangle = \left[-\frac{\hbar^2}{2\mu}\nabla^2 - \frac{Ze^2}{4\pi\epsilon_0 r} \right] |\Psi\rangle = E|\Psi\rangle . \tag{2.4}$$

Since the Coulomb potential in Eq. 2.2 is spherically symmetric, the wavefunction in Eq. 2.4 can be written in spherical polar coordinates,

$$\Psi_{n,l,m_l}(r,\theta,\phi) = R_{n,l}(r) Y_{l,m_l}(\theta,\phi), \tag{2.5}$$

where $R_{n,l}(r)$ is the radial function, which corresponds to the principal quantum number ($n = 1, 2, 3, ...$), and $Y_{l,m}$ is the spherical harmonic which corresponds to both the angular momentum quantum number ($l = 0, 1, 2, 3, ..., n-1$) and the magnetic quantum number ($m_l = -l, -l+1, ..., l-1, l$).

It is possible to separate Eq. 2.4 into one angularly dependent equation,

$$\left[\frac{1}{\sin\theta}\frac{d}{d\theta}\left(\sin\theta \frac{d}{d\theta} \right) + \frac{1}{\sin^2\theta}\frac{d^2}{d\phi^2} \right] Y_{l,m_l}(\theta,\phi) = -l(l+1) Y_{l,m_l}(\theta,\phi), \tag{2.6}$$

and one radially dependent equation,

$$\left[\frac{\hbar^2}{2\mu}\frac{1}{r^2}\frac{d}{dr}\left(r^2 \frac{d}{dr} \right) - \frac{\hbar^2}{2\mu}\frac{l(l+1)}{r^2} + \frac{Ze^2}{4\pi\epsilon_0 r} + E \right] R_{n,l}(r) = 0, \tag{2.7}$$

where the term with the negative sign is a repulsive force known as the centrifugal barrier potential, which together with the Coulomb potential, gives the effective potential

$$V_{\text{Effective}} = \frac{\hbar^2}{2\mu}\frac{l(l+1)}{r^2} - \frac{Ze^2}{4\pi\epsilon_0 r}. \tag{2.8}$$

From the Schrödinger equation it is possible to determine the energy eigenvalues, E_n, of a hydrogen atom. This is given by

$$E_n = -\frac{\mu}{2\hbar^2 n^2}\frac{Z^2 e^4}{(4\pi\epsilon_0)^2}. \tag{2.9}$$

Here, one can see that the eigenenergy is only dependent on the principal quantum number, n, which is a special case for a hydrogen-like system. A detailed solution of the Schrödinger equation for a hydrogen-like system can be found in several text books, for example in *Physics of Atoms and Molecules* by B. H. Bransden and C. J. Joachain [85].

2.1.2 Fine and Hyperfine Structure

Besides its charge ($-e$) and mass (m_e), the electron has another property called spin. The absolute value of the spin is defined by $|\boldsymbol{s}| = \sqrt{s(s+1)}\hbar$, where s is the spin quantum number and the two components in the $\pm$z direction are $s_z = \pm\frac{1}{2}\hbar$. Moreover, an electron with charge $-e$, which moves in a circular orbit with the orbital angular momentum l around the nucleus, will give rise to a magnetic moment.

The interaction between the electron spin and the angular momentum is called the spin-orbit coupling and gives rise to a splitting of the energy levels within an atom. The electron spin induces a magnetic moment, $\boldsymbol{\mu}_s$, defined as

$$\boldsymbol{\mu}_s = -\mathrm{g}_s(\mu_{\mathrm{B}}/\hbar)\boldsymbol{s}, \tag{2.10}$$

where $\mathrm{g}_s \approx 2$ is the so-called Landé factor and μ_{B} is the Bohr magneton, which interacts with the magnetic field originating from the angular momentum of the electron. This angular momentum is, according to Biot-Savart's law, $\boldsymbol{B}_l = \frac{\mu_0 Ze}{4\pi r^3 m_e}\boldsymbol{l}$. This results in an energy shift ΔE_{FS}, in the rest-frame of the nucleus, which is given by

$$\begin{aligned}\Delta E_{\mathrm{FS}} = -\left\langle \boldsymbol{\mu}_s \cdot \boldsymbol{B}_l \right\rangle &= \mathrm{g}_s\mu_{\mathrm{B}}\left\langle \frac{\mu_0 Ze}{8\pi r^3 m_e\hbar}(\boldsymbol{s}\cdot\boldsymbol{l})\right\rangle \\ &\approx \left\langle \frac{\mu_0 Ze^2}{8\pi m_e^2 r^3}(\boldsymbol{s}\cdot\boldsymbol{l})\right\rangle.\end{aligned} \tag{2.11}$$

The energy levels will therefore be split into the fine structure components with energies equal to

$$E_{\text{FS}} = E_n - \langle \boldsymbol{\mu}_s \cdot \boldsymbol{B}_l \rangle = E_n + \left\langle \frac{\mu_0 Z e^2}{8\pi m_e^2 r^3} (\boldsymbol{s} \cdot \boldsymbol{l}) \right\rangle . \tag{2.12}$$

Next, the total angular momentum, $\boldsymbol{j}$, which is dependent on the orbital angular momentum l and the electron spin s, is introduced as $\boldsymbol{j} = \boldsymbol{l} + \boldsymbol{s}$ where the absolute value is given by $|\boldsymbol{j}| = \sqrt{j(j+1)}\hbar$. By defining the so-called spin-orbit coupling constant $a = \left\langle \frac{\mu_0 Z e^2 \hbar^2}{8\pi m_e^2 r^3} \right\rangle$, where r is the average distance between the nuclei and the electron, the fine structure energy in Eq. 2.12 can be written as

$$E_{\text{FS}} = E_n + \frac{a}{2}[j(j+1) - l(l+1) - s(s+1)]. \tag{2.13}$$

In addition to the fine structure splitting, there is an even finer structure, the so-called hyperfine structure, which is caused by the interaction between the valence electrons and the nucleus. Just like the electron, the nucleus has a spin that is defined as $|\boldsymbol{I}| = \sqrt{I(I+1)}\hbar$, where I is the nuclear spin quantum number whose projection onto the z-axis is defined by $IZ = m_I$ with $-I \leq m_I \leq +I$. The spin gives rise to a magnetic moment $\boldsymbol{\mu}_N = \mathrm{g}_N \frac{\mu_K}{\hbar} \boldsymbol{I}$, where g_N is the g-factor and the nuclear magneton, μ_K, defined as $\mu_K = \hbar e / 2m_{\text{P}}$. The interaction between the magnetic moment of the nucleus and the magnetic field, B_J, generated by the electrons at the site of the nucleus results in a shift in energy, ΔE_{HFS}, called the hyperfine structure

$$\Delta E_{\text{HFS}} = -\langle \boldsymbol{\mu}_N \cdot \boldsymbol{B}_J \rangle = -|\boldsymbol{\mu}_N| \cdot B_J \cos(\phi(J, I)), \tag{2.14}$$

where the angle between $\boldsymbol{J}$ and $\boldsymbol{I}$ is denoted as $\phi(J, I)$. Introducing the total angular momentum of the atom, $F = J + I$, and the hyperfine structure constant, $A = \frac{\mathrm{g}_N \mu_K B_J}{\sqrt{J(J+1)}}$, the energy in Eq. 2.14 can be written as

$$\Delta E_{\text{HFS}} = \frac{A}{2}[F(F+1) - J(J+1) - I(I+1)]. \tag{2.15}$$

The hyperfine splitting is typically orders of magnitude smaller compared to the energy shifts associated with the fine structure. A schematic figure of the fine and hyperfine structure in the hydrogen atom can be seen in Figure 2.1. A more detailed discussion on the fine and hyperfine structure can be found in several atomic physics text books, for example in the the book *Atoms, Molecules and Photons - An Introduction to Atomic-, Molecular- and Quantum Physics* by W. Demtröder [24].

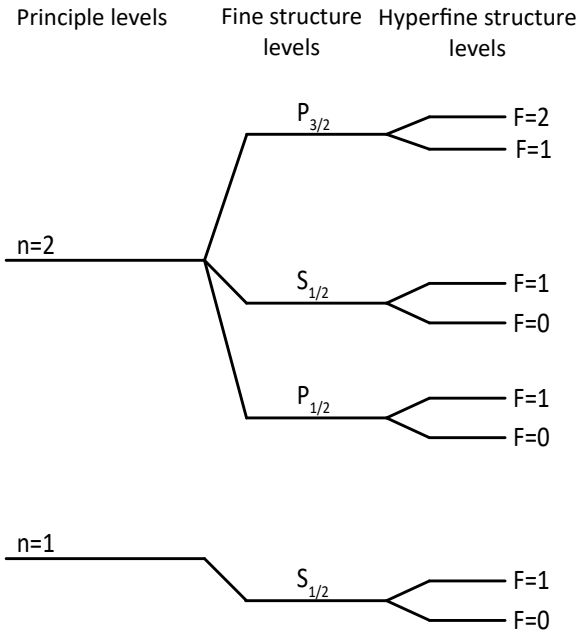

Figure 2.1: A schematic diagram (not to scale) of the fine structure and hyperfine structure levels within the hydrogen atom.

2.1.3 Multi-Electron Systems

When looking at multi-electron systems with N electrons, the model becomes more complex since the interaction between the electrons needs to be accounted for. The Schrödinger equation for an atom with N electrons is then given by

$$H\Psi(\boldsymbol{r}_1, \boldsymbol{r}_2, \dots, \boldsymbol{r}_N) = E\Psi(\boldsymbol{r}_1, \boldsymbol{r}_2, \dots, \boldsymbol{r}_N), \tag{2.16}$$

where the non-relativistic Hamiltonian, excluding spin-orbit coupling, is written as

$$H = -\sum_{i}^{N} \frac{\hbar^2}{2m}\nabla_i^2 - \sum_{i}^{N} \frac{Ze^2}{4\pi\epsilon_0 r_i} + \sum_{i,j>i}^{N} \frac{e^2}{4\pi\epsilon_0 |r_i - r_j|}. \tag{2.17}$$

The first term of the Hamiltonian in Eq. 2.17 relates to the kinetic energy of the individual electrons, the second term is related to the electron-nucleus

interaction, and the third term is the electron-electron repulsion. Since this last term, the electron-electron repulsion, needs to be taken into account, the Hamiltonian cannot, in most cases, be solved analytically. Instead, various approximations and numerical methods need to be used.

One of the most frequently used methods is the Hartree-Fock approximation, which is an independent particle model, where the interaction between the electrons is taken into account by assuming that each electron interacts with a mean field which approximates the interaction between all of the outer electrons. The energy of the system, assuming that the wavefunction is normalized, is given by

$$E = \langle \Psi | \, H \, | \Psi \rangle \,, \tag{2.18}$$

where the wavefunction Ψ can be written using determinants in order to account for the Pauli exclusion principle, which follows from the antisymmetry principle. In the general form, Ψ can be written as a Slater determinant

$$\Psi = \frac{1}{\sqrt{N!}} \begin{vmatrix} \psi_1(1) & \psi_2(1) & ... & \psi_N(1) \\ \psi_1(2) & \psi_2(2) & ... & \psi_N(2) \\ \vdots & \vdots & \ddots & \vdots \\ \psi_1(N) & \psi_2(N) & ... & \psi_N(N) \end{vmatrix}. \tag{2.19}$$

Here, ψ includes both spin function and angular and radial components.

Using the variational method, which can be used to find an approximation to the lowest energy by using a "trail wavefunction" and iterating the parameters such that the solution converges, a better approximation of the energy can be obtained. This is explained in detail in text books by B. H. Bransden and C. J. Joachain [85] and W. Demtröder [24].

LS and jj coupling

Due to the N character of the total angular momentum, there are more possibilities for spin-orbit coupling interactions in multi-electron systems. In the coupling scheme for many light atoms, the orbital angular momenta, and spin for the individual electrons is presumed to form one resultant orbital angular momentum ($\mathbf{L} = \sum_i \mathbf{l}_i$) and one resultant spin angular momentum ($\mathbf{S} = \sum_i \mathbf{s}_i$). These two terms are then combined to form the total angular momentum $\mathbf{J} = \mathbf{L} + \mathbf{S}$ which is referred to as the **L-S** coupling. The individual atomic levels in a system is based on the possible values that these quantum numbers can take for a specific configuration. This is called the term symbol and the terms are arranged according to $^{2S+1}L_j$, where n is the principal quantum number and $2S+1$ is referred to as the multiplic-

ity, which corresponds to the number of fine structure components and *j* is the total angular momentum.

If the coupling energy between an individual electron's magnetic momentum and its spin momentum is greater compared to the interactions between the different electrons, the spin and angular momentum of each of the individual electron, e_i, couple to yield a resultant angular momentum $j_i = l_i + s_i$ which then couples to the total angular momentum $\mathbf{J} = \sum_J j_i$. This coupling mechanism is called j-j coupling and is more commonly observed in heavier atoms. In the textbooks by W. Demtröder [24] and S. Svanberg [86], detailed discussions and further information regarding the coupling mechanism can be found.

2.1.4 Optical Transitions

An atom can change its electron configuration by absorbing or emitting a photon. In order for a transition between two states in an atom or ion to occur (i.e. for a photon to be absorbed), the selection rules have to be obeyed. In this section, a brief introduction to the selection rules can be found, while a more detailed description of the selection rules is given in *Atomic and Molecular Spectroscopy* by S. Svanberg [86].

Besides energy conservation, the angular momentum must be conserved and certain symmetry rules must be obeyed in order for a transition to take place. To the first order, this can be described by the transition dipole matrix element

$$M_{if} = \int \Psi_f^* \vec{\mu} \Psi_i d\tau. \tag{2.20}$$

Here, Ψ_i and Ψ_f are the wavefunctions for the initial (i) and final, (f) state and $\vec{\mu}$ is the dipole moment operator (which is a function of $\vec{r}$).

The transition probability from an initial state to a final state depends on the strength of the coupling between the two states as well as the density of the final state. The transition probability (P_{if}) per unit time can, according to Fermi's Golden Rule, be written as

$$\frac{d\mathrm{P}_{if}}{dt} = \frac{2\pi}{\hbar} |M_{if}|^2 \rho_f, \tag{2.21}$$

where ρ_f corresponds to the density of the final state.

In addition to the electric dipole transition (E1), there are also higher order transitions e.g. electric quadrupole transitions (E2), magnetic dipole (M1), quadrupole (M2) transitions, and additional higher order transitions. The dominating effect of an interaction between the electron in an atom and the electromagnetic field is governed by the electric dipole transition,

while the coupling to the magnetic component in the electromagnetic wave describes the magnetic dipole transitions. Hence, the electric dipole transitions have higher probability and are therefore called "allowed" transitions. Higher order transitions are called forbidden, however they can still occur. The selection rules can differ slightly depending on transition, spin-orbit coupling, and hyperfine structure but the rigorous rules are

$$\begin{aligned} &\Delta J = 0, \pm 1, \text{ where } J = 0 \nleftrightarrow 0 \\ &\Delta M_J = 0, \pm 1, \text{ where } M_J = 0 \nleftrightarrow 0, \text{ if } \Delta J = 0 \\ &\pi_f = -\pi_i \text{ for E1, M2, E3} \\ &\qquad\qquad \text{and} \\ &\pi_f = \pi_i \text{ for M1, E2, M3.} \end{aligned} \tag{2.22}$$

Here, J is the total angular momentum number ($J = L + S$), the total magnetic quantum number is denoted by M_J and π is the parity. In addition to this, different cases of spin-orbit coupling and transitions between hyperfine structure exist. Further information regarding this can be found in atomic physics textbooks.

2.2 Negative Ions

The fundamental difference between a neutral atom and its negative ion is the nature of the potential that binds the additional electron to the neutral system. In a neutral system or positive ion, an electron at a far distance from the nucleus experiences the Coulomb potential, which scales with $1/r$ where r is the distance between the center of the nucleus and the electron. On the other hand, when it comes to negative ions, there is no long range force acting on the surplus electron due to the parent atom having zero net charge. Instead, the net binding force is extremely short ranged and it is therefore not possible to describe negative ions by only taking the independent particle model into account. Instead, it is necessary to include the electron correlations directly in the theoretical models [87]. The extra electron does not experience any net attraction from the neutral atomic core, but instead their interaction gives rise to a polarization effect on the core when it approaches the electron cloud that surrounds the nucleus, which in turn induces an electric dipole. The induced electric dipole exerts an attractive force back onto the additional electron which makes it possible for the electron to be bound to the neutral atomic core. The induced electric dipole scales with distance as $1/r^4$. The induced dipole, $V_{\text{Pol}}(r)$, which also

includes the atomic polarizability term α, together with the centrifugal potential, $V_{\text{Ang}}(r)$, which is dependent on the angular momentum, l, creates the effective potential which is described by[1]

$$V_{\text{Effective}}(r) = V_{\text{Ang}}(r) + V_{\text{Pol}}(r) \propto \frac{l(l+1)}{2r^2} - \frac{\alpha}{2r^4}. \tag{2.23}$$

An illustration of the effective potential for different angular momentum l and the centrifugal barrier, with the Coulomb potential for comparison is shown in Figure 2.2. Here, it is possible to get an indication of how much relative energy is needed in order to photodetach electrons with different angular momenta. For an s-electron the detachment energy is considerably smaller compared to the energy needed to detach p- and d- electrons.

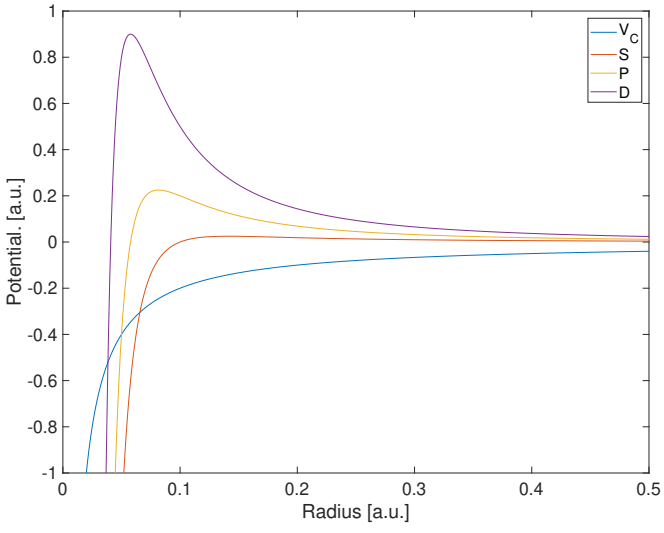

Figure 2.2: An illustration of the effective potential of the polarization induced potential and the centrifugal barrier for different angular momentum l (S, P, D) with the Coulomb potential (V_C) as a reference.

The energy gained by the system by binding the surplus electron (i.e. the binding energy) is referred to as the electron affinity (EA) and can be

[1]Note that this equation cannot be used for small distances since it breaks down when the surplus electron is located on a distance from the nucleus which is comparable to the radial distance of the electrons occupying a neutral atom.

expressed as

$$\mathrm{EA}(X) = E_{\text{ground state}}(\mathrm{X}) - E_{\text{ground state}}(\mathrm{X}^-). \tag{2.24}$$

Here, $E_{\text{ground state}}(\mathrm{X})$ and $E_{\text{ground state}}(\mathrm{X}^-)$ are referred to as the lowest energy levels of a neutral atom (X) and its corresponding negative ion (X^-). This is graphically shown in Figure 2.3.

Most elements can form negative ions and can just as the neutral atoms and positive ions be described with wavefunctions. However, the short-range of the force in the case of negative ion results in much smaller binding energies, typically one order of magnitude smaller than the so-called ionisation potential (IP), which is the energy required to remove an electron from a neutral atom. Another difference is that negative ions, in most cases, do not have any bound excited states with opposite parity except for some rare cases such as lanthanum [76], cerium [77], osmium [78], thorium [61] and uranium [79]. More extensive overviews of negative ions can be found in the reviews of D. Pegg [36] and T. Andersen [37].

2.3 Photodetachment Spectroscopy

Since negative ions are weakly bound systems, their extra electrons can be easily liberated, leaving a neutral atom and a continuum state of a free electron [35]. This can occur through different processes, e.g. particle-particle collisions, interactions between the negative ions, by a strong external electrical field or photon-particle interactions. In this work, photon-particle interactions, or laser photodetachment, is used to investigate negatively charged systems.

The photodetachment process, where a photon with an energy of $h\nu$ (where ν is the frequency) is absorbed by a negatively charged ion, X^-, resulting in a neutral atom, X, and a free electron e^-, can be described by

$$\mathrm{X}^- + \gamma \rightarrow \mathrm{X} + e^-. \tag{2.25}$$

To fully describe the behavior of the total cross section of the photodetachment process, full quantum mechanical calculations have to be taken into account. However, the general behavior of the total cross section, σ_{Total}, over a large range of photon energies, $h\nu$, is described by M. Amusia [88] which states that[1]

$$\sigma_{\text{Total}} \propto \sqrt{\mathrm{EA}}\frac{\sqrt{(h\nu - \mathrm{EA})^3}}{(h\nu)^3}. \tag{2.26}$$

[1]Note that this is valid when $h\nu > EA$.

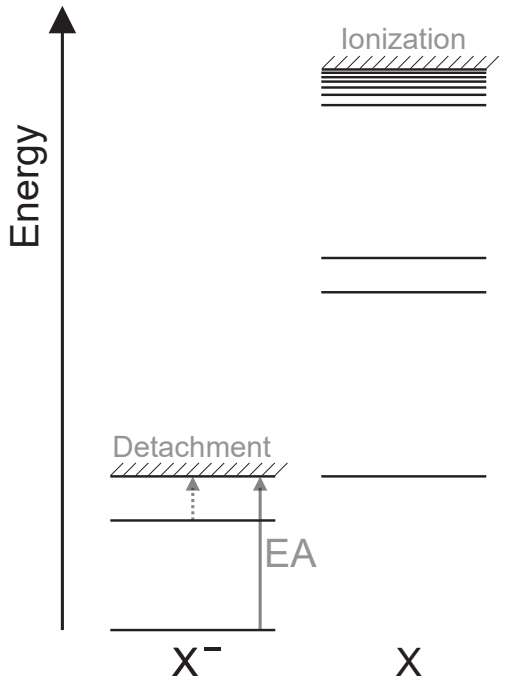

Figure 2.3: Energy level diagram of an atom X, and its negative ion X^-. The electron affinity (EA) is defined with a solid arrow. The neutral atom has several excited states (note that only a few are marked here) while the negative ion only has a few, if any, excited states. The dashed arrow indicates the energy needed to detach an electron in the excited state in the negative ion. The detachment level of the negative ion as well as the ionization level of the neutral atom have also been marked.

This behavior can be seen in Figure 2.4. Here, it is possible to see that for energies equal to or higher than the electron's binding energy the photodetachment processes can occur while for energies smaller than the electron's binding energy (i.e. energies below the EA) the process cannot take place. Above the photodetachment threshold, the overlap between the wavefunction of the negative ion and the tail of the wavefunction corresponding to the free electron increases and hence the probability of detachment also increases until it reaches its peak at approximately a value corresponding to 2·EA. However, higher photon energies will introduce an oscillation in

the wavefunction of the free electron which results in a decrease in overlap between the wavefunctions, hence, the cross section approaches zero.

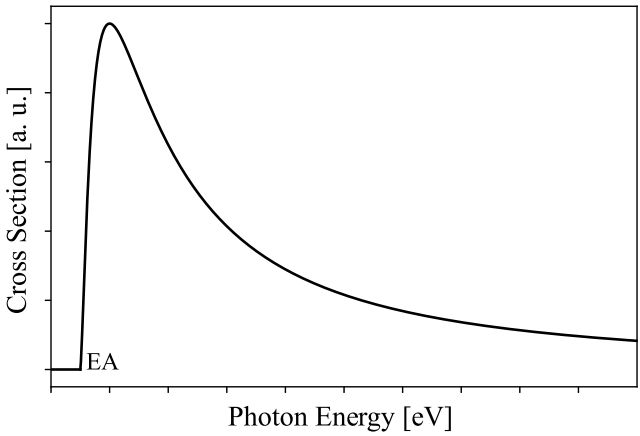

Figure 2.4: The general behavior of the total photodetachment cross section over a large range of energies. The photodetachment threshold, corresponding to the electron affinity (EA), has been marked.

In addition to the general model there is a threshold law which was described by Wigner in 1948 [89] when he made an assumption that the effective potential, described in Equation 2.23, is dominated by the centrifugal term at large distances between the electron and the core of the residual atom, i.e. at small energies above threshold. From this assumption Wigner derived an expression which describes the cross section of the photodetachment near threshold known as the Wigner law:

$$\sigma_{P.D} \propto \begin{cases} E_{\mathrm{e}}^{l+1/2} = (\hbar\omega - E_{\mathrm{Th}})^{l+1/2} & \text{for } \hbar\omega \geq E_{\mathrm{Th}}, \\ 0 & \text{for } \hbar\omega < E_{\mathrm{Th}}. \end{cases} \tag{2.27}$$

Here, E_{e} is the energy of the detached electron, $\hbar\omega$ is the energy of the incoming photon and E_{Th} corresponds to the energy needed for the surplus electron to be ejected from the system. When the photodetachment process occurs, the detached electron is emitted with an angular momentum, l, which follows the selection rules (assuming electric dipole approximation),

$$\Delta l = \pm 1, \tag{2.28}$$

Hence, the free electron resulting from the photodetachment process will have an angular momentum corresponding to

$$l = l_0 \pm 1, \tag{2.29}$$

where l_0 is the angular momentum of the electron in its bound state. Due to the angular momentum selection rules, described in Equation 2.28, the photodetachment can result in different onsets according to the Wigner law. The threshold behavior for the first three partial waves where $l = 0, 1$ or 2 can be seen in Figure 2.5.

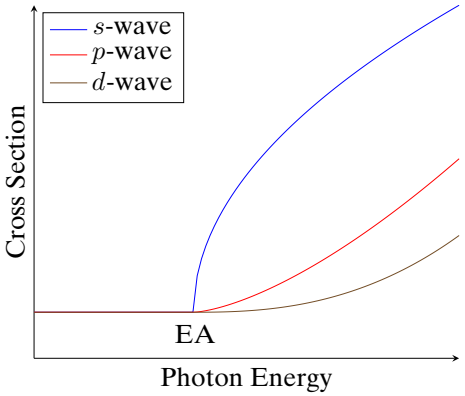

Figure 2.5: Sketch showing the general behavior of the cross section for each s-, p- and d-waves (where $l = 0, 1, 2$), at the photodetachment threshold. All according to the Wigner threshold law of Equation 2.27.

2.4 Excited States and Lifetimes

In neutral atoms and positive ions, where the long range Coulomb interaction is dominant, an infinite series of bound excited states can be found. Since the Coulomb attraction is effectively screened in negative ions, an infinite number of bound excited states cannot be supported. This makes the appearance of excited states in negative ions less common when compared to positive ions and neutral atoms. However, typically negative ions do possess one or a few excited states which are normally fine and hyperfine structure splittings of the ground state of the negative ion.

Excited states in negative ions are usually long lived since electric dipole (E1) transitions between the ground state and the excited state are, with

few exceptions, forbidden due to the states having the same parity[1]. This means that the excited electron can only decay through magnetic dipole (M1) transitions or higher order transitions but since these transitions are weak, the lifetimes of these states are generally several orders of magnitude larger than electric dipole transitions, and can reach lifetimes of 100 of seconds.

When investigating the excited states in negative ions, specific states can be probed by varying the photon energy, and hence photodetachment of electrons from a certain level can occur. A schematic image of the energy levels is shown in Figure 2.3. The different transitions of the excited states in the negative ions will also result in different onsets in the Wigner threshold when investigating the photodetachment cross section. In addition to the photodetachment cross section, the lifetime of the excited states can also be determined.

2.5 Doubly Excited States

Even though bound excited states in negative ions are, in general, not very common, it is possible for excited states to exist in the continuum, above the negative ion detachment level. A negative ion can be excited into a doubly excited state by absorbing a photon with sufficient energy. Doubly excited states in negative ions were first observed in the late 1970s by Bryant *et al.* when studying negative ions of hydrogen [90]. Since then a number of negative ions with doubly excited states have been studied [91, 92, 93, 94, 95].

Doubly excited states are formed when a negative ion absorbs a photon with sufficient energy to simultaneously excite two electrons, and these states later decay into a lower lying state within the neutral atom and a free electron. This can be compared to auto-ionizing states in neutral atoms and positive ions. Here, the electron correlation is extremely important, which makes these states important to study when it comes to atomic theoretical calculations [96].

When studying doubly excited states, these states will be observed as resonances in the photodetachment cross section. Two types of resonances can be observed, the so-called Feshbach and Shape resonances. Feshbach resonances refer to doubly excited states which are bound with respect to a state in the neutral atom. These binding energies are usually very small compared to the so-called parent state. Here, the decay process in-

[1]Exceptions are La^- [76], Ce^-, [77] Os^- [78], Th^- [61] and U^- [79]

volves one emitted free electron while the other electron transitions to a lower lying state within the atom. Shape resonances imply doubly excited states which are, due to the centrifugal barrier, bound above its parent state where the transition to the parent state can occur through tunneling. The transitions from the ground state in a negative ion into a doubly excited state are shown in Figure 2.6. A more detailed description of the topic can be found in the review of H. S. W. Massey [97] and in the thesis of J. Rohlén [98].

2.6 Molecular Ions

Molecular ions are more complex systems compared to atomic ions. This is because the electronic states in the molecular ions are additionally split into vibrational and rotational states which are typically separated by energies of the order of meV. This results in many closely lying states and hence the descriptions of the dissociation process, as well as the detachment cross section are more complex as compared to an atomic ion. Hence, the electron affinity is less well defined. The EA defined for atomic negative ions translates closest to the adiabatic electron affinity (EA) of a molecule which corresponds to the transition energy from the ground vibrational/rotational state of the negative ion to the ground vibrational/rotational state of the neutral molecule [99]. This can be described by:

$$\mathrm{EA(AB)} = E\left|\mathrm{AB}^{-}, \nu' = 0,\ J' = 0\right\rangle - E\left|\mathrm{AB}, \nu = 0,\ J = 0\right\rangle, \qquad (2.30)$$

where AB is the neutral molecule, AB^{-} its corresponding negative ion and ν and J are the vibrational and rotational states for the respective molecules.

Experimentally, molecular ions are often created inside an ion source at a high temperature, where the population of the vibrational and rotational states will follow a Boltzmann distribution. This means that photodetachment from closely lying excited states in the anion and the ground state in the neutral molecule can occur, which will result in a less discrete cross section onset. This makes it impossible to accurately determine the adiabatic EA which is the energy needed to detach the negative without changing the distance of the nuclei. However, it is possible to measure the so-called Vertical Detachment Energy (VDE). This value gives an upper limit for the adiabatic EA [99]. In order to measure the adiabatic EA with a higher precision, the ions need to be stored and cooled until they relax into their

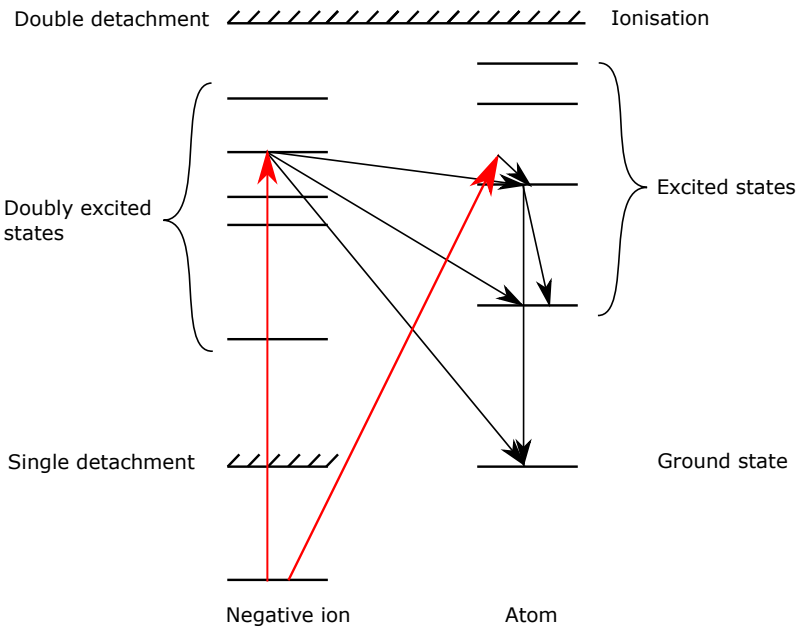

Figure 2.6: Energy level diagram of a negative ion. An electron in the negative ion can be detached directly into a state in a neutral atom or via a doubly excited state the negative ion when a photon is absorbed (red arrows). When the electron is in an excited state in the neutral it can later decay to a lower energy level or into the ground state of the neutral atom (black arrows). Figure courtesy of D. Leimbach.

vibrational ground state. This can be performed at storage rings like DESIREE [100], where the molecular ions can be stored and cooled down into their vibrational ground state. Furthermore, a process where the neutral molecule might capture an electron may occur, which leads to the formation of a short-lived state which then dissociates. This process is called Dissociative Electron Attachment (DEA) [101]. A schematic image of the molecular energy levels (including the vibrational- and rotational levels)

and the transitions corresponding to the adiabatic EA, the VDE and the DEA is shown in Figure 2.7 [1].

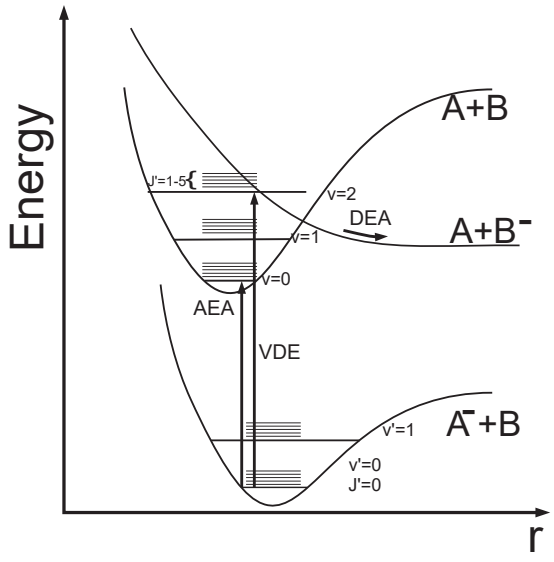

Figure 2.7: A qualitative diagram of the potential energy, including the vibrational ν and rotational J states, of a neutral molecule, AB, and its corresponding anions, AB^- and A^-B. Here, the vertical detachment energy (VDE), the electron affinity (EA) and the dissociation through electron detachement (DEA) are indicated.

If a sufficient amount of energy is imparted to a molecule, the molecular bonds may break causing it to split into two or more neutral or ionic fragments. This process is called molecular dissociation and can be induced by e.g. collisions with other molecules, atoms, ions, or by photons.

In the case where positively charged molecules are investigated through collision-induced processes, a single charged molecule, AB^+, which collides with a neutral atom, can dissociate via two different dissociation schemes:

$$AB^+ + \text{atom} \rightarrow \begin{cases} A^+ + B + \text{atom} \\ A + B^+ + \text{atom} \end{cases} \tag{2.31}$$

The cross section of the dissociation process can be investigated by collision-induced dissociation processes. It is also possible to determine the disso-

[1]Note that not all negative ions have lower energy compared to its neutral [99].

ciation channels and the electronic state of the dissociation products [102, 103, 104].

Molecular dissociation is also used as an alternative method to create atomic ions. Some atomic ions may not be produced and extracted from an ion source in sufficiently high quantities. However, the production rate may be improved if the ions are produced and extracted in molecular ion beams instead of atomic ion beams [105]. If this is part of the production scheme, the molecules need to be dissociated before the experimental measurements are carried out. One example where this production and preparation process is of interest is in medical applications, especially within CERN-MEDICIS and the MEDICIS-Promed project, where the isotope ^{11}C is studied as a possible candidate within hadron therapy [106]. Here, the carbon is extracted from the target-ion source unit as CO^+ [107], as this molecule has been shown to be more volatile compared to atomic carbon and can therefore be extracted from the target-ion source with higher yields [108]. The CO^+ molecules then have to be dissociated prior to medical applications. The collisional dissociation process of CO^+ was investigated in Paper VII.

CHAPTER 3

ION BEAM FACILITIES

There are several different ion beam facilities around the world where both positive and negative ions can be created. In such facilities, the ions are created in ion sources and extracted as beams. Both stable and radioactive isotopes can be produced. The different facilities used for the experiments discussed in this thesis are described in this chapter.

Regardless the way the ions are created, they all have to be transported in vacuum, typically in the pressure range of $10^{-6} - 10^{-8}$ mbar, in order to reach the experimental stations. Vacuum is needed to avoid collisions between the ions and residual particles since these collisions will destroy the ions and also generate background leading to a lower signal-to-noise ratio during measurements. When studying negative ions, the vacuum needs to be better quality as compared to when studying positive ions. This is due to the fact that the electron affinity is usually smaller compared to the ionization potential, hence negative ions are more fragile compared to the positively charged ions.

3.1 Ion Beam Manipulation

While ions can be produced through several different techniques, the manipulation of the resultant beams can be done in similar ways (depending on the energies of the ions). A brief overview of different ion beam manipulation techniques, as well as different characterization methods are described in the following sections. A more detail discussion of this can be found in the textbook by H. Wiedemann [109].

3.1.1 Beam Emittance

Beam emittance, ϵ, is a property used to characterize the size (volume) and quality of an ion beam. It describes the region that the particles occupy by including six phase space variables (three space coordinates and their three respective mechanical momentum coordinates) which are defined in three separate two-dimensional beam emittances [110, 111]. The emittance is often divided into longitudinal emittance and transverse emittance. The longitudinal emittance characterizes the phase and energy distribution along the ion beam axis, while the transverse emittance describes the space and momentum spread in the two axes perpendicular to the longitudinal axis. The momentum of a particle along a certain axis is, in general, described as having an angle, θ, relative to the axis. From this, it follows that the emittance will have dimensions of angle times length, most commonly expressed in units of π mm mrad [1].

According to Liouville's theorem, the emittance is always conserved for an ion beam that is only influenced by conservative fields. However, the emittance may change by influence from scattering on residual gas, laser cooling, space charge effects which, in these cases, make Liouville's theorem invalid [112].

3.1.2 Beam Optics

The simplest way to manipulate charged particles is by creating an external magnetic or electric field which can interact with the ions. The force which is acting on the charged particle is described by the Lorentz force, $\boldsymbol{F}_{\text{Lorentz}} = q(\boldsymbol{E} + \boldsymbol{v} \times \boldsymbol{B})$, where q and $\boldsymbol{v}$ are the charge and the velocity of the particle, and $\boldsymbol{E}$ and $\boldsymbol{B}$ correspond to the electric and magnetic field respectively. In order to steer and deflect the ions, a homogeneous electric field can be used, generated from two parallel metal plates to which a bias voltage is applied. Since the ions in the beam repel each other, it is important to be able to (re)focus the beam. This can be done, for example, using an electrostatic Einzel lens. Here, the electrodes consist of three cylinders, where the first and the last cylinder are normally on ground potential while the middle electrode is biased with an adjustable static potential yielding an inhomogeneous electric field. As the ions enter the Einzel lens, ions further from the central beam axis are deflected more strongly by the electric field, which focuses the beam to a point. It is also possible to use electrostatic quadrupoles for focusing purposes. This element will focus the beam in

[1] Note that some sources will include the factor π in the numerical value and instead write the unit of the emittance as mm mrad.

one axis while defocusing it in the other. Hence, it is common to arrange these elements in duplets or triplets in order to focus the beam in both directions. Furthermore, quadrupoles can also be used as deflectors if the ion propagation axis is perpendicular to the field direction.

3.1.3 Mass Separation Magnet

When the ion beam is extracted from an ion source, it can consist of many different elements, isotopes or molecular species i.e. many different masses. In order to study a specific species, it is necessary to separate the desired species from the rest of the ion beam, which can be accomplished through mass separation using for example a dipole mass separator magnet.

A mass separator magnet uses a strong, homogeneous magnetic field to spatially separate by their mass to charge ratio. When ions are guided into the mass separator magnet, they will travel along different trajectories depending on their mass to charge ratio. This is because a particle with charge q and mass m, which is moving through a magnetic field of strength B with a velocity of v will experience a centrifugal force ($F_{\text{centrifugal}} = \frac{mv^2}{r}$) equal to the Lorentz force ($F_{\text{Lorentz}} = qvB$) which will result in a circular motion with radius r. This expression can be written as

$$qvB = \frac{mv^2}{r}. \tag{3.1}$$

Since all ions are accelerated over the same electric potential, U, the velocity of the ions is only dependent on the mass and charge of the particle and can be written as

$$v = \sqrt{\frac{2qU}{m}}. \tag{3.2}$$

By combining Eq. 3.1 and Eq. 3.2, the radius of curvature can be defined as

$$r = \frac{1}{B}\sqrt{\frac{2mU}{q}}. \tag{3.3}$$

From this it is possible to see that for a given radius of curvature of the ion trajectory is dependent on the mass-to-charge ratio and the magnetic field strength. The element of interest can therefore be separated from the rest of the initial beam by applying a magnetic field which guides this specific mass in a central trajectory through the small apertures of the magnet, while ions with lower or higher masses will have either a smaller or a larger radius and will therefore be blocked and not exit the magnet.

The ability to separate the different masses is determined by the mass resolution of the dipole separator magnet. This is defined as

$$R = \frac{m}{\Delta m}, \tag{3.4}$$

where Δm is the resolving power which is defined by the full width at half maximum of the mass peak. The mass resolution of a separator magnet is limited by the energy distribution of the ion source, as well as possible imperfections and inhomogenities in the magnetic field.

3.1.4 Time-of-Flight Measurements

In the time-of-flight spectrometry one makes use of the fact that ions with the same kinetic energy, but with different masses, will have different velocities. If the ions in an ion beam are accelerated by the same electric potential, U, the classical kinetic energy, E, of each ion is given by

$$E = qU = \frac{1}{2}mv^2. \tag{3.5}$$

Therefore two ions with different masses (m) but the same charge (q) will, after being accelerated by the same potential, have different velocities (v).

After acceleration, the velocity of a charged particle will not change in a field-free drift region. If the drift length (l_{drift}) is known and the flight time (t) of the ion is measured, the velocity of the ion can be determined since $v = l_{\text{drift}}/t$. Eq. 3.5 can then be written as

$$qU = \frac{1}{2}m\left(\frac{l_{\text{drift}}}{t}\right)^2 \Longleftrightarrow t = \frac{l_{\text{drift}}}{\sqrt{2U}}\sqrt{\frac{m}{q}}, \tag{3.6}$$

where the first term is constant, assuming that the experimental setup does not change for a specific measurement ($A = \frac{l_{\text{drift}}}{\sqrt{2U}}$). If the drift length is sufficiently long, the different species will become spatially separated and by time-resolved detection the different masses can be resolved.

3.1.5 Radio-Frequency Quadrupole Cooler and Buncher

Radio-Frequency Quadrupole (RFQ) devices have been used at different research facilities and laboratories worldwide for several years [113, 114, 115] where they are used for ion beam preparation and, most importantly, for improvements of the ion beam. The losses in an ion beam is proportional to the emittance of the beam, which according to Liouville's theorem, is conserved under the influence of conservative fields [116]. However, the emittance can be improved by cooling the ions, which can be done

through collisional impact between the ions in a so-called buffer gas inside the Radio-Frequency Quadrupole cooler and buncher (RFQcb). During the cooling process, the ions are confined by a radio-frequency field which is present inside the apparatus. There is also a possibility of bunching (spatially compressing) the ions, which can increase the signal-to-noise ratio and is for example, beneficial when studying radioactive isotopes produced in low quantities [55]. This is an advantageous technique when performing fluorescence-detected collinear laser spectroscopy since it reduces the laser-induced background [117]. By guiding laser beams through the RFQcb, it opens up for the possibility of optical pumping of the trapped ions within the apparatus [118, 119]. Additionally, non-resonant laser photodetachment of negative ion beams within the RFQcb can be used to suppress isobaric contaminants within the ion beam since the interaction time between the ions and laser beam is increased when the ions are trapped within the RFQcb [120]. The RFQcb can also be used as a mass filter due to the presence of the mass dependent radio-frequency field inside the RFQcb. This, together with the possibility of extending the laser-ion interaction time by trapping the ions, is of great advantage where highly purified ion beams are of great importance, for example within the Accelerator Mass Spectrometry (AMS) community [121, 122].

At the ISOLDE facility at CERN, an RFQcb, ISCOOL, has been integrated downstream the second mass separator magnet at the HRS (High-Resolution Separator) beamline at the on-line facility (described later in this chapter). The apparatus is used to cool the ions by collisional impact between the injected ions and, typically, a high purity helium buffer gas which is maintained at a constant pressure inside the trap. This serves an important purpose at ISOLDE, as it reduces the energy spread and the transverse emittance of the ion beam [123] and hence, the quality of the ion beam will be improved before the ions are sent to the downstream experiments at the ISOLDE beamlines. Post mass separation, the emittance is typically 10-40 π mm mrad (the acceptance emittance of ISCOOL is $\sim 30\ \pi$ mm mrad) and by cooling the ions in ISCOOL the emittance can be reduced to 3π mm mrad (95% efficiency) [55]. Furthermore, ISCOOL provides a feature where the ions can be extracted either as a bunch or in continuous mode. A schematic image of ISCOOL is illustrated in Figure 3.1, where all the main components are labeled.

ISCOOL (as well as its replica integrated with the beamline at the Offline 2 facility described later in this chapter) can be divided into three different regions: the injection region, the cooling (or buffer gas) region, and the extraction region. It consists of three main components: the radio-frequency

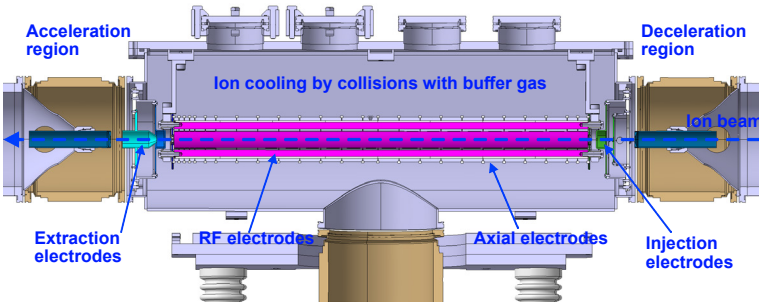

Figure 3.1: A schematic figure of the RFQcb, ISCOOL, which is located at the ISOLDE on-line facility. Here the main components, such as injection and extraction region, radio frequency rods, axial electrodes and buffer gas region, are all marked along with the direction of the ion beam. Figure courtesy of C. Muñoz Pequeño.

(RF) field, the buffer gas, and the axial direct current (DC) field. These regions and components are all described briefly below and can all be seen in Figure 3.1. A more detailed description of ISCOOL can be found in theses by I. Podadera Aliseda [124] and C. Babcock [125].

Injection and Extraction Region

When the ion beam reaches ISCOOL, it can have an energy of up to 60 keV. However, in order to inject the ions into the RFQcb, and the cooling region, the ions have to be decelerated. If the ion beam would have an energy of several keV and interact with the buffer gas without any electrical beam confinement elements, the collisions between the two elements would cause the ion beam to expand and the majority of the ion beam would not be transmitted through the RFQcb.

The deceleration is achieved by letting the ions pass by a grounded injection electrode, followed by two other electrodes, both biased with a voltage. The ions will interact with the electric field and decelerate to an energy of approximately 200 eV before they interact with the buffer gas.

After cooling, and possible bunching (see below), the ions are then extracted from the RFQcb by interacting with the electric field associated with the extraction plate. This electrode is biased with a voltage in order to accelerate the ions towards the two extraction electrodes which, together with a grounded electrode, will accelerate the ions up to their initial energy (pre injection).

The ion optics inside the ISCOOL have been designed and optimized in order to minimize the beam losses and minimize the expansion of the ion beam during extraction [124]. Furthermore, it is necessary to decrease the pressure of the buffer gas in the region between the extraction plate and the first extraction electrode since this is where the acceleration of the ions takes place after the cooling process. If a large amount of buffer gas is defusing into this region, where there is no beam confining RF field, this will cause the emittance of the ion beam to increase due to collisions between the ions and the gas. Hence, it is important to have sufficiently powerful differential pumping sectors, both in the injection and extraction regions, in order to maximize collisional losses [1].

The Buffer Gas

When the ions or molecules enter the RFQcb cavity they will interact with the buffer gas through elastic collisions. The purpose of this is to reduce the transverse motion of the injected ions and hence improve the emittance and improve the energy spread within the ion beam [123]. In this region, the ions will drift for a distance equal to one mean free path before it collides with a helium atom. The mean free path (l) of an ion in a helium gas in thermal equilibrium is given by

$$\bar{l} = \frac{k_{\mathrm{B}}T}{\sqrt{2}\pi \mathrm{P}(r_{\mathrm{ion}} + r_{\mathrm{gas}})^2}, \tag{3.7}$$

where k_{B} is the Boltzmann constant, T is the temperature, P is the pressure and r_{ion} and r_{gas} are the radii of the ion and the gas atom. The collisions repeat until the ions reach the end of the gas region, which is 800 mm long in total, or until the ions are scattered with an angle which makes the ions collide with the surrounding surfaces and are lost. When the ions are elastically scattered, energy will be transferred between the ions and the atoms in the gas, which will result in the damping of the oscillations of the ions until they reach thermal equilibrium with the surrounding buffer gas and thus cooling the ions which then end up on the axis of the beamline.

The nominal pressure of the buffer gas inside the cooling region at ISCOOL is around 0.1 mbar, as this has proven to give the lowest emittance [126, 125]. However, the actual pressure at ISCOOL cannot be directly measured and can therefore only be estimated [2].

[1] This has been upgraded for the RFQcb at the Offline 2 facility. Here, the pumping capacity in the injection and extraction region is significantly higher compared to ISCOOL.

[2] A vacuum gauge is placed in the vicinity of the RFQcb. This monitors the pressure

At ISOLDE, the most commonly used buffer gas used is helium, but in this thesis, a mixture of helium and neon, in addition to pure helium gas, was used for investigations of molecular dissociation. This is described in Paper VII.

The Radio-Frequency Field

The purpose of the RF field is to confine and focus the beam in the center of the beam axis during the cooling process. The RF field is applied to the four long electrodes (rods) that are located along the beam axis inside the RFQcb. The RF field is produced by an oscillating and amplified voltage which is applied to these rods. Each opposite pair of electrodes share the same polarity (either positive or negative) and the polarity of the pairs is then switched at a known frequency (in this case in the order of kHz). The behaviour of the ions in the oscillating (sinusoidal) field can be mathematically described using the so-called Mathieu equation, which is a special case of the Hill equation [127]. The solutions to the equation of motion can be either stable or unstable which is defined by the geometry of the apparatus and should therefore be taken into account when selecting voltage and frequency in order to get a stable ion trajectory. In general, it is also possible to utilise other waveforms e.g. a square wave [128]. In this case, where a square wave is implemented, the solution of the Hill equation is given by a linear ordinary differential equation called the Meissner equation. ISCOOL is operated using sinusoidal wave forms, but other waveforms have been investigated within the RFQcb at Offline 2 [129]. The theory behind the equation of motion is discussed in detail in the textbook by P. H. Dawson [127].

The Longitudinal DC Field

As previously stated, it is possible to operate ISCOOL in either a continuous or bunched mode. In the first case, the ion beam is extracted as a continuous beam but when switching to bunched mode it is possible to prevent the beam from escaping the cooler and in that way create a bunched ion beam. The four RF electrodes are surrounded by 25 circular, electrically isolated electrodes which can all be independently biased with a voltage, creating a longitudinal DC field which is used to extract the ions as a single bunch. In most cases when ISCOOL operates in bunching mode, the axial potential applied to the circular electrodes will form a potential slope

in the surrounding beamline and by that an approximate pressure inside the interaction region is estimated.

with a potential well and barrier at the end, similar to that illustrated in Figure 3.2. The ions are prevented from escaping the RFQcb by applying a potential, greater than the energy of the ions, to an electrode at the very end of the buffer gas region, just before the extraction region. Once the ions have been cooled and trapped in the potential well, it is possible to lower the voltage on the last electrode in order to extract the ion bunch. Since particles of the same charge are trapped inside the RFQcb, they will exert a repulsive force on each other when trapped in the potential well. The number of trapped ions in the RFQcb is therefore limited by the space charge effect which is caused by the Coulomb interaction between the ions inside the potential well [127]. For ISCOOL the space charge limit is 10^8 ions [55].

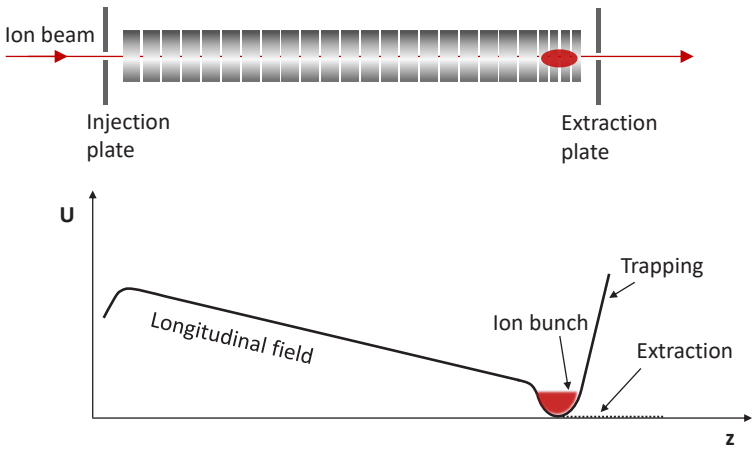

Figure 3.2: The longitudinal DC electrodes inside the RFQcb (upper image) and the potential well created by the voltage applied to the electrodes when operating ISCOOL in bunching mode (lower image). The potential barrier at the end of the potential well is present while trapping the ions but switched to ground potential during extraction.

When operating ISCOOL in continuous mode, the voltages on the axial electrodes are either set to zero or held at low potentials creating a shallow potential curve.

Bunched operation mode was used during the molecular dissociation test described in Paper VII.

3.1.6 Beam Diagnostics

Ions are extracted and accelerated inside vacuum chambers and sometimes over long distances. Hence, it is important to be able to get information regarding the properties of the ion beam, such as its intensity, spatial position and structure, and the beam envelope. To do this, different detecting devices can be used.

Faraday cups (FCs) are one example of these devices can be used for intensity measurements. An FC consists of a metallic cup where the ions are detected. The ions impinge on the back of the metal cup and transfer their charge, which then is detected and measured as an electric current. When the ions impinge with a kinetic energy in excess of a few keV, secondary electrons can be created but these are suppressed by applying a bias voltage (around -100 V) at the entrance of the cup. The minimum current that a Faraday cup can detect is typically of the order of pA, the upper limit is determined by the ability of the metal to absorb power from the incoming ion beam.

There are also more sensitive detection devices, such as microchannel plates (MCPs) [130], channel electron multipliers (CEMs) [131], and MagneTOF detectors [132] which use the electron multiplication technique in order to detect particles. Here, the incoming particles impinge on a dynode, resulting in the creation of secondary electrons. These secondary electrons are then directed towards another dynode or section of the same dynode, biased with a higher positive voltage. This can be repeated several times until the incoming particle's charge has been amplified such that it can be measured by conventional electronics. This multiplication technique makes it possible to perform single particle detection.

For monitoring the spatial position in either one or two dimensions, shape and envelope of the ion beam inside the vacuum chambers, wire scanners made of wire grids can be used. In these cases the ion beam interacts with the thin metal wires and creates an electric current in the wire which then can be detected. This can then be converted into a transversal position of the ion beam within the beamline.

3.2 Radioactive Ion Beam Facilities

In 1896, the French scientist Henri Becquerel discovered evidence for radioactivity when working with phosphorescent materials [133, 134, 135]. By placing a sample of uranium salt on top of a photographic plate, he noticed that the plate was dimmed. He concluded that the radiation emitted

from the uranium had caused the plate to react as if it was exposed to light. A few years later, thorium was also found to be radioactive, as well as polonium and radium which were discovered by Marie Skłodowska-Curie and Pierre Curie [135, 136]. Furthermore, discoveries of isotopes were made [137, 138], which later was displayed in the so-called table of nuclides.

Radioactive isotopes are commonly used in society, such as to fuel the chain reaction in nuclear reactors [139], for military purposes [140], and for medical purposes such as cancer therapy and diagnostics [141].

Some long-lived radioactive isotopes do occur naturally in reasonable quantities, but a large number of isotopes have to be created artificially in nuclear reactors or accelerators in order to produce sufficient quantities for studies. Accelerators are especially suitable for short-lived isotopes since the isotopes are created in ion beams which are transported directly towards the experiment. There are two common types of techniques which are usually used when producing radioactive ion beams, the *in-flight* technique [142] and the *Isotope Separator On-Line (ISOL)* technique [143].

In the in-flight technique, a thin target consisting of light elements is bombarded with a primary beam of heavy ions. This results in fragmentation reactions where the products have approximately the same direction and energy as the primary beam. The ions are then mass separated and guided towards the experimental setups.

The advantage of the in-flight method is that the process is not sensitive to chemical properties or to the half-life of the isotopes. The half-life of the extractable isotopes is only limited by the flight time of the ions from the target to the experimental station, which is typically on the order of μs. Hence, isotopes with a half-life down to a few μs can be produced [144]. However, due to the random recoil momentum of the produced fragments, the angular and energy distributions of the produced ions are usually large which results in a larger emittance [144]. A few examples of in-flight facilities are the Super-FRS at GSI [60] (Darmstadt, Germany), the Radioactive Ion Beam Factory (RIBF) at RIKEN (Tokyo, Japan) [57, 58] and IGISOL at the University of Jyväskylä (Jyväskylä, Finland) [59]. A detailed description of the in-flight technique and some of the facilities can be found in articles by Blumenfeld *et al.* [145] and the *In-Flight Separation of Projectile Fragments* by Morrissey and Sherrill [144] which is a part of the *The Euroschool Lectures on Physics with Exotic Beams, Vol. I*.

The method utilized in ISOL facilities is based on using a thick, hot target for the isotope production which gives a large total cross-section for the production [146]. The target material is irradiated with a beam of light ions (e.g. protons) in order to create the isotopes. There are three main reaction channels for the ISOL production: spallation, fragmentation and

fission, illustrated in Figure 3.3. The isotopes then diffuse from the target

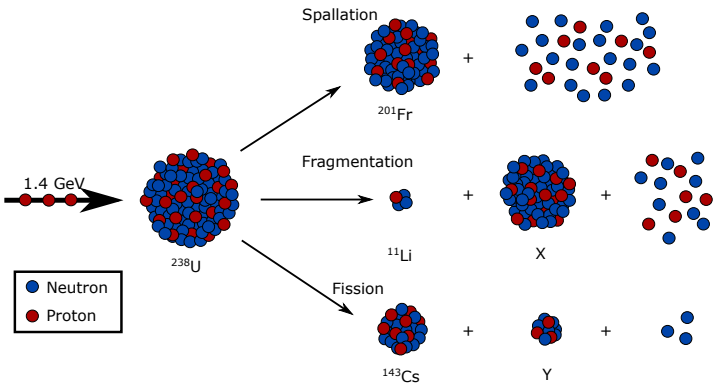

Figure 3.3: The three main nuclear reactions induced when a proton beam of 1.4 GeV collides with a ^{238}U . Figure courtesy of D. Leimbach [147].

and effuse into an ion source where the atoms/molecules are ionized and further extracted, accelerated, and mass separated in order to select the isotope of interest. Since the isotopes are produced at rest, low-energy experiments are suitable, but there is also a possibility to post-accelerate the isotopes after mass selection [148].

In general, a large number of isobars of different elements are produced in the target simultaneously which makes it difficult to produce ion beams with high purity using the ISOL method. This can be improved by careful selection of the ion source and target material based on the isotope of interest. However, the production of e.g. refractory elements is challenging since high temperatures are required in order to make the elements sufficiently volatile such that they can be extracted from the target. A few examples of ISOL facilities around the world are SPIRAL at GANIL (Caen, France) [149], ISAC at TRIUMF (Vancouver, Canada) [56] and ISOLDE at CERN (Geneva, Switzerland) [55]. A more extensive overview of the ISOL technique can be found in articles by Blumenfeld *et al.* [145] and *Isotope Separation On Line and Post Acceleration* by Van Duppen [150] which is a part of *The Euroschool Lectures on Physics with Exotic Beams, Vol. II*.

3.2.1 ISOLDE Infrastructure

The Isotope Separator On-Line DEvice (ISOLDE) [55] is located at the Conseil Européen pour la Recherche Nucléaire (CERN) [151]. It consists of one ISOL (on-line) facility where protons are used to irradiate target-ion source and two non-radioactive, "off-line" laboratories, Offline 1 and Offline 2, where the latter is the most recently built laboratory. These facilities and laboratories, along with the ion beam production, are described in the following sections.

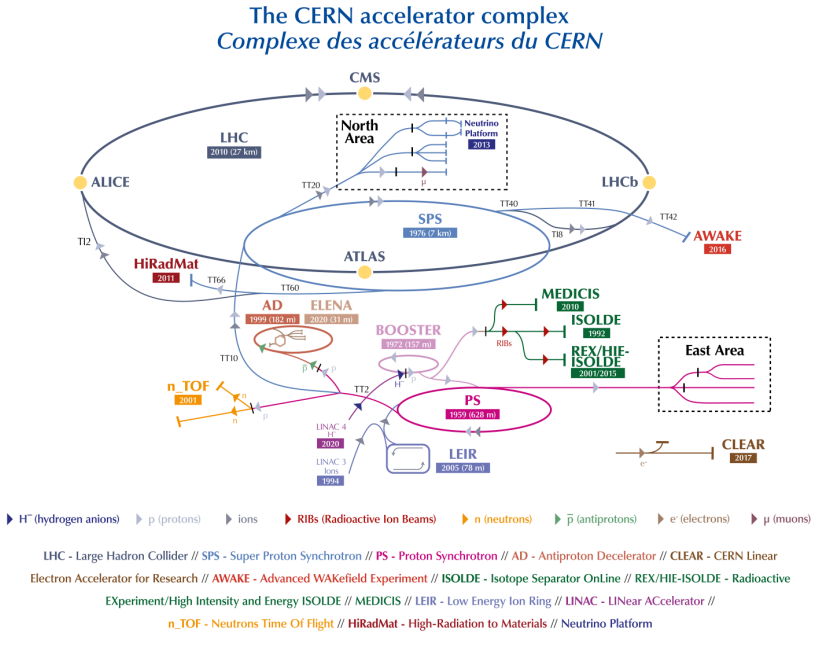

Figure 3.4: CERN accelerator complex. Courtesy of E. Lopienska [152].

3.2.2 ISOLDE On-Line Facility

The ISOLDE facility is a radioactive ion beam facility which bases its production of radioactive isotopes on the ISOL technique [55]. Here, radioactive ion beams with energies of up to 60 keV can be produced for low energy experiments. There is also the possibility for post-acceleration after mass

separation up to an energy of 10 MeV/u [153, 154]. The isotopes are used for research in different areas of science, for example, in atomic and nuclear physics, solid state physics, fundamental physics, biology and nuclear medicine.

ISOLDE consists of two target stations, i.e. Front-Ends, where it is possible to place target-ion source units which can then be heated up and irradiated with a pulsed proton beam of 1.4 GeV. The protons come from the Proton Synchrotron Booster (PS Booster), which is a part of the accelerator complex at CERN as seen in Figure 3.4.

The target stations at ISOLDE are attached to two different beamlines, namely the General-Purpose Separator (GPS) and the High-Resolution Separator (HRS). The GPS beamline has one mass separator magnet with a resolution $R = \frac{m}{\Delta m}$ of approximately 800. The HRS on the other hand, has two magnets and overall resolution of approximately 6000 [55]. In order to guide the ions through the beamlines and towards the experiments, electrostatic optical elements are used. After mass selection in the GPS beamline, the ions can be guided to the central beamline, General High Mass (GHM) beamline, or the General Low Mass (GLM) beamline; the latter is where the GANDALPH (Gothenburg ANion Detector for Affinity measurements by Laser PHotodetachment) chamber is installed temporarily for negative ion experiments. When using the HRS beamline, the ions can be guided to the central beamline and further to different experimental setups. Here, it is also possible to use the RFQcb, ISCOOL. For the experiments later described, both the GPS and the HRS beamlines have been used. A layout of the two beamlines at ISOLDE can be seen in Figure 3.5, together with the specific instrumentation integrated into both beamlines as well as the ToF detector described later in this chapter and in Paper VIII which was used to perform the measurements presented in Paper VII.

3.2.2.1 Ion Beam Production at ISOLDE

By letting bunches of protons bombard a thick target, it is possible to produce radioactive nuclei at the ISOLDE facility. The material which the target is made from varies depending on the needs. They can be formed from solids, powder, or liquids, however the area of target material design is an incessantly ongoing development. The nuclei are produced in the target through spallation, fragmentation or fission. In order to make the particles diffuse out of the target in a relatively short time and reduce the probability of them sticking to the surface, the target is heated up to approximately 2000°C. The particles then diffuse out of the target through

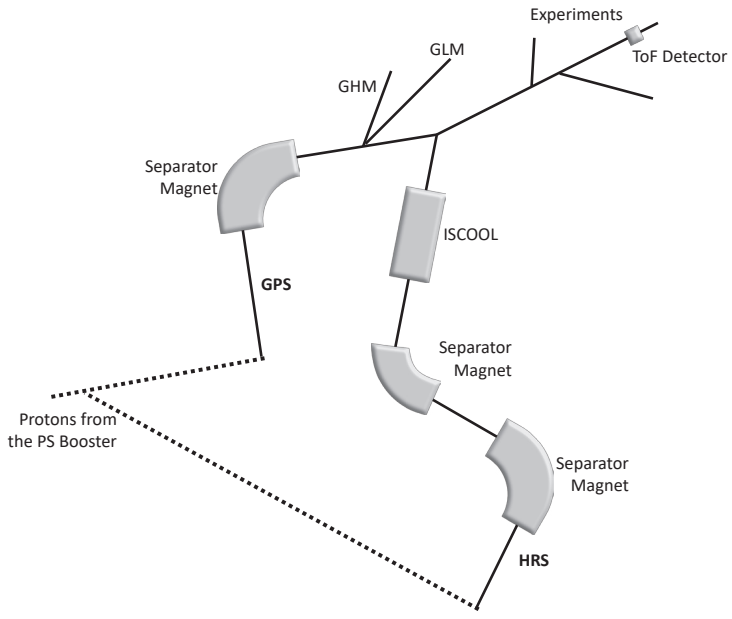

Figure 3.5: A schematic layout of the beamline structure at the ISOLDE on-line facility.

the transfer line, where they are ionized, either thermally, by a plasma, or by photons. The target container and the transfer line are heated independently since, in general, it is important to have a high temperature on the transfer line in order to avoid elements condensing on the surfaces.

Furthermore, there is a possibility of injecting a gas into the target-ion source. This feature was used during the molecular dissociation tests described in this thesis. In order to extract the ions from the target-ion source unit, an electrostatic field gradient is applied between the unit itself and the so-called extraction electrode, which accelerates the ions out of the source and towards the experimental stations.

The three most common target-ion source units used at ISOLDE are the surface ion source, the plasma ion source (the Forced Electron Beam Induced Arc Discharge - FEBIAD [155]) and the laser ion source (the Versatile Arc Discharge and Laser Ion Source - VADLIS [156]). In positive surface ion sources the atoms are ionized by contact with a heated surface

with high work function. Here, the surface material can remove an electron from the atom if the work function of the material is higher than the ionization potential of the element. Examples of metals with high work functions which are typically used in these ion sources are tantalum and tungsten, which have work functions between 4-4.5 eV [157]. When it comes to negative ion sources, materials with low work functions, typically less than 3 eV, are needed to created a beam of negative ions. A common material is lanthanum hexaboride (LaB_6), which has a work function of approximately 2.6 eV [158]. Plasma ion sources ionize the atoms through impact with a plasma created by the acceleration of electrons inside the ion source. The plasma is confined inside the ion source using a magnetic field. In laser ion sources, a combination of lasers are used in order to step-wise excite the electrons in the atom towards the ionization potential corresponding to the atom. In order to do this, the lasers have to be chosen to match the excitation scheme of the element of interest. These ion sources used at ISOLDE are described in detail in the thesis of D. Leimbach [147].

When the isotopes have been ionized, they are extracted from the target-ion source as an ion beam with a maximum energy of 60 keV.

3.2.3 ISOLDE Offline Laboratories

Before all target-ion source units are installed at the ISOLDE on-line facility they have to be characterized and quality controlled. This is primarily done at Offline 1 [159] which is a non-radioactive mass separator. In the past, Offline 1 has been used for both target quality controls and target and ion sources developments, together with the ISOLDE on-line facility. However, since the time dedicated to pure machine developments at the on-line is very limited, and during ISOLDE operation, the Offline 1 facility is mostly used for target-ion source control, a dedicated testing and development facility has been built. This new facility is called Offline 2 and the planning and construction of this facility forms part of this thesis work.

The Offline 2 facility is, like Offline 1, a non-radioactive facility. It contains a mass separator beamline and a laser laboratory which is located in a separate room adjacent to the mass separator.

Unlike Offline 1, the beamline at Offline 2 has been constructed to mimic the ISOLDE on-line beamline. It consists of a ISOLDE Frontend, a mass separator magnet, ion beam optics and ion beam analyzers that are all identical to the ones which can be found at the on-line beamline, as well as a Radio-Frequency Quadrupole cooler and buncher (RFQcb) which mimics ISCOOL [160, 124, 161]. There is also a possibility to connect further instrumentation (detectors, etc.) at the end of the beamline. A layout of the

Offline 2 beamline can be seen in Figure 3.6.

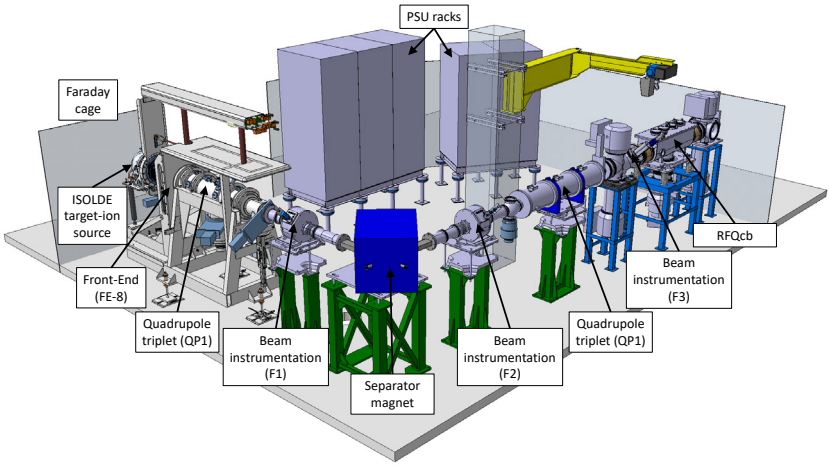

Figure 3.6: A layout of the Offline 2 beamline where the main elements have been labelled. The ion production takes place in the ISOLDE target-ion source located at the Frontend. Here, the first quadrupole triplet of the beamline is placed as well. The beam instrumentation (Faraday cups and ion beam scanners) are located up- and downstream of the magnet, in the vicinity of the focal points (F1 and F2). Another quadrupole triplet placed before the RFQcb as well as a Faraday cup which is located at the third focal point (F3). There is also a possibility of installing movable equipment (for example detectors) downstream of the RFQcb, outside of the Faraday cage.

Since both Offline 1 and Offline 2 are non-radioactive facilities the ion production is not driven by the bombardment of protons on the target. Instead, a sample of an element is placed in the target-ion source which is then heated thermally, which makes the particles diffuse out of the unit.

The fact that the ion beam production at Offline 2, as well as transportation, can mimic the ISOLDE on-line beamline is critical as new developments and improvements are highly important since ion beam requirements have increased along the study of radioactive ion beams over the last decades [145]. Further information about the Offline 2 facility can be found in Papers IX and X.

3.2.4 GANDALPH

The Gothenburg ANion Detector for Affinity measurements by Laser PHotodetachment (GANDALPH) is an experimental apparatus designed for experiments utilizing Laser Photodetachment Threshold spectroscopy (LPT) processes of radioactive isotopes at an energy above 15 keV. The setup consists of electrostatic deflectors, collimators which define the interaction region, beam diagnostics for monitoring the negative ion beam current, detectors for low ion flux detection, an alpha particle detector, and a neutral particle detector which is described briefly below.

3.2.4.1 Neutral Particle Detector

The neutral particle detector (NPD) integrated with the GANDALPH beamline (as well as the RADAR beamline and the Doppler spectrometer at GUNILLA which are discussed later in this chapter) are based on the design of Hanstorp [162]. The detector consists of a transparent and conductive plate, which is called the target plate, and a Channel Electron Multiplier (CEM). The target plate has to be both optically transparent in order for the laser light to be transmitted through the plate and at the same time conductive in order to produce secondary electrons when the neutral particles created from the photodetachment process impinge on the plate. When a neutral particle impacts the target plate, a few secondary electrons are emitted and guided towards the CEM where they are multiplied by a factor of 10^9 and detected. In the original design, the target plate consisted of a glass plate with a coating composed of tin-doped indium oxide (In_2O_3:Sn), which created a transparent and conducting target [162]. The transparency for this composition is approximately 80% in the range from visible wavelength to far infrared and the efficiency of the detector is about 40% for 3 keV particles [162]. However, for shorter wavelengths, the transmission significantly decreases. Furthermore, when the photon energy is increased above the material work function, a larger amount of photoelectrons are created by the laser pulse through the photoelectric effect, which leads to a large electron background that can saturate the detector. Due to this, the target plate was replaced by a graphene coated quartz plate. This increased the transmissivity to more than 95% all the way from the far infrared region to the ultraviolet region [163] and the efficiency of the NPD is nearly 100% [164]. To further decrease the detection of photoelectrons, a metal grid or a bend plate can be placed at the entrance of the CEM. This grid can be switched with a potential that prevents electrons produced at the target from entering the CEM. The tin-doped indium oxide target plate

was used in the experiment described in Paper I but upgraded to a graphene coated quartz plate before measuring the electron affinity of astatine (presented in Paper II). The NPD toghether with the GANDALPH beamline are described in further detail in Paper III, I and II.

3.2.5 Fast Time-of-Flight Detector

The fast Time-of-Flight detector was constructed for detection of a broad span of beam currents, ranging from single ion counts up to μA. This was of interest since the ion beam current (i.e. the dissociation rate) in the molecular dissociation test presented in Paper VII was unknown. A detector like this was not available previously at ISOLDE; conventional Faraday cups can only measure beam currents down to around 0.25 pA, and regular MCP detectors and other electron multipliers cannot handle higher beam currents as the signal will saturate the detector and result in premature aging of the device.

The ToF detector consists of a secondary electron emission plate, electrostatic mirrors, and an MCP detector, which makes it suitable for single ion counting in addition to high beam current detection. The secondary electron emission (SEE) plate is a copper plate coated with an approximately 200 nm thick film of lithium fluoride (LiF). When the ions impinge on the plate, secondary electrons will be emitted from the plate and then accelerated and deflected 90° via electrostatic mirrors toward the MCP detector. The electrostatic mirrors consist of an oxygen free copper frame where gold coated tungsten (AuW) wires with diameter 20 μm have been tensioned and placed with 1 mm pitch. The detector efficiency is approximately 94% and since the SEE plate is easily replaced, it is also possible to use the detector when measuring radioactive ion beams, since contamination is not a significant issue if the plate can be replaced with a new, non-contaminated plate. Further information regarding the ToF detector can be found in Paper VIII.

3.3 GUNILLA

The Gothenburg University Negative Ion Laser LAboratory (GUNILLA) [165, 166] is a research facility where a broad range of stable negative ions can be produced. Here, Laser Photodetachment Threshold spectroscopy (LPT) experiments can be conducted as well as detection of Rydberg atoms.

Stable negative ions are created in a Cesium sputter source and are accelerated further downstream to a mass separator magnet. Post mass se-

lection, the ions of interest are transported to the desired experimental apparatus. A schematic layout of GUNILLA is shown in Figure 3.7.

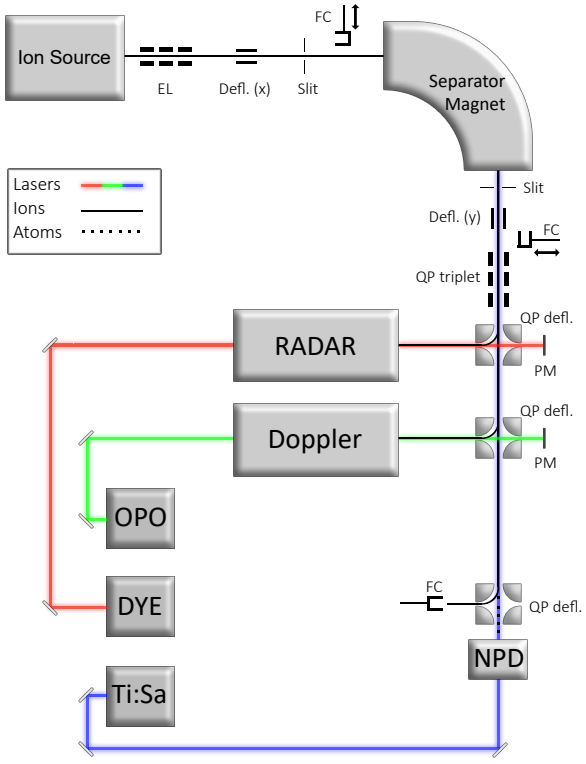

Figure 3.7: A schematic layout of GUNILLA. The ions are created in the ion source and extracted into the beamline. The Einzel Lens (EL), deflectors in x and y direction (Defl. (x) and (y)), the quadrupole triplet (QP Triplet) and the quadrupole deflectors (QP Defl.) are used to manipulate the ions towards the three different spectrometers, RADAR, Doppler or NPD. Three high intensity lasers (Optical Parametric Oscillators (OPO), Dye and Ti:Sa) produce laser beams which can be directed into the experimental setups using optical mirrors. Note that the beams generated from all lasers can be guided to all the different experimental arrangements. Faraday cups (FC), a Neutral Particle Detector (NPD) and Power Meters (PM) are used for beam diagnostics. Besides these, there are additional detectors integrated in the three spectrometer sectors.

Ion Beam Production at GUNILLA

The ion source is a conventional cesium sputter source of type PS-120 from Peabody Scientific and it is based off the design by Middelton [167]. The source consists of a surface ionizer, which is a spherical tantalum surface (the anode), and a rod made of aluminium (the cathode). When the cesium is heated to somewhere in range 100°C to 150°C it vaporizes and diffuses into the ion source and onto the ionizer. When the cesium atoms reach the ionizer, which is kept at a temperature of 1300°C, they are ionized by surface ionization. The positively charged cesium ions are then accelerated toward the cathode which is typically held at -3 kV relative to the anode. There is a small hole in the middle of the cathode where it is possible to place the target material, i .e. the element of interest. When the energetic positive cesium ions impinge on the cathode, the atoms and molecules of the target material will be sputtered. Since the cathode is cooled to room temperature, a part of the vaporized cesium will condense on the cathode surface. The neutral cesium layer will contribute to a lowering of the work function at the cathode surface and will increase the possibility for the sputtered atoms or molecules to capture an additional electron and become negatively charged [168]. Hence the cesium, which has a very low ionization energy, is used both for sputtering as well as an electron donor.

The spread in initial kinetic energy between the ions created in the sputtering process will be rather large. This will lead to Doppler broadening which, in turn, will reduce the resolution of the measurements. This is due to the sputtering process in the ion source. When the cesium atoms are accelerated onto the cathode material, the sputtered atoms will have outgoing energies ranging from a few eV up to 20 eV, since an energy spread of about 20 eV. If this was entirely due to a thermal process, the energy spread in the beam would instead be around 25 meV at room temperature since $E \propto k_B T$, where k_B is the Boltzmann constant and T is the temperature. It is possible to decrease the spread in energy by accelerating the ions over the same electrical potential [169]. The velocity spread (Δv) can be described by the uncertainty in the kinetic energy (E) in the beam according to

$$\frac{dE}{dv} = \frac{d(\frac{mv^2}{2})}{dv} = mv. \tag{3.8}$$

Here, the mass and velocity of the ions are denoted by m and v, respectively. This expression can be approximated to

$$\frac{\Delta E}{\Delta v} = mv, \tag{3.9}$$

which in turn can be written as

$$\Delta v = \frac{\Delta E}{\sqrt{2mE}}. \tag{3.10}$$

From Eq. 3.10 it can be seen that the velocity spread will decrease with respect to the ions emitted from the ion source when they are accelerated over the same electrical potential. This technique is called velocity compression and was first described in 1976 by Kaufman [169]. The ions are, therefore, accelerated to a kinetic energy of typically 6 keV and the ion current prior to mass selection is generally a couple of μA.

Ion Beam Transportation

When the ions have been accelerated out from the ion source they are transported to the beamlines under vacuum of the order of 10^{-8} mbar. The ions are guided through the beamline toward the experimental arrangements using electrostatic elements including quadrupole triplets, deflectors and lenses. Since the ion beam exiting the ion source generally consists of several ion and molecule species, a mass separator magnet, with a mass resolution of $R = \frac{m}{\Delta m} \approx 500$, is used in order to mass select the ion of interest [166]. The ion beam current can easily be monitored throughout the beamline using the Faraday cups placed both upstream and downstream of the separator magnet.

3.3.1 RADAR

The Rydberg Atom Detector for Anion Research (RADAR) [170] is a part of the GUNILLA beamline. It is the first experimental arrangement located after the separator magnet. RADAR is designed to measure the photodetachment thresholds of different elements by combining Laser Photodetachment Threshold Spectroscopy (LPTS) with Resonant Ionisation Spectroscopy (RIS). Since the detachment threshold is dependant on the angular momentum of the outgoing electron, according to the Wigner law [89] described in Equation 2.27, this can result in a different onset of the detachment above the ground state threshold (as described in Section 2.3). If the onset of the photodetachment process is slow, e.g. corresponds to the behaviour of a p-wave, it is difficult to determine the electron affinity with a high precision. Instead, it is possible to excite the negative ion, from its ground state, into a higher excited state in the neutral atom, and after this, the atom can be exited further into a Rydberg state and later ionized using the field ionizer. This would result in a sharp onset of the photodetachment

process which facilitates a more precise determination of the electron affinity.

The mass separated ion beam is deflected by 90° into the interaction region where it is overlapped with two laser beams. The pulses from these two lasers will be set to have different arrival times in order to first detach the surplus electron, and then excite the neutral atom into a Rydberg state, thereby creating a Rydberg atom. The Rydberg atom then enters the Field Ionizer (FI) region. This region consists of 11 parallel plates to which a voltage gradient is applied, where the gradient at the beginning of the FI region is weak enough that it has a negligible effect on the Rydberg atoms of interest, but gets increasly stronger towards the end, such that it ionizes the atoms of interest. This will decelerate all the positive ions created in the RIS process and hence they will exit the FI with a decreased kinetic energy compared to their initial energy.

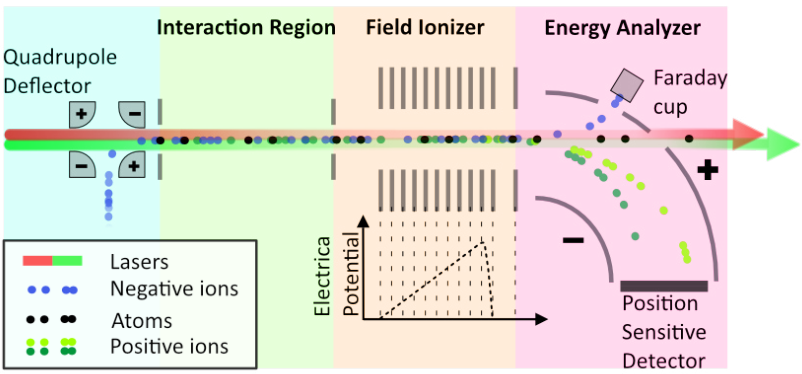

Figure 3.8: A schematic figure of the RADAR spectrometer at GUNILLA. The negativly charged ions are deflected 90° into the interaction region by a quadrupole deflector where they are overlapped with the laser beams. The field ionizer is located downstream the interaction region. This is where excited Rydberg atoms are field ionized. The ions and atoms are then separated by charge and energy. The neutral atoms continue in a straight path while the negative ions are deflected into a Faraday cup. The positively charged ions are deflected into the energy analyzer where the radius of curvature of the particles is energy dependent, followed by a position sensitive detector which detect the positive ions.

In order to spatially separate the Rydberg atoms of interest from the positive ions created through e.g. collisionally induced detachment processes

and two-photon ionization processes, an electrostatic mass analyzer was used. This consists of two electrostatic plates which deflect the ions by 90° onto a position sensitive detector, and due to their differences in kinetic energy, the ions will then be spatially separated when reaching the detector surface. The neutrals will, however, be unaffected by the mass analyzer and continue straight forward. A schematic figure of RADAR can be seen in Figure 3.8.

Due to several apertures along the beam path, the ion beam tuning process can be a bit cumbersome. To facilitate the beam tuning, an NPD has been installed at the end of the beamline. This makes it possible to monitor the neutrals created in the photodetachment process and in that way, improve the overlap between the ion and laser beams. This NPD is described in Section 3.2.4.1.

3.3.2 The Doppler Spectrometer

The Doppler Spectrometer is a collinear spectrometer at GUNILLA. A schematic overview of the spectrometer can be seen in Figure 3.9. The setup consists of a quadrupole deflector which deflects the mass separated ion beam into a 20 cm long interaction region defined by two apertures with a diameter of 6 mm. Here, it is possible to perform Laser Photodetachment Threshold (LPT) spectroscopy experiments by overlapping the negative ions with a co- or counter-propagating laser beam. The neutral atoms produced in the photodetachment processes will then travel toward the NPD (described in Section 3.2.4.1) where they will be detected.

Furthermore, a 30 cm long cylindrical electrode is located in the interaction region and can be used to tune the exact laser frequency experienced by the ions by tuning the velocity of the ions. This is done by applying a bias to this electrode which will change the kinetic energy of the ions and via the Doppler shift will tune them into resonance with the photon energy. Applying a positive potential to the electrode will increase the kinetic energy whereas a negative potential will result in a decrease. Depending on the laser setup (co- or counter-propagating) this will either result in an increase or decrease in the Doppler shift. Using this technique is equivalent to tuning the laser wavelength but it can be beneficial if the laser exhibits instability when performing wavelength scans, or if the investigation requires making smaller changes in wavelength than what is possible with a specific laser.

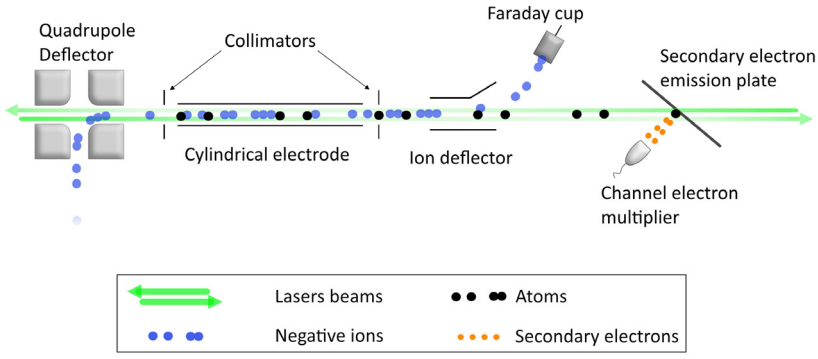

Figure 3.9: A schematic overview of the Doppler spectrometer. The negative ion beam is deflected by a quadrupole deflector into the interaction region where it is overlapped with a laser beam. The neutral atoms which are produced in the photodetachment process reach the neutral atom detector where they impinge on the plate and secondary electrons are emitted and detected by a Channel Electron Multiplier (CEM). The undetached negative ions are deflected into a Faraday cup.

3.4 The DESIREE Facility

The Double ElectroStatic Ion Ring ExpEriment (DESIREE) [171] is a research facility at Stockholm University, Sweden, which is used for studies of atomic and molecular (and clusters) ions. It consists of two cryogenic ion beam storage rings, which are merged together in an interaction region. The rings have a circumference of approximately 8.8 m each, the pressure inside the beamline is 10^{-14} mbar and it is kept at a temperature of approximately 13 K [171, 45] which is achieved by cryogenic cooling. A schematic figure of the DESIREE storage rings can be seen in Figure 3.10.

At DESIREE, the ions can be stored and studied over time. For example, ions of different charge states can be produced and stored in the two merging rings and overlapped in an interaction region between the two rings. It is also possible to measure the radiative lifetimes of excited states in negative ions. The lifetimes of excited states in negative ions can be on the order of several seconds or longer. This is because the fine structure transitions are almost exclusively forbidden such that the de-excitations occur using E2, M1 or higher order transitions. So in order to measure these

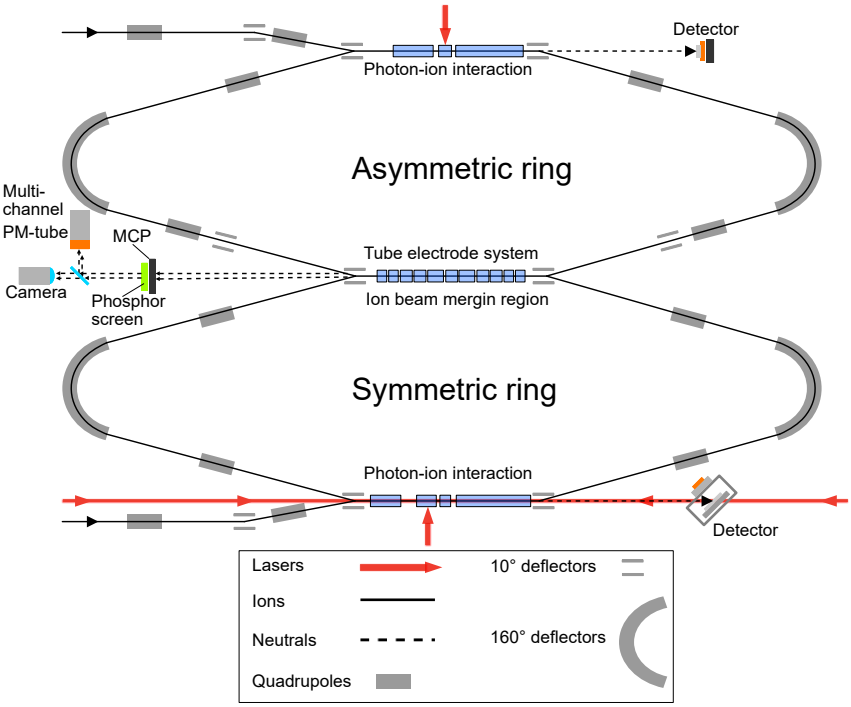

Figure 3.10: A schematic overview of the DESIREE storage rings. Here, some of the ion optics have been included as well as the detectors and the laser beam paths.

lifetimes, the ions have to be stored for several lifetimes[1]. Furthermore, lifetime studies of doubly excited metastable states can also be conducted by storing the ions. In these measurements, the produced ions will undergo an autodetachment process and decay to neutral atoms.

The advantage of using storage rings instead of ion traps when studying ions is the easy access to the ion beam, which improves the interaction time between ions and other particles or photons. Furthermore, the Doppler shift is well defined, the energies for collisions between ions and other particle are well controlled, and due to the geometry of the rings, it is possible to detect both charged and neutral particles from the studied interactions [171].

[1]At the DESIREE storage ring, ions have been stored for more than one hour [172].

All these conditions make it possible to conduct lifetime measurements of negative ions since these measurements require low background collisions due to the low population of excited states in some ions.

At DESIREE, the ions are produced in a cesium sputter source of type SNICS II [167] using the same technique which is used at GUNILLA. For a more detailed description of the ion beam production see Section 3.3.

After production, the ions are extracted and accelerated towards a 90° mass selection magnet where the ions of interest are selected and further guided into the DESIREE storage rings using ion optics. A number of Faraday cups placed strategically along the beamline can be used to monitor the ion beam current. In the experiments presented in this thesis only the symmetric ring is used for ion beam storage.

The ion beam current which is injected into the storage rings is kept as low as possible in order to minimize the ion-ion interactions in the beam since this would reduce the quality of the ion beam. A more detailed description of the facility can be found in [171, 45].

CHAPTER 4

EXPERIMENTS, RESULTS AND DISCUSSION

Negative ions can be studied in various ways, as discussed in Chapter 1. In this thesis, the electron affinities of different elements and isotopes, both stable and radioactive, have been studied, as well as the radiative lifetimes of excited states in a stable negative ion. Since both stable and radioactive isotopes have been studied, and due to the fact that radioactive isotopes have to be produced at radioactive isotope facilities, the experiments included in this thesis have been conducted at a number of different ion beam facilities: ISOLDE at CERN, GUNILLA at the University of Gothenburg and DESIREE at the University of Stockholm. An overview of these facilities is given in Chapter 3. This chapter includes brief introductions to the experiments described within this thesis as well as their corresponding results and discussions. In this chapter, the results from the experiments I have been involved in as a Ph.D student are presented and summarized in individual sections. The results are described in full detail in the appended papers.

4.1 Experimental Resolution

For the photodetachment measurements, which have been performed on both radioactive and stable ions, the geometry of the interaction between the ion beam and the laser beam has to be considered. The angle between the two beams can range from 0° to 180°, where the most commonly used are the 90° and the 0°/180°, often referred to as crossed and collinear beam geometries. In the crossed beam geometry, the resolution is relatively small compared to a collinear geometry but the volume of the ion beam and laser

beam can be precisely determined using the animated-crossed-beam technique which allows for absolute cross section measurements [173, 174]. In collinear geometries on the other hand, the interaction volume is evidently larger compared to the crossed geometry which results in high resolution, and this technique is typically used when measuring relative cross sections. In these measurements, a large Doppler shift will occur. The Doppler shift which occurs when the beam geometry is either parallel (ν_p) or anti-parallel (ν_a) can be described using the relativistic Doppler expression

$$\nu_{p,a} = \nu_0 \frac{1 \pm (v/c)}{\sqrt{1-(v/c)^2}}, \tag{4.1}$$

where ν_0 is the unshifted frequency, v is the velocity of the ions, and c denotes the speed of light. By measuring the photodetachment threshold in both co- and counter propagating laser and ion beam schemes the Doppler free threshold can be determined by calculating the geometrical mean value of the two respective thresholds ν_p and ν_a [175]. This gives

$$\sqrt{\nu_p \nu_a} = \sqrt{\frac{\nu_0(1+v/c)}{\sqrt{1-(v/c)^2}} \frac{\nu_0(1-v/c)}{\sqrt{1-(v/c)^2}}} = \sqrt{\nu_0 \nu_0} = \nu_0. \tag{4.2}$$

Another problem which arises in spectroscopy is the so-called Doppler broadening. This is due to the energy spread in the ion beam which arises from the non-zero temperature in the ion source as mentioned in Chapter 3.3. However, this can be reduced if the ions are accelerated over the same electrical potential, known as velocity compression [169]. Hence, due to velocity compression in the longitudinal plane, the Doppler broadening is reduced which results in a higher resolution.

Due to the divergence between the ion and laser beam when they are overlapped, the moving ions will observe different laser frequencies which in turn will give rise to an uncertainty in the photon frequency. The uncertainty of the frequency, $\Delta\nu$, can be written as

$$\Delta\nu = \nu_0 \left(1 - \frac{v}{c}\cos(\theta + \Delta\theta)\right) - \nu_0 \left(1 - \frac{v}{c}\cos(\theta)\right), \tag{4.3}$$

where the angle between the ions and laser beam is denoted by θ, the spread in the angle is $\Delta\theta$, and v and ν_0 correspond to the ion velocity and the laser frequency in the laboratory rest frame, respectively. For an experimental arrangement where the two beams are in a collinear geometry, where $\theta = 0$ and $\Delta\theta$ is small, the expression in Eq. 4.3 can be simplified to

$$\Delta\nu = \nu_0 \frac{v}{c}(-\cos\Delta\theta + 1) \approx \nu_0 \frac{v}{c}\left(-1 + \frac{(\Delta\theta)^2}{2} + 1\right) = \frac{v(\Delta\theta)^2}{2\lambda_0}. \tag{4.4}$$

If the ion and laser beams are perpendicular to each other, i.e. $\theta = \pi/2$, and using the small angle approximation, the expression for the uncertainty of the frequency can be simplified to

$$\begin{aligned}\Delta\nu &= -\nu_0\frac{v}{c}\cos(\pi/2+\Delta\theta) = -\nu_0\frac{v}{c}\cos(\pi/2)\cos(\Delta\theta) - \sin(\pi/2)\sin(\Delta\theta) \\ &\approx -\nu_0\frac{v}{c}\Delta\theta = \frac{v\Delta\theta}{\lambda_0}.\end{aligned} \tag{4.5}$$

Since Eq. 4.5 contains a linear term, a large difference in frequency uncertainty will arise when the angle deviates slightly from 90° (i.e. deviations smaller than 1°), this is not the case for the collinear geometry (where $\theta = 0$). Furthermore, due to the cosine dependence in the equations above, a small variation from an angle of 90° in a perpendicular ion/laser beam geometry will result in a larger Doppler broadening compared to small deviations from the interaction angle in a parallel ion/laser beam geometry.

In conclusion, it is more difficult to align the ion and laser beams collinerarly, but it is favorable due the large interaction volume which leads to a large signal sensitivity. Furthermore, the decrease in Doppler broadening will result in a high resolution.

4.2 Photodetachment of Radioactive Isotopes (Paper I and II)

The first photodetachment measurement of a radioactive negatively charged isotope (^{128}I) was performed in 2016 at the ISOLDE on-line facility using the GANDALPH spectrometer. This measurement was a significant milestone towards the measurement of the electron affinity of astatine which was measured a few years later using the same technique in a similar experimental arrangement.

The iodine isotopes were produced using a thorium/tantalum foil target and extracted with an energy of 20 keV. The ions were then mass selected and the ions of interest were guided towards the GANDALPH spectrometer, which was connected to the ISOLDE GLM beamline, where they were deflected into the interaction region. In the interaction region, the ion beam was overlapped with a laser beam generated with a tunable titanium:sapphire (Ti:Sa) laser with a repetition rate of 10 kHz and a bandwidth of 10 GHz [176], which is a part of the ISOLDE RILIS (Resonance Ionisation Laser Ion Source) laser system used in the production of positive ion beams at ISOLDE [177]. The maximum power of the laser beam

was measured to be 450 mW after the interaction region and the electron affinity was determined by measuring the photodetechment cross section in a co-propagating geometry and correcting for the Doppler shift.

Due to the outgoing electron being a *p*-electron, the photodetachment threshold is an *s*-wave threshold which results in a sharp onset. Unfortunately, due to time limitations, the photodetachment threshold could not be measured in both co- and counter ion/laser beam geometries, which would have allowed reduction of the Doppler shift to all orders. Instead, the ion beam velocity was determined by recording the data for the photodetachment threshold of $^{127}I^-$ and using its well-known EA to determine the ion beam energy. This procedure is explaind in detail in Paper I. This made it possible to determine the EA with sufficient precision to see it being in good agreement with the value determined by Peláez *et al.* [43]. This procedure lead to a higher uncertainty in the EA value which made it impossible to resolve the isotope shift. The electron affinity of the radioactive isotope ^{128}I ($t_{1/2} = 25$ min [178]) was determined to be 3.059 052(38) eV. The photodetachment cross section of $^{128}I^-$ can be seen in Figure 4.1. Here, the energy scale has been corrected for the Doppler shift using the calculated velocity. The photodetachment measurement of astatine was conducted using the upgraded version of the GANDALPH spectrometer (presented in Paper III). As astatine is a homologue to iodine, the outgoing electron will also give rise to a sharp onset due to the *s*-wave threshold. The astatine atoms were created in a target consisting of a Th/Ta composition, ionized by a ISOLDE-MK4 negative ion surface ion source [179] and further extracted and guided towards the GANDALPH spectrometer where the ions were overlapped with a laser beam with a power of 20-30 mW in the laser-ion beam interaction region. The laser setup used in the photodetachment experiment is a part of the ISOLDE RILIS laser system and consisted of a *Nd*:YAG InnoSlab laser with 10 kHz repetition rate where the third harmonic output was used to pump a commercial dye laser (Credo Dye, Sirah Laser-und Plasmatechnik GmbH) used with the dye Coumarin 503 in an ethanol solution. The laser beam was scanned in the region of 510 nm-514 nm based on theoretical prediction of the electron affinity value of astatine [180].

The measurement was performed in co- and counter propagating geometries and the geometrical mean of the two geometries was used to eliminate the effects caused by the Doppler shift. The electron affinity of ^{211}At was determined to be 2.415 78(7) eV. This value, together with the previously measured ionization potential [181], gave an electronegativity of ^{211}At of 5.87 eV. The limiting factors for a higher precision measurement

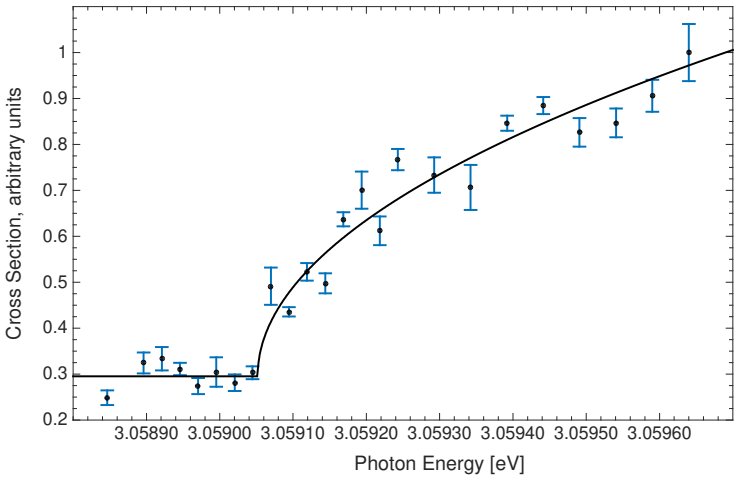

Figure 4.1: Normalized photodetachment cross section of $^{128}I^-$ as a function of laser photon energy. The error bars represent the statistical uncertainty (one sigma). The Wigner threshold law fit is represented by the solid black line. The energy scale has been corrected for the Doppler shift.

are dominated by the linewdith of the laser used in this experiment which was 12 GHz, corresponding to 50 μeV.

Several theoretical calculations of the electron affinity of astatine have been done throughout the years, but the calculated values have not been in agreement with each other [182, 183, 180, 184, 185]. Therefore, in addition to the experimental measurement made on astatine, the group of A. Borschevsky at the Van Swinderen Institute for Particle Physics and Gravity at the University of Groningen performed theoretical investigations of the electron affinities of astatine and iodine (^{127}I) using the computational software DIRAC15 program package [186]. The calculations were done by taking the contributions of quantum electrodynamics and the Breit correction, as well as higher order excitations, into account and implementing a coupled-cluster method which accounts for the electron correlation effects and the relativistic Coulomb interaction. This state-of-the-art relativistic quantum mechanical calculation yielded an electron affinity of astatine of 2.414(16) eV, which is in agreement with the experimentally determined value.

4.3 High Precision Measurements of the EA of Stable Isotopes (Paper IV and V)

The electron affinities of cesium and rubidium were determined using the RADAR spectrometer [170] at the GUNILLA beamline using a combination of LPTS and RIS.

The negatively charged cesium/rubidium ions were produced in the cesium sputter ion source at GUNILLA. The ions were extracted at an energy of 6 keV, mass selected and further guided into the RADAR spectrometer where the partial photodetachment cross section for Cs^- and Rb^- were investigated by exciting the negative ion into the $6p\ ^2P_{3/2}$ and $5p\ ^2P_{3/2}$ states of the neutral atoms, respectively. The neutral atoms were then further excited into the $25d\ ^2D_{5/2}$ Rydberg state for Cs and $37d\ ^2D_{5/2}$ Rydberg state for Rb, where they could be field ionized by the potential applied to the circular electrodes integrated in the beamline. It should be noted that for the Cs experiment eleven circular electrodes were used to create the potential gradient while for the Rb experiment only four were used. The diameter of the apertures in these plates were also increased from 3 mm to 6 mm for the Rb experiment. The reason why the beamline and the field ionizer was modified slightly between the two experiments was mainly due to issues with ion beam transmission, which was significantly smaller compared to the Cs experiment. Hence, in order to increase the transmission, a few of the circular electrodes were removed. This has no effect on the precision in the experiment, as the ionization process is only slightly shifted in position. The laser excitation schemes for Cs^- and Rb^- are shown in Figure 4.2 and Figure 4.3 respectively. Here, the photodetachment wavelength is denoted by λ_1 which originates from a tunable laser while λ_2 corresponds to photons set to a fixed wavelength. The field ionization process of the Rydberg atom is denoted by a black curved arrow in both figures.

Both a dye laser and an optical parametric oscillator (OPO) were used for these experiments. The dye laser, which was used for the photodetachment processes in the Cs and Rb experiments is a Sirah PrecisionScan dye laser, pumped by a 10 Hz pulsed Nd:YAG laser. For the Cs experiment, this was used with a solution of DCM dye in dimethyl sulfoxide (DMSO) and gave a pulse energy of about 1.7 mJ, while for the Rb experiment this was used with a Rhodamine B solution resulting in a pulse energy of about 0.5 mJ exiting RADAR. The resonance excitation step in the Cs experiment was done using an OPO of type MOPO:SL from the Quanta Ray

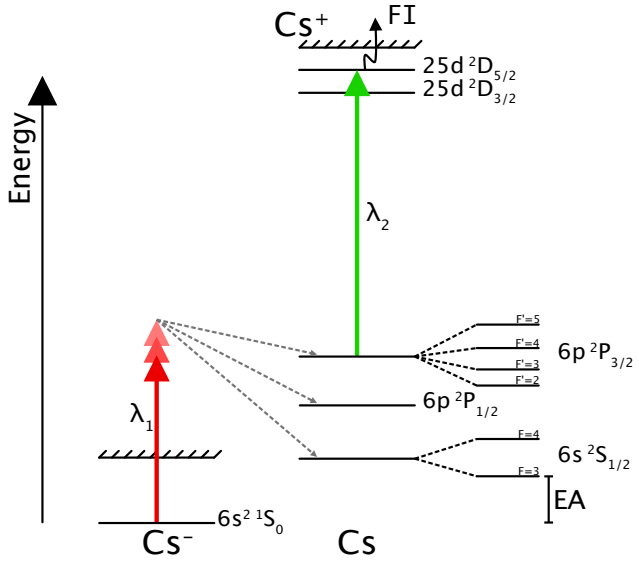

Figure 4.2: Partial energy level diagram (not to scale) for both negatively charged and neutral Cs. The negative ion absorbs a photon (λ_1) where the wavelength can be tuned (red arrows). The ion can decay into three different neutral states via electron emission (dashed arrows). The residual Cs atom in the $6p\ ^2P_{3/2}$ excited state then absorbs a photon (λ_2) at a fixed wavelength for resonant excitation to the Rydberg state, $25d\ ^2D_{5/2}$ (green arrow). Finally, the Rydberg atom undergoes the field ionization (F.I.) process (curved black arrow).

series by Spectra Physics, pumped by a Nd:YAG laser with a 10 Hz repetition rate. To reduce the power broadening effects and to minimize the background created by a two-step photodetachment/photoexcitation process from photons generated by the OPO, the pulse energy was limited to a value of 10 µJ. For the Rb experiment, this step was performed using a commercial OPO of type NT342C-10-SH/SF-WW manufactured by EKSPLA, pumped by a Nd:YAG laser with a repetition rate of 10 Hz, with a pulse energy of about 50 µJ measured after the RADAR spectrometer.

The timing between the two laser pulses was determined by maximizing the atomic population in the intermediate state and the data acquisition was triggered after the second laser pulse with respect to the particle time-of-flight from the interaction region in RADAR to the MCP detector. The measurements were performed in both co- and counter-propagating

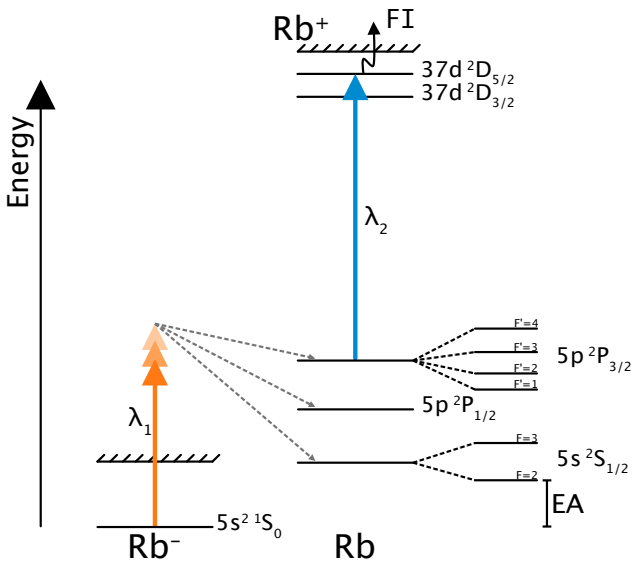

Figure 4.3: A partial energy level diagram (not to scale) for both negatively charged and neutral Rb. Here the photons corresponding to the photodetachment process (λ_1) and the resonant ionization (λ_2) are indicated by orange arrows and a blue arrow respectively. The negative Rb ion absorbs a photon, λ_1 and is photodetached and excited into the $5p\ ^2P_{3/2}$ state in the Rb atom. The residual atom in this state then absorbs a photon, λ_2, and is resonantly excited into the Rydberg state, $37d\ ^2D_{5/2}$. In the final step, this Rydberg atom is field ionized (F.I.), indicated by the black arrow in the figure.

geometries in order to allow reduction of the Doppler shift to all orders.

The threshold data obtained in the Cs experiment was fitted using the following equation

$$(\sigma \circledast g)(E_n) = \sigma(E_n) \sum_{E_m} g(E_n - E_m), \tag{4.6}$$

which is a discrete convolution between a Gaussian normalized function,

$$g(E_n - E_m) = \left(\frac{1}{\sigma_g \sqrt{2\pi}} \right) e^{-(E_n - E_m)^2/(2\sigma_g^2)}, \tag{4.7}$$

and the Wigner function

$$\sigma(E_{\mathrm{m}}) = \begin{cases} A + B\sum_{F}(2F+1)\times \\ \left(E_{\mathrm{m}} - \left(E_{\mathrm{Th}} + E_{\mathrm{hfs,F}}\right)\right)^{l+1/2} & \text{for } E_{\mathrm{m}} \geq (E_{\mathrm{Th}} + E_{\mathrm{hfs,F}}), \\ A & \text{for } E_{\mathrm{m}} < (E_{\mathrm{Th}} + E_{\mathrm{hfs,F}}). \end{cases} \tag{4.8}$$

Here, the photon energy is represented by E_m while E_{Th} and $E_{\mathrm{hfs,\,F}}$ are the photodetachment threshold energy and the energy corresponding to the hyperfine level, F, in the $6p\ ^2P_{3/2}$ state for Cs. The angular momentum is denoted by l, which in the case for both Cs and Rb is $l = 0$, A and B correspond to the background and the amplitude of the fit respectively. A representative graph of the obtained data from a co-propagation scheme in the Rb experiment is presented in Figure 4.4.

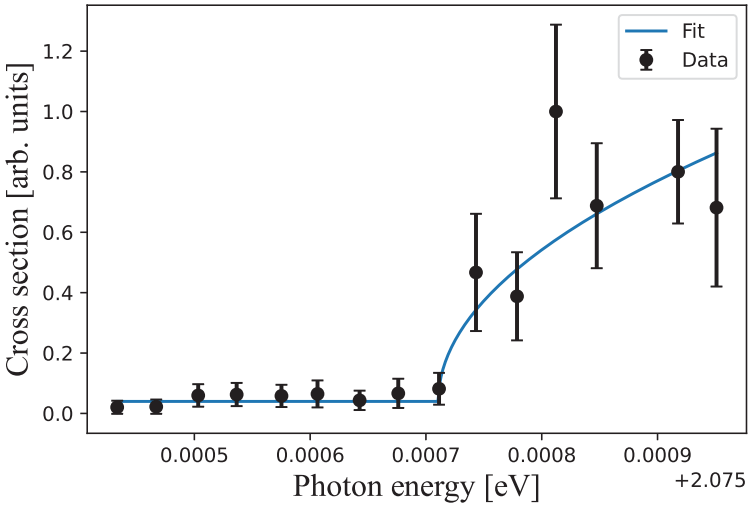

Figure 4.4: The photodetachment cross section measured in the Rb experiment as a function of the relative photon energy where the neutral Rb atom is excited to the $5p\ ^2P_{3/2}$ state. The data was obtained in a co-propagating geometry and fitted using Eq. 4.8. The fit is represented by a solid line.

Furthermore, the σ_g parameter describes the energy spread of the ions and the contribution of the linewidth of the laser responsible for the photodetachment processes and hence determines a limit to the experimental

resolution. The threshold data obtained in the Rb experiment was fitted using only the Wigner function in Eq. 4.8 and the hyperfine levels corresponding to the $5p\ ^2P_{3/2}$ state of Rb.

The geometrical mean of the co- and counter-propagating geometries were calculate to correct for the Doppler shift, i.e.

$$E_{\mathrm{Th}}^{\mathrm{Corr}} = \left(E_{\mathrm{Th}}\uparrow\uparrow \cdot E_{\mathrm{Th}}\uparrow\downarrow\right)^{1/2}. \tag{4.9}$$

The energy difference between the ground state of the neutral atoms and its corresponding excited state ($6P_{3/2}(F=2)$ for Cs and $5P_{3/2}(F=1)$ for Rb) was subtracted from the corrected $E_{\mathrm{Th}}^{\mathrm{Corr}}$ value. The electron affinity for Cs was determined to be EA(Cs)=$471.5987(6)$ meV which is in excellent agreement with previously measured values [187, 188, 32, 189] and an improvement of the previously most accurate value determined by Scheer *et al.* [189]. Furthermore, the electron affinity of Rb was determined to be EA(Rb)=$485.898(4)$ meV which is both an improvement and in agreement with the previous measurement [190].

The reason why the data obtained in the two experiments were fitted using different methods was that the linewidth of the laser could not be measured for the Rb experiment, and the near threshold statistics were not good enough to use the convolution method since this resulted in an unrealistic spread in the obtained fitting parameter corresponding to the linewidth. An estimation of the effect of the laser linewidth was instead done by investigating the shift between the convolution fit and pure Wigner fit using simulated data. This resulted in an average shift of $3(3)$ μeV which was compensated for in the final analysis and the uncertainty was added to the final uncertainty value. This, together with other systematical errors, is described in detail in Paper V.

In addition to the determination of the electron affinity of Rb, the lifetime of the excited $^2P_{3/2}$ state in the neutral Rb was measured. This was done by monitoring the detection of the yield of positive ions as a function of the delay time between the two laser pulses. When the time delay is set to be on the order of the lifetime, the excited atoms might decay to the ground state before they interact with λ_2. Hence, the lifetime of the state can be measured. To determine the lifetime from these measurements, an exponential function was used, which gave the decay constant corresponding to the lifetime of the state. The lifetime was determined to be 24.3(2.4) ns which is in good agreement with the previous measurement done by Theodosiou *et al.* [191]. Following this, it has been shown that this technique can be used to determine short lifetimes of excited states.

4.4 Radiative Lifetime Measurement of excited states in Rhodium (Paper VI)

Radiative lifetimes of excited states in the negative ion of rhodium were measured in a single ring experiment at the electrostatic storage ring facility DESIREE (Double ElectroStatic Ion-Ring ExpEriment). Rhodium anions were produced in a cesium sputter source and injected into the symmetric storage ring. Subsequently, the ion beam was overlapped with a laser beam a collinear geometry and the production of neutral atoms was measured as a function of storage time. First, the photon energy was set well above the detachment threshold for the respective states. The resulting data was fitted with one or more exponential functions depending on the measured the state. In that way, the ion beam storage time was determined to be $803(90)$ s. More details can be found in Paper VI. From previous experiments, the binding energies of the the $4d^8 5s^2\ ^3F_3$ and $4d^8 5s^2\ ^3F_2$ excited states were known [192, 189]. In addition to those, a highly mixed $^1D_2 + ^3P_2 + ^3F_2$ excited was observed for the first time. These states are indicated in Figure 4.5, which is a schematic figure of the energy levels of Rh^-. In addition to the measurements, theoretical calculations were carried out using either only the valence-valence (VV) correlation model or including core-valence correlation contributions (VV+CV). The $4d^8 5s^2\ ^3F_3$ and $4d^8 5s^2\ ^3F_2$ states were measured at the same photon energy yielding a double exponential function. In order to determine which lifetime corresponded to which state, theoretical calculations of the respective lifetimes had to be implemented. The lifetimes of the $^3F_3$ and $^3F_2$ states were determined to be $\tau = 3.22(33)$ s and $\tau = 21.3(20)$ s, respectively. The data obtained for these two states, along with the fits, is shown in Figure 4.6. The binding energy of the newly observed, highly mixed, bound state was determined to be < 0.62 eV and its lifetime was measured to be $\tau = 11.8(15)$ s. This does, however, not compare well with the theoretically calculated lifetime, which was found to be $\tau = 1.7(1)$ s. This difference could be due to the presence of a predicted unbound mixed state, in the continuum. The theoretically calculated energy of this state is 1037 meV (VV) or 1107 meV (VV+CV) above the ground state in the negative ion, depending on the theoretical model used for the calculation. Furthermore, an autodetaching state was observed for the first time where the measured lifetime was shown to be $\tau = 318(20)$ µs.

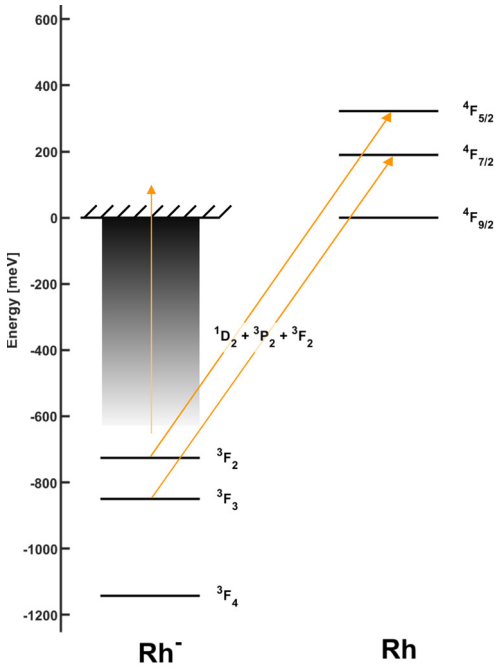

Figure 4.5: Energy level diagram of Rh^-.

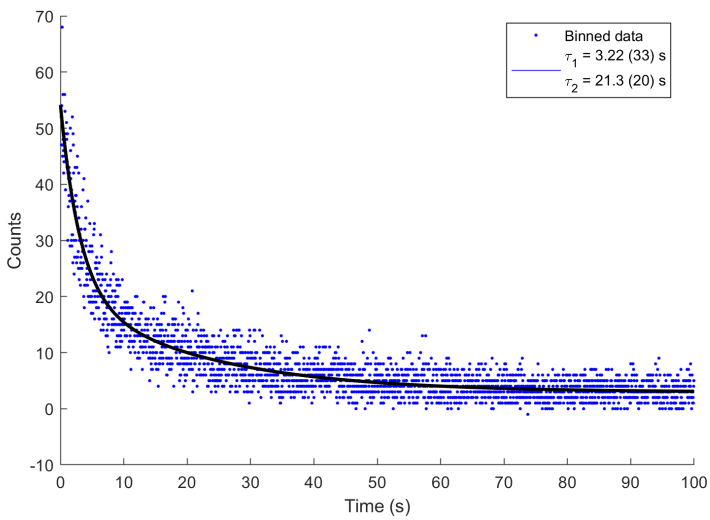

Figure 4.6: Lifetimes of the $^2F_3$ and $^3F_3$ states in Rh^-.

4.5 Molecular dissosciation study on CO^+ (Paper VII)

In order to extend the number of isotopes and molecules available for experiments at the ISOLDE facility, it is of interest to study processes that take place inside the RFQcb when molecular ions are injected and cooled. The initial intention of the RFQcb is to cool and also, if wanted, bunch the ions, however molecules injected into the device may also dissociate via collisional impact with the buffer gas. The interest in molecular dissociation is also related to medical applications, for example within CERN-MEDICIS and the MEDICIS-Promed project, where ^{11}C is studied as a possible treatment ion for hadron therapy [106]. Since carbon monoxide is more volatile compared to atomic carbon, the carbon is extracted from the target material in molecular form which has, in previous work at ISOLDE, shown to give higher yields [193]. This means that the molecules have to be dissociated before they can be used for medical purposes since it is the atomic ion that is used in the medical applications.

To investigate this, ion beams of both CO^+ or N_2^+ molecules were produced at ISOLDE in order to investigate whether collision-induced dissociation processes occur inside the RFQcb, ISCOOL, at ISOLDE. The molecules were produced by injecting either carbon monoxide (CO) or diatomic nitrogen (N_2) gas into a standard FEBIAD target-ion source [155] which was installed on the HRS Front-End. The mass separated molecular beams were then injected into the RFQcb, ISCOOL, where they were decelerated to about $200\,\text{eV}$ before they interacted with the buffer gas inside the apparatus. After the cooling process, the ions were re-accelerated to the initial energy of $40\,\text{keV}$.

For this experiment, two buffer gases were used separately, either helium or a mixture of helium and neon (90:10), in order to alter the center-of-mass energy in the collisions between the molecules and the atoms in the buffer gas and to determine the change in dissociation rate between the change of condition. The center of mass energy for head-on collisions when CO^+ and N_2^+ molecules with an energy of $200\,\text{eV}$, collide with He is around $25\,\text{eV}$, and when colliding with Ne, the center of mass energy is increased to $83\,\text{eV}$, which is above the dissociation energies for both molecules [194, 195].

ISCOOL was operated in bunched mode throughout the test and the buffer gas pressure inside ISCOOL was adjusted to give the best ion transmission in the mass region of interest before starting the measurement and it was thereafter held constant.

Since the intention was to cool down the molecules completely before

extracting them, the RFQcb was filled with ions in 20 µs-5 ms pulses and at a repetition rate of 5 Hz. The cooling time was set to 5 ms throughout the test.

The radio-frequency (RF) field applied to the RFQcb will determine which mass will pass through the apparatus and thus be extracted. In order to investigate the mass regions of interest (CO/N_2 to C), the RF field was altered between 680 kHz and 780 kHz, in steps of 10 kHz. However, scanning from 680 kHz means that the frequency corresponding to atomic mass 28 was not fully reached. The reason for this was that the total beam of this mass would completely saturate the detector since the detector was in a single ion counting mode. As a result, the peak corresponding to mass 28 in the obtained mass spectra is much lower than the actual signal.

The ToF detector assembly, described briefly in Section 3.2.5 and in detail in Paper VIII, was mounted on an extractable mount in the ISOLDE central beamline, approximately 10 meters downstream the RFQcb extraction point, as illustrated in Figure 3.5. The signal from the MCP detector was fed into a LeCroy Waverunner 1 GHz 20 GS/s oscilloscope which performed the electronic read out and digitization. The oscilloscope had been programmed to count the secondary electrons and sum them into a histogram of Time-of-Flight where t_0 was the release from ISCOOL and t_x was the time it took for the ions to reach the detector.

The mass scale was calibrated by measuring the flight times of ions with known m/q. The obtained data points were then fitted to Eq. 3.6 and the leading edge of the full width at half maximum (FWHM) was used as the reference point. For this investigation, the atomic mass 8, 16 and 28, corresponding to carbon (C), oxygen (O) and carbon monoxide (CO), were used as reference masses. Figure 4.7 shows an envelopes of one of the mass scans when injecting CO^+ and N_2^+ into ISCOOL. Note that the radio-frequency applied to the RFQcb was not scanned all the way to match mass 28, i.e. that of CO^+, since the signal from the primary beam then would saturate the detector. Hence, the height of the peak at mass 28 appears much lower than the actual signal.

The foremost result of the experiment is that the rate of the dissociation of the molecules inside ISCOOL is extremely low. The primary injected beams dominate the fragments extracted from the RFQcb. However, it is possible to observe a small molecular dissociation within the RFQcb containing either pure helium buffer gas or a mixture of helium and neon (90:10). The ratios vary depending on molecule and RFQcb operation mode and the detected dissociation signal of CO^+ is larger than for N_2^+. The result might seem somewhat surprising at first, since the col-

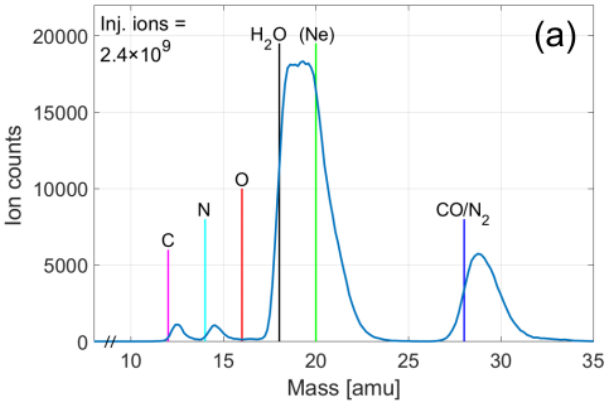

Figure 4.7: A graphs showing the envelope of a mass scan when injecting molecular beams of CO^+ into He. The vertical lines indicate to the masses of C^+, N^+, O^+, H_2O^+, Ne^+ and CO^+/N_2^+ with respect to the leading edge of the envelopes. The number of ions injected the scan is noted in the upper left corner of the graph. Note that the frequency was not scanned to match mass 28, hence, the height of this peak appears much lower than the actual signal.

lisional energies between the molecules and the buffer gas are well above the dissociation energies of both molecules. However, the main reason for a dissociation to occur will be an electronic excitation of the molecular ion to an anti-bonding state where it then dissociates. Moreover, the maximum center of mass collision energy will only be acquired in head-on collisions which will only be the case for a small fraction of the collisions, since the majority of the ions will undergo multiple, non head-on collisions where they gradually lose energy when they enter the RFQcb, such that the energy is eventually so low that they cannot dissociate. From this, it can be presumed that the dissociation process will only take place at or near the entrance of the RFQcb.

The results show that dissociation of CO^+ inside ISCOOL is not a very efficient way to produce C^+, since only a small fraction of the injected ions will dissociate. However, the investigation shows that it may be possible to use the RFQcb to cool and bunch molecules with only very small losses. A possible application may be within the MEDICIS-Promed project where possible schemes of injecting radioactive ion beams into a synchrotron-based medical accelerator have been investigated [196].

CHAPTER 5

CONCLUSION AND OUTLOOK

The work included in this thesis can be divided into an experimental part and a technical part. The experimental part includes electron affinity measurements, lifetime measurements of excited states in negative ions and molecular dissociation inside the RFQcb, ISCOOL. The technical part, on the other hand, includes the design, commissioning and testing of the Offline 2 ion beam facility, the upgrade of the experimental spectrometer GANDALPH and building and a testing of a time-of-flight detector.

A major result of my thesis work is the first ever determination of electron affinities of short-lived radioisotopes using the GANDALPH spectrometer. This opens up the field of negative ion research to a new area of the periodic table, such as actinides and heavy elements. The commissioning of GANDALPH was performed along with the first experiment of photodetachment spectroscopy of a radioactive negative ion. This work is described in Paper I where the electron affinity of $^{128}I^-$ was successfully measured and determined to be $3.059\,052(38)$ eV. With this milestone reached and some further upgrades to GANDALPH (described in Paper III), the first unknown photodetachment threshold of the radioactive anion, astatine, could be measured. The EA was experimentally determined to be $2.415\,78(7)$ eV (Paper II). Within this work, relativistic quantum mechanical calculations were performed to theoretically determine the electron affinity of astatine. This yielded an electron affinity of $2.414(16)$ eV, which is in excellent agreement with the experimentally determined value. Astatine is of great interest in the field of Targeted Alpha Therapy (TAT) [68, 70], where the isotope ^{211}At is a good candidate due to its half-life of 7.2 h, as well as the fact that it decays into a non-toxic and non radioactive isotope by emitting an α-particle with a suitable kinetic energy of 6.0 - 7.5

MeV [69]. The value of the electron affinity combined with the previously determined ionization potential [1] yields the electronegativity of the element. This is a key number to describe an elements chemical property which is of importance in quantum chemical computations performed to find a suitable biochemical process to attach ^{211}At to an antibody.

By combining laser photodetachment threshold spectroscopy with resonance ionization, we have demonstrated a state-selective technique which enables high precision measurements of EAs of the alkali metals and other elements detaching with a *p*-wave. As a proof of principle the electron affinities of cesium and rubidium were measured with an accuracy of a few μeV. The EA of Cs was determined to be $471.5987(6)$ meV, which is in excellent agreement with previously measured values [187, 188, 189, 31], while the electron affinity of Rb was determined to be $485.898(4)$ meV which is also in excellent agreement with previous measurements [190]. Furthermore, the lifetime of the excited $^2P_{3/2}$ in Rb atom was determined to be 24.3(2.4) ns, which is in good agreement with the tabulated value presented by Theodosiou *et al.* [191]. This gives not only a good indication that the excited state of interest was reached but also that this technique can be used to determine short lifetimes of excited states.

At DESIREE, the radiative lifetimes of the excited states, $^3F_3$, $^3F_2$ and the mixed $^1D_2 +^3 P_2 +^3 F_2$ state in Rh^- were determined to be $3.22(33)$ s, $21.3(20)$ s and $11.8(15)$ s, respectively. While the $^3F_3$, $^3F_2$ excited states were observed previously, the highly mixed state and an additional autodetaching state with a lifetime of $318(20)$ μs were observed for the first time. The binding energy of the bound mixed state was found to be < 0.62 eV. The lifetimes of the two lowest lying states were in excellent agreement with the theoretical calculations. The energy of the highest lying state (the $^1D_2 +^3 P_2 +^3 F_2$ state) showed some discrepancy with theory, which may be due to the presence of another unbound state which has been theoretically predicted.

The possibility of molecular dissociation of CO^+ and N_2^+ within the RFQcb, ISCOOL, has been investigated within the framework of this thesis. By using a new ToF detector (described in Paper VII) and observing the time-of-flight spectra of the cooled molecules extracted from the RFQcb, which contained either pure helium buffer gas or a gas mixture of helium and neon (90:10), one can see that a small fraction of the molecules did undergo dissociation. However, the fraction is orders of magnitude smaller compared to the fraction that remained in molecular form. Our results showed that injecting these molecules into ISCOOL is not a very efficient way of producing ion beams of only atomic ions, but on the other hand, the results indicate that the RFQcb can be used where the experimental

requirements are to cool and bunch ions in molecular form. It could be of interest to investigate dissociation processes of other ions with lower dissociation thresholds where the production of the constituent atomic ion is not available in sufficient quantities. It could also be of interest to investigate other buffer gases with heavier masses to investigate different impact energies.

The Offline 2 facility, described in Paper IX and X is a new, non-radioactive laboratory at ISOLDE, CERN. This facility has been designed to mimic the production of radioactive isotopes at the ISOLDE on-line facility and will serve as a test facility where developments of, for example, new target-ion sources, ion beam manipulation techniques and hardware can be performed. In addition to the mass separator, a dedicated laser room has been installed in the facility which will enable a range of technical developments, such as extending the wavelength coverage of the existing tunable solid-state titanium:sapphire lasers through stimulated Raman scattering in diamond [197, 198]. The first ion source campaigns benefitting from the completed Offline 2 infrastructure are the LIST (Laser Ion Source and Trap) [199, 200] and PI-LIST (Perpendicularly Illuminated Laser Ion Source and Trap) [201] development programmes. These ion sources allow for production of high purity ion beams of exotic isotopes and laser spectroscopy with isobaric selection. The improvements developed at Offline 2 can be implemented at the ISOLDE on-line facility without having to interfere with the on-going research.

The results and developed tools presented in this thesis provide new insights into anions and broaden the research field for future investigations of negative ions. The experiments on radioisotopes at ISOLDE mark a major milestone by allowing investigations of short-lived negative ions. While the EA of ^{128}I is the first ever measured EA of a radioisotope, the measurement of astatine represents a milestone not only towards investigations of heavy and super heavy elements but also is of high relevance for the use of astatine in TAT. As a next step, the measurement of the EA of polonium is planned [202], as well as the isotope shift in chlorine, where the isotope shift for the stable isotopes, ^{35}Cl and ^{37}Cl, already has been experimentally determined [203] but with low precision. The interest in the isotopic shift in negative ions results from the dominance of electron correlation effects in the specific mass shift, which is an indispensable ingredient when e.g. extracting nuclear charge radii or electric and magnetic multipole moments from isotope shift measurements [204, 205, 206, 207, 208, 209]. A proposal [210] has already been approved for beam time at the ISOLDE facility and is expected to take place in the fall of 2023. Another large interest for negative ions at CERN is within the antiProton Unstable Matter Annihilation

(PUMA) experiment [83]. Here, heavy elements with negative charge will be trapped together with antiprotons, and the annihilation products will then be detected.

By combining the measurement technique used when determining the EA of Cs and Rb, i.e. laser photodetachment spectroscopy and resonant ionization, with the radioactive beam technique applied for the studies of ^{128}I and ^{211}At, the EA of francium will be determined. The production yield of positive Fr ions at ISOLDE is quite high due to the low ionization potential of Fr [211]. However, in order to create negatively charged Fr ions, one would have to use a charge exchange cell [212]. Francium is the heaviest alkali metal and its EA is currently unknown, but theoretically predicted to be 0.491(5) eV [213]. Completing this measurement would complete the EA measurements of the alkali metal group, leading to a better understanding of electron correlation and relativistic effects of heavy elements. Furthermore, this method will be employed for elements of other groups where a three level excitation laser scheme will be necessary, due to high ionization potentials.

Furthermore, the mapping of the lifetimes of different elements will be expanded. Of particular interest here are lanthanum and thorium, both elements which are highly relevant for laser cooling of negative ions. There are also plans to measure the electron affinity of the three naturally occurring isotopes of silicon. This will be performed using the same technique as utilized to determine the electron affinity of ^{16}O and ^{18}O [44], which is, until this day, the most accurate measurement of the electron affinity as well as the isotope shift in a negative ion. In addition to this, the hyperfine structure of silicon will also be investigated.

In conclusion, the work performed in this thesis contributes to the field of negative ion research both with technical developments and newly determined and high precision measurements of fundamental properties of negative ions. This is of interest, for theoretical studies of negative ions since they provide important and valuable information regarding electron correlation. In addition, this also provides valuable information for other research areas such as plasma physics [66], medicine [68] and chemistry [2] where negative ions are used.

ACKNOWLEDGEMENTS

There are many people who have contributed in different ways and made it possible for me to finish my doctoral studies and write this thesis. I would like to thank all of you but then this section would be way too long. However, there are some people I would like to thank in particular:

- My supervisor Professor Dag Hanstorp, who gave me the opportunity to be a part of the negative ion group at the department of physics at the University of Gothenburg. He is one of the most positive and understanding persons I have ever met. He has always taken the time to answer my questions and given me good advice, no matter how busy his own schedule has been. His inspiration, deep knowledge, expertise in physics and support and patience have made it possible for me to finally complete my thesis.

- My examiner Raimund Feifel for all the support throughout my PhD studies and the rest of the department of physics at the University of Gothenburg.

- The ISOLDE and RILIS teams, especially Sebastian Rothe who helped a lot during my time at CERN and also Jochen, Bernard, Ermano, Andrés and Richard.

- Friends and office mates at ISOLDE, Bea, Carlos, Nhat-Tan, Yisel and Ferran for much support, many great laughs and all the ”smoking” breaks.

- Ludi for all the help and assistance in the lab and all the interesting physics and cooking discussions.

- Richard, for not only proof reading this thesis and helping me improve my writing but also for being a very good friend.
- Remi for valuable corrections and comments on my thesis and for many nice discussions during the coffee breaks.
- Mats and Jan-Åke for all the help and support with everything from LabVIEW and electronics to drilling holes.
- A huge thanks to David, who not only brought GANDALPH back from the Balrog and made him into the white wizard but also helped a lot with most of my work. You're a great colleague and a very good friend.
- Miranda, my dear friend and colleague, thank you for all the assistance, the pep talks and support and also for bringing amazing coffee to the office.
- My class mate, Julia who became my colleague and very good friend. Thank you for many great and successful working hours together and for all the good laughs (and for the coffee and "nabaner" breaks of course).
- Jakob for always being willing to discuss and answer questions and never saying no to a coffee. Also, thank you for all the fun classes I got to teach and for the template for this thesis.
- Jessica for all the assistance in the lab and many great discussions. You are a true "funkel".
- My dear Gothenburg and Stockholm colleagues and friends, especially Moa, Yaz, Javier, José, Andreas, Sebastian and everyone else in the group and on the 8th floor.
- Thanks to my great friends outside of work, especially Viktoria, Sara, Johanna, Lisa, Hirepan and Afshin. You've kept me sane during all these years. And a special, warm thank you to Jenny for all the support and love throughout the years.
- A big warm thank you to my mom, dad, brothers and sister and the rest of my family as well. Thank you for all your love and support. And I cannot forget Kevin, my forever puppy, whom came into our lives like a little tornado of happiness. Thank you for always making my days brighter.

- Finally, I would like to thank Ida who came into my life at a very stressful time, better known as the final time of a PhD. Thank you for your support and for making me laugh, for wanting to discuss physics and other science related things, and for being understanding even at times when I wasn't myself. Jag älskar Dig.

Annie Ringvall Moberg
Göteborg
29th March, 2023

BIBLIOGRAPHY

[1] Sebastian Rothe et al. "Laser photodetachment of radioactive 128 I – Laser photodetachment of radioactive". In: *Journal of Physics G: Nuclear and Particle Physics* 44.10 (2017), p. 104003. DOI: 10.1088/1361-6471/aa80aa.

[2] David Leimbach et al. "The electron affinity of astatine". In: *Nature Communications* 11.1 (2020), pp. 1–9. DOI: 10.1038/s41467-020-17599-2.

[3] D. Leimbach et al. "Upgrades of the GANDALPH photodetachment detector towards the determination of the electron affinity of astatine". In: *Nuclear Instruments and Methods in Physics Research, Section B: Beam Interactions with Materials and Atoms* 463 (Jan. 2020), pp. 277–279. DOI: 10.1016/j.nimb.2019.05.015.

[4] José E Navarro Navarrete et al. "A high-resolution measurement of the electron affinity of cesium". In: *Submitted to Physical Review A* (2023).

[5] Annie Ringvall-Moberg et al. "The electron affinity of rubidium: A state selective measurement". In: *In preparation* (2023).

[6] J. Karls et al. "Lifetimes of excited states in Rh-". In: *In preparation* (2023).

[7] A. Ringvall Moberg et al. "Time-of-Flight study of molecular beams extracted from the ISOLDE RFQ cooler and buncher". In: *Nuclear Instruments and Methods in Physics Research, Section B: Beam Interactions with Materials and Atoms* 463 (2020), pp. 522–524. DOI: 10.1016/j.nimb.2019.03.014.

[8] S. Warren et al. "A new fast time of flight detector for single ion counting to high flux radioactive beams at ISOLDE". In: *Review of Scientific Instruments* 90.10 (2019), p. 103313. DOI: 10.1063/1.5122715.

[9] Annie Ringvall et al. "The Offline 2 facility at ISOLDE, CERN". In: (2022). DOI: 10.17181/CERN-OPEN-2022-015.

[10] S. Warren et al. "Offline 2, ISOLDE's target, laser and beams development facility". In: *Nuclear Instruments and Methods in Physics Research, Section B: Beam Interactions with Materials and Atoms* 463 (2020), pp. 115–118. DOI: 10.1016/j.nimb.2019.07.016.

[11] J. Ballof et al. "A concept for the extraction of the most refractory elements at CERN-ISOLDE as carbonyl complex ions". In: *European Physical Journal A* 58.5 (2022), pp. 1–18. DOI: 10.1140/epja/s10050-022-00739-1.

[12] Vadim Maratovich Gadelshin et al. "First laser ions at the CERN-MEDICIS facility". In: *Hyperfine Interactions* 241.1 (2020). DOI: 10.1007/s10751-020-01718-y.

[13] B. Pullman. *The atom in the history of human thought*. Oxford University Press, USA, 2001, pp. 31–33.

[14] The Nobel Prize in Physics 1906. *NobelPrize.org. Nobel Prize Outreach AB, cited 2021-08-27*. DOI: https://www.nobelprize.org/prizes/physics/1906/summary/.

[15] J J. Thomson M.A. F.R.S. "XL. Cathode Rays". In: *The London, Edinburgh, and Dublin Philosophical Magazine and Journal of Science* 44.269 (1897), pp. 293–316. DOI: 10.1080/14786449708621070.

[16] J J. Thomson F.R.S. "On the structure of the atom: aninvestigation of the stability and periods of oscillation of a number of corpuscles arranged at equalintervals around the circumference of a circle; with application of the results to the theory of atomicstructure". In: *The London, Edinburgh, and Dublin Philosophical Magazine and Journal of Science* 7.39 (1904), pp. 237–265. DOI: 10.1080/14786440409463107.

[17] Professor E. Rutherford F.R.S. "LXXIX. The scattering of α and β particles by matter and the structure of the atom". In: *The London, Edinburgh, and Dublin Philosophical Magazine and Journal of Science* 21.125 (1911), pp. 669–688. DOI: 10.1080/14786440508637080.

[18] N. Bohr. "I. On the constitution of atoms and molecules". In: *The London, Edinburgh, and Dublin Philosophical Magazine and J. Sc* 26.151 (1913), pp. 1–25. DOI: 10.1080/14786441308634955.

[19] N. Bohr. "XXXVII. On the constitution of atoms and molecules". In: *The London, Edinburgh, and Dublin Philosophical Magazine and Journal of Science* 26.153 (1913), pp. 476–502. DOI: 10.1080/14786441308634993.

[20] N. Bohr. "LXXIII. On the constitution of atoms and molecules". In: *The London, Edinburgh, and Dublin Philosophical Magazine and Journal of Science* 26.155 (1913), pp. 857–875. DOI: 10.1080/14786441308635031.

[21] Albert Einstein. "Über einen die Erzeugung und Verwandlung des Lichtes betreffenden heuristischen Gesichtspunkt". In: *Annalen der Physik* 322 (1905), pp. 132–148. DOI: 10.1002/andp.19053220607.

[22] E. Schrödinger. "An undulatory theory of the mechanics of atoms and molecules". In: *Physical Review* 28.6 (1926), pp. 1049–1070. DOI: 10.1103/PhysRev.28.1049.

[23] Paul Adrien Maurice Dirac and Ralph Howard Fowler. "The quantum theory of the electron". In: *Proceedings of the Royal Society of London. Series A, Containing Papers of a Mathematical and Physical Character* 117.778 (1928), pp. 610–624. DOI: 10.1098/rspa.1928.0023.

[24] Wolfgang Demtröder. *Atoms, Molecules and Photons An Introduction to Atomic-, Molecular- and Quantum*. Springe, 2010.

[25] J J. Thomson. "Bakerian Lecture: Rays of positive electricity". In: *Proceedings of the Royal Society A: Mathematical, Physical and Engineering Sciences* 89.607 (1913), pp. 1–20. DOI: 10.1098/rspa.1913.0057.

[26] Rupert Wildt. "Negative Ions Oe Hydrogen and the Opacity". In: *Astrophysical Journal* 89 (1939), pp. 295–301. DOI: 10.1086/144048.

[27] Thomas J. Millar, Catherine Walsh, and Thomas A. Field. "Negative ions in space". In: *Chemical Reviews* 117.3 (2017), pp. 1765–1795. DOI: 10.1021/acs.chemrev.6b00480.

[28] Lewis M. Branscomb and Stephen J. Smith. "Experimental Cross Section for Photodetachment of Electrons from H – and D –". In: *Physical Review* 98.4 (May 1955), pp. 1028–1034. DOI: 10.1103/PhysRev.98.1028.

[29] Lewis M. Branscomb et al. "Photodetachment Cross Section and the Electron Affinity of Atomic Oxygen". In: *Physical Review* 111.2 (July 1958), pp. 504–513. DOI: 10.1103/PhysRev.111.504.

[30] D. R. Hartree and W Hartree. "Self-Consistent Field, with Exchange, for Beryllium". In: *Proceedings of the Royal Society of London. Series A - Mathematical and Physical Sciences* 150.869 (1935), pp. 9–33. DOI: 10.1098/rspa.1935.0085.

[31] H. Hotop and W. C. Lineberger. "Binding Energies in Atomic Negative Ions". In: 14.3 (1975), pp. 539–5769. DOI: 10.1063/1.555524.

[32] H. Hotop and W. C. Lineberger. "Binding Energies in Atomic Negative Ions: II". In: *Journal of Physical and Chemical Reference Data* 14.3 (July 1985), pp. 731–750. DOI: 10.1063/1.555735.

[33] T Andersen et al. "Binding Energies in Atomic Negative Ions : III". In: 28.6 (1999), pp. 1511–1533. DOI: 10.1063/1.556047.

[34] Chuangang Ning and Yuzhu Lu. "Electron Affinities of Atoms and Structures of Atomic Negative Ions". In: *Journal of Physical and Chemical Reference Data* 51.2 (2022). DOI: 10.1063/5.0080243.

[35] H. S.W. Massey. "Negative ions". In: *Adv. at. mol. phys.* 15.C (Jan. 1979), pp. 1–36. DOI: 10.1016/S0065-2199(08)60293-6.

[36] David J Pegg. "Structure and dynamics of negative ions". In: *Reports on Progress in Physics* 67.6 (June 2004), pp. 857–905. DOI: 10.1088/0034-4885/67/6/R02.

[37] T. Andersen. "Atomic negative ions: structure, dynamics and collisions". In: *Physics Reports* 394.4-5 (May 2004), pp. 157–313. DOI: 10.1016/J.PHYSREP.2004.01.001.

[38] J. Cooper and R. N. Zare. *Angular distribution of photoelectrons*. Jan. 1968. DOI: 10.1063/1.1668742.

[39] D. Hanstorp, C. Bengtsson, and D. J. Larson. "Angular distributions in photodetachment from O-". In: *Physical Review A* 40.2 (1989), pp. 670–675. DOI: 10.1103/PhysRevA.40.670.

[40] Mikael Eklund et al. "Tomography of photoelectron distributions produced through strong-field photodetachment of Ag". In: *Physical Review A* 102.2 (2020). DOI: 10.1103/PhysRevA.102.023114.

[41] Christophe Blondel, Christian Delsart, and François Dulieu. "The photodetachment microscope". In: *Physical Review Letters* 77.18 (Oct. 1996), pp. 3755–3758. DOI: 10.1103/PhysRevLett.77.3755.

[42] W. Chaibi et al. "Effect of a magnetic field in photodetachment microscopy". In: *European Physical Journal D* 58.1 (2010), pp. 29–37. DOI: 10.1140/epjd/e2010-00086-7.

[43] R. J. Peláez et al. "Pulsed photodetachment microscopy and the electron affinity of iodine". In: *Journal of Physics B: Atomic, Molecular and Optical Physics* 42.12 (2009), p. 7. DOI: 10.1088/0953-4075/42/12/125001.

[44] Moa K. Kristiansson et al. "High-precision electron affinity of oxygen". In: *Nature Communications* 13.1 (2022). DOI: 10.1038/s41467-022-33438-y.

[45] H T Schmidt et al. "First storage of ion beams in the Double Electrostatic Ion-Ring Experiment: DESIREE". In: *Review of Scientific Instruments* 84.5 (2013), p. 55115. DOI: 10.1063/1.4807702.

[46] D. M. Pendergrast and J. N. Yukich. "Observed Landau structure in photodetachment from trapped [Formula Presented]". In: *Physical Review A - Atomic, Molecular, and Optical Physics* 67.6 (2003), p. 5. DOI: 10.1103/PhysRevA.67.062721.

[47] James E. Wells and J. N. Yukich. "Photodetachment spectroscopy from the lowest threshold of S". In: *Physical Review A - Atomic, Molecular, and Optical Physics* 80.5 (2009), pp. 1–4. DOI: 10.1103/PhysRevA.80.055403.

[48] Anne Joiner, Robert H. Mohr, and J. N. Yukich. "High-resolution photodetachment spectroscopy from the lowest threshold of O-". In: *Physical Review A - Atomic, Molecular, and Optical Physics* 83.3 (2011), pp. 2–5. DOI: 10.1103/PhysRevA.83.035401.

[49] Y Nakano et al. "A cryogenic electrostatic storage ring project at RIKEN". In: *Journal of Physics: Conference Series*. Vol. 388. PART 14. Nov. 2012, p. 142027. DOI: 10.1088/1742-6596/388/14/142027.

[50] R. Von Hahn et al. "The cryogenic storage ring CSR". In: *Review of Scientific Instruments* 87.6 (June 2016), p. 063115. DOI: 10.1063/1.4953888.

[51] K. C. Chartkunchand et al. "Measuring the 2D3/2 Ni- excited state lifetime in DESIREE". In: *J. Phys.: Conference Series* 635.9 (2015), pp. 9–10. DOI: 10.1088/1742-6596/635/9/092142.

[52] D. Müll et al. "Metastable states of Si- observed in a cryogenic storage ring". In: *Physical Review A* 104.3 (2021), pp. 1–13. DOI: 10.1103/PhysRevA.104.032811.

[53] Pradip K. Ghosh. *Ion traps*. Oxford: Clarendon Press, 1995.

[54] John N. Yukich, Tobias Kramer, and Christian Bracher. "Observed photodetachment in parallel electric and magnetic fields". In: *Physical Review A - Atomic, Molecular, and Optical Physics* 68.3 (2003), p. 8. DOI: 10.1103/PhysRevA.68.033412.

[55] R. Catherall et al. "The ISOLDE facility". In: *Journal of Physics G: Nuclear and Particle Physics* 44.9 (2017). DOI: 10.1088/1361-6471/aa7eba.

[56] G. C. Ball et al. "Physics with reaccelerated radioactive beams at TRIUMF-ISAC". In: *J. Phys. G: Nucl. Part. Phys.* 38.2 (2011). DOI: 10.1088/0954-3899/38/2/024003.

[57] T. Suda. "Present status of the RIKEN Radioactive Ion Beam Factory, RIBF". In: *Journal of Physics: Conference Series* 267.1 (2011). DOI: 10.1088/1742-6596/267/1/012008.

[58] T. Kubo et al. "BigRIPS in-flight separator at RIKEN RI beam factory (RIBF)". In: *AIP Conference Proceedings* 1224.May (2010), pp. 492–498. DOI: 10.1063/1.3431457.

[59] I D Moore et al. "The IGISOL technique-three decades of developments". In: *Hyperfine Interact* 223 (2014), pp. 17–62. DOI: 10.1007/s10751-013-0871-0.

[60] H. Geissel et al. "The Super-FRS project at GSI". In: *Nuclear Instruments and Methods in Physics Research, Section B: Beam Interactions with Materials and Atoms* 204 (2003), pp. 71–85. DOI: 10.1016/S0168-583X(02)01893-1.

[61] Rulin Tang et al. "Candidate for Laser Cooling of a Negative Ion: High-Resolution Photoelectron Imaging of Th –". In: *Phys. Rev. Lett.* 123.20 (Nov. 2019), p. 203002. DOI: 10.1103/PhysRevLett.123.203002.

[62] Xiaoxi Fu et al. "Electron affinity measurements of lanthanide atoms: Pr, Nd, and Tb". In: *Physical Review A* 101.2 (Feb. 2020), p. 022502. DOI: 10.1103/PhysRevA.101.022502.

[63] M. C. McCarthy et al. "Laboratory and Astronomical Identification of the Negative Molecular Ion C 6 H -". In: *The Astrophysical Journal* 652.2 (2006), pp. L141–L144. DOI: 10.1086/510238.

[64] MRC McDowell. "On the formation of H2 in hi regions". In: *The Observatory* 81 (1961), pp. 240–243.

[65] Teresa Ross et al. "The Search for H – in Astrophysical Environments". In: *The Astrophysical Journal* 684.1 (2008), pp. 358–363. DOI: 10.1086/590242.

[66] D.E. Post, K. Borrass, and J.D. Callen. *ITER physics*. May 1991.

[67] Robert S. Mulliken. "A new electroaffinity scale; Together with data on valence states and on valence ionization potentials and electron affinities". In: *The Journal of Chemical Physics* 2.11 (1934), pp. 782–793. DOI: 10.1063/1.1749394.

[68] Young-Seung Kim and Martin W Brechbiel. "An overview of targeted alpha therapy". In: *Tumor Biology* 33.3 (2012), pp. 573–590. DOI: 10.1007/s13277-011-0286-y.

[69] D. Scott Wilbur. *Enigmatic astatine*. 2013. DOI: 10.1038/nchem.1580.

[70] David Teze et al. "Targeted radionuclide therapy with astatine-211: Oxidative dehalogenation of astatobenzoate conjugates". In: *Scientific Reports* 7.1 (2017). DOI: 10.1038/s41598-017-02614-2.

[71] Daniela Schulz-Ertner, Oliver Jäkel, and Wolfgang Schlegel. "Radiation Therapy With Charged Particles". In: *Seminars in Radiation Oncology* 16.4 (2006), pp. 249–259. DOI: 10.1016/j.semradonc.2006.04.008.

[72] Alban Kellerbauer and Jochen Walz. "A novel cooling scheme for antiprotons". In: *New Journal of Physics* 8.3 (Mar. 2006), pp. 45–45. DOI: 10.1088/1367-2630/8/3/045.

[73] Steven Chu et al. "Three-dimensional viscous confinement and cooling of atoms by resonance radiation pressure". In: *Physical Review Letters* 55.1 (July 1985), pp. 48–51. DOI: 10.1103/PhysRevLett.55.48.

[74] A. Aspect et al. "Laser cooling below the one-photon recoil energy by velocity-selective coherent population trapping". In: *Physical Review Letters* 61.7 (Aug. 1988), pp. 826–829. DOI: 10.1103/PhysRevLett.61.826.

[75] William D. Phillips and Harold Metcalf. "Laser deceleration of an atomic beam". In: *Physical Review Letters* 48.9 (Mar. 1982), pp. 596–599. DOI: 10.1103/PhysRevLett.48.596.

[76] C. W. Walter et al. "Candidate for Laser Cooling of a Negative Ion: Observations of Bound-Bound Transitions in La –". In: *Physical Review Letters* 113.6 (Aug. 2014), p. 063001. DOI: 10.1103/PhysRevLett.113.063001.

[77] C. W. Walter et al. "Infrared photodetachment of Ce-: Threshold spectroscopy and resonance structure". In: *Phys. Rev., A. - Atomic, Molecular, and Optical Physics* 76.5 (Nov. 2007), p. 052702. DOI: 10.1103/PhysRevA.76.052702.

[78] René C. Bilodeau and Harold K. Haugen. "Experimental Studies of Os – : Observation of a Bound-Bound Electric Dipole Transition in an Atomic Negative Ion". In: *Physical Review Letters* 85.3 (July 2000), pp. 534–537. DOI: 10.1103/PhysRevLett.85.534.

[79] Rulin Tang et al. "Electron affinity of uranium and bound states of opposite parity in its anion". In: *Physical Review A* 103.5 (May 2021), p. L050801. DOI: 10.1103/PhysRevA.103.L050801.

[80] G. Cerchiari et al. "Ultracold Anions for High-Precision Antihydrogen Experiments". In: *Physical Review Letters* 120.13 (Mar. 2018), p. 133205. DOI: 10.1103/PhysRevLett.120.133205.

[81] D. J. Larson et al. "Sympathetic cooling of trapped ions: A laser-cooled two-species nonneutral ion plasma". In: *Physical Review Letters* 57.1 (July 1986), pp. 70–73. DOI: 10.1103/PhysRevLett.57.70.

[82] M. Ahmadi et al. "Investigation of the fine structure of antihydrogen". In: *Nature* 578.7795 (2020), pp. 375–380. DOI: 10.1038/s41586-020-2006-5.

[83] T. Aumann et al. "PUMA, antiProton unstable matter annihilation: PUMA collaboration". In: *European Physical Journal A* 58.5 (2022), pp. 1–69. DOI: 10.1140/epja/s10050-022-00713-x.

[84] Louis de Broglie. "XXXV. A tentative theory of light quanta". In: *The London, Edinburgh, and Dublin Philosophical Magazine and J. Sc.* 47.278 (1924), pp. 446–458. DOI: 10.1080/14786442408634378.

[85] B Bransden and C Joachain. *Physics of Atoms and Molecules*. 1983.

[86] Sune Svanberg. *Atomic and Molecular Spectroscopy: Basic Aspects and Practical Applications*. 4. Springer Berlin, Heidelberg, 1991. DOI: https://doi.org/10.1007/978-3-642-18520-5.

[87] David J. Pegg. "Structure and dynamics of negative ions". In: *Reports on Progress in Physics* 67.6 (2004), pp. 857–905. DOI: 10.1088/0034-4885/67/6/R02.

[88] M.Y. Amusia. *Atomic Photoeffect*. Vol. 21. 1. Springer Science & Business Media, 1990, pp. 1–12. DOI: 10.1007/978-1-4757-9328-4.

[89] Eugene P. Wigner. "On the Behavior of Cross Sections Near Thresholds". In: *Physical Review* 73.9 (May 1948), pp. 1002–1009. DOI: 10.1103/PhysRev.73.1002.

[90] H. C. Bryant et al. "Observation of resonances near 11 eV in the photodetachment cross section of the H- ion". In: *Physical Review Letters* 38.5 (Jan. 1977), pp. 228–230. DOI: 10.1103/PhysRevLett.38.228.

[91] U. Ljungblad et al. "Observation of doubly excited states in Li–". In: *Physical Review Letters* 77.18 (Oct. 1996), pp. 3751–3754. DOI: 10.1103/PhysRevLett.77.3751.

[92] Gunnar Haeffler et al. "Observation of resonance structure in the Na - photodetachment cross section". In: *Physical Review A - Atomic, Molecular, and Optical Physics* 59.5 (May 1999), pp. 3655–3659. DOI: 10.1103/PhysRevA.59.3655.

[93] I. Yu. Kiyan et al. "Spectrum of doubly excited states in the K– ion". In: *Physical Review Letters* 84.26 (June 2000), pp. 5979–5982. DOI: 10.1103/PhysRevLett.84.5979.

[94] A. O. Lindahl et al. "Experimental studies of partial photodetachment cross sections in K - below the K(72P) threshold". In: *Physical Review A - Atomic, Molecular, and Optical Physics* 85.3 (Mar. 2012), p. 033415. DOI: 10.1103/PhysRevA.85.033415.

[95] A. O. Lindahl et al. "Observation of thresholds and overlapping resonances below the 10 2P 1/2 and 2P3/2 thresholds in the photodetachment of Cs -". In: *Physical Review A - Atomic, Molecular, and Optical Physics* 88.5 (Nov. 2013), p. 053410. DOI: 10.1103/PhysRevA.88.053410.

[96] Gregor Tanner, Klaus Richter, and Jan Michael Rost. "The theory of two-electron atoms: Between ground state and complete fragmentation". In: *Reviews of Modern Physics* 72.2 (Apr. 2000), pp. 497–544. DOI: 10.1103/RevModPhys.72.497.

[97] David R. Bates. "Negative ions: Structure and spectra". In: *Advances in Atomic, Molecular and Optical Physics* 27.C (Jan. 1990), pp. 1–80. DOI: 10.1016/S1049-250X(08)60148-2.

[98] Johan Rohlén. "Excited States in Negative Ions". PhD thesis. PhD thesis. University of Gothenburg, 2014.

[99] Jonathan C. Rienstra-Kiracofe et al. "Atomic and molecular electron affinities: Photoelectron experiments and theoretical computations". In: *Chemical Reviews* 102.1 (2002), pp. 231–282. DOI: 10.1021/cr990044u.

[100] Henning T Schmidt et al. "DESIREE as a new tool for interstellar ion chemistry". In: *International Journal of Astrobiology* 7.3-4 (2008), pp. 205–208. DOI: 10.1017/S1473550408004229.

[101] Rachel M. Thorman et al. "The role of low-energy electrons in focused electron beam induced deposition: Four case studies of representative precursors". In: *Beilstein Journal of Nanotechnology* 6.1 (2015), pp. 1904–1926. DOI: 10.3762/bjnano.6.194.

[102] S. Rosén et al. "Absolute cross sections and final-state distributions for dissociative recombination and excitation of CO + (v = 0) using an ion storage ring". In: *Physical Review A - Atomic, Molecular, and Optical Physics* 57.6 (June 1998), pp. 4462–4471. DOI: 10.1103/PhysRevA.57.4462.

[103] VR Bhardwaj, D Mathur, and K Vijayalakshmi. "Collision-induced dissociation of CO 2+ ions". In: *Phys. Rev. A* 58.4 (1998), pp. 2834–2843.

[104] P. Lablanquie et al. "Experimental and theoretical investigation of the spectroscopy and dynamics of multiply charged CO cations". In: *Physical Review A* 40.10 (Nov. 1989), pp. 5673–5689. DOI: 10.1103/PhysRevA.40.5673.

[105] J Ballof et al. "Radioactive boron beams produced by isotope online mass separation at CERN-ISOLDE". In: *European Physical Journal A* 55.5 (2019). DOI: 10.1140/epja/i2019-12719-1.

[106] R. S. Augusto et al. "New developments of 11C post-accelerated beams for hadron therapy and imaging". In: *Nuclear Instruments and Methods in Physics Research, Section B: Beam Interactions with Materials and Atoms* 376 (2016), pp. 374–378. DOI: 10.1016/j.nimb.2016.02.045.

[107] S. Stegemann et al. "Production of intense mass separated 11C beams for PET-aided hadron therapy". In: *Nuclear Instruments and Methods in Physics Research, Section B: Beam Interactions with Materials and Atoms* 463.May 2019 (2020), pp. 403–407. DOI: 10.1016/j.nimb.2019.04.042.

[108] T. M. Mendonca et al. "Production and release of ISOL beams from molten fluoride salt targets". In: *Nuclear Instruments and Methods in Physics Research, Section B: Beam Interactions with Materials and Atoms* 329.2014 (2014), pp. 1–5. DOI: 10.1016/j.nimb.2014.03.003.

[109] Helmut Wiedemann. *Particle Accelerator Physics*. Vol. 7. 4. Springer-Verlag Berlin Heidelberg. DOI: 10.1080/08940889408261288.

[110] Martin Reiser. *Theory and Design of Charged Particle Beams*. Weinheim: WILEY-VCH Verlag GmbH & Co. KGaA, 2008. DOI: 10.1002/9783527617623.

[111] S. Jr. Humphries. *Charged particle beams*. Ed. by United States: Wiley-Interscience. 1990.

[112] Santiago Bernal. "Emittance and space charge". In: *A Practical Introduction to Beam Physics and Particle Accelerators*. IOP Publishing, 2016. DOI: 10.1088/978-1-6817-4076-8ch4.

[113] A. Nieminen et al. "Beam cooler for low-energy radioactive ions". In: *Nuclear Instruments and Methods in Physics Research Section A: Accelerators, Spectrometers, Detectors and Associated Equipment* 469.2 (Aug. 2001), pp. 244–253. DOI: 10.1016/S0168-9002(00)00750-6.

[114] Y. Liu et al. "Collisional cooling of negative-ion beams". In: *Nuclear Instruments and Methods in Physics Research Section B: Beam Interactions with Materials and Atoms* 187.1 (Jan. 2002), pp. 117–131. DOI: 10.1016/S0168-583X(01)00844-8.

[115] G. Darius et al. "Linear radio frequency quadrupole for the cooling and bunching of radioactive ion beams". In: *Review of Scientific Instruments* 75.11 (Nov. 2004), pp. 4804–4810. DOI: 10.1063/1.1809296.

[116] J. Liouville. "Note sur la Théorie de la Variation des constantes arbitraires." In: *Journal de mathématiques pures et appliquées* 3.1 (1838), pp. 342–349.

[117] E Mané et al. "An ion cooler-buncher for high-sensitivity collinear laser spectroscopy at ISOLDE". In: *European Physical Journal A* 42.3 (2009), pp. 503–507. DOI: 10.1140/epja/i2009-10828-0.

[118] B. Cheal et al. "Laser Spectroscopy of Niobium Fission Fragments: First Use of Optical Pumping in an Ion Beam Cooler Buncher". In: *Physical Review Letters* 102.22 (June 2009), p. 222501. DOI: 10.1103/PhysRevLett.102.222501.

[119] C. Babcock et al. "Quadrupole moments of odd-A 53–63Mn: Onset of collectivity towards N = 40". In: *Physics Letters B* 760 (Sept. 2016), pp. 387–392. DOI: 10.1016/J.PHYSLETB.2016.07.016.

[120] Y Liu et al. "Isobar suppression by photodetachment in agas-filled rf quadrupole ion guide". In: *Appl. Phys. Lett* 87 (2005), p. 113504. DOI: 10.1063/1.2046732.

[121] P Andersson et al. "Nearly complete isobar suppression by photodetachment". In: *Journal of Applied Physics* 107.2 (2010), p. 26102. DOI: 10.1063/1.3291104.

[122] Martin Martschini et al. "The ILIAMS project – An RFQ ion beam cooler for selective laser photodetachment at VERA". In: *Nuclear Instruments and Methods in Physics Research Section B: Beam Interactions with Materials and Atoms* 456 (Oct. 2019), pp. 213–217. DOI: 10.1016/J.NIMB.2019.04.039.

[123] A. Kellerbauer et al. "Buffer gas cooling of ion beams". In: *Nuclear Instruments and Methods in Physics Research Section A: Accelerators, Spectrometers, Detectors and Associated Equipment* 469.2 (Aug. 2001), pp. 276–285. DOI: 10.1016/S0168-9002(01)00286-8.

[124] Ivan P. Aliseda. "New developments on preparation of cooled and bunched Radioacive Ion Beams at ISOL-facilities: The ISCOOL project and the Rotating Wall Cooling". In: *Ph.D. Thesis* July 2006 (2006), p. 234.

[125] Carla Babcock. "Collinear Laser Spectroscopy of Manganese Isotopes using the Radio Frequency Quadrupole Cooler and Buncher at ISOLDE". In: *Ph.D. Thesis* (2015).

[126] Carla Babcock and Tim Giles. "Upgrade of the radio frequency quadrupole cooler and buncher for the HIE-ISOLDE project". In: *Nuclear Instruments and Methods in Physics Research, Section B: Beam Interactions with Materials and Atoms* 317.PART B (2013), pp. 484–487. DOI: 10.1016/j.nimb.2013.08.020.

[127] P.H. Dawson. *Quadrupole Mass Spectrometry and its Applications*. Amsterdam: Elsevier, 1976. DOI: 10.1016/C2013-0-04436-2.

[128] Mathew Smith et al. "First tests of the TITAN digital RFQ beam cooler and buncher". In: *Hyperfine Interact* 173 (2006), pp. 171–180. DOI: 10.1007/s10751-007-9554-z.

[129] S. Warren and T. Giles. "Radio-frequency waveform investigation for ion transport within the RFQcb at ISOLDE's Offline 2 facility". In: *Journal of Instrumentation* 16.07 (July 2021), P07058. DOI: 10.1088/1748-0221/16/07/P07058.

[130] Joseph Ladislas Wiza. "Microchannel plate detectors". In: *Nuclear Instruments and Methods* 162.1-3 (1979), pp. 587–601. DOI: 10.1016/0029-554X(79)90734-1.

[131] G. W. Goodrich and W. C. Wiley. "Continuous Channel Electron Multiplier". In: *Rev. Sci. Instrum.* 33.7 (July 1962), pp. 761–762. DOI: 10.1063/1.1717958.

[132] ETP Ion Detect. *MagneTOF ™: A New Class of Robust Sub-nanosecond TOF Detectors with Exceptional Dynamic Range*. 2013.

[133] Henri Becquerel. "Sur les radiations émises par phosphorescence". In: *Comptes Rendus* 122 (1896), pp. 420–421.

[134] Henri Becquerel. "Sur les radiations invisibles émises par les corps phosphorescents". In: *Comptes Rendus* 122 (1896), pp. 501–503.

[135] Pierre Radvanyi and Jacques Villain. "The discovery of radioactivity". In: *Comptes Rendus Physique* 18.9-10 (2017), pp. 544–550. DOI: 10.1016/j.crhy.2017.10.008.

[136] P Curie and M Sklodowska-Curie. "Sur une substance nouvelle radioactive, contenue dans la pechblende". In: *Comptes Rendus Hebdomadaires des Séances de l'Académie des Sciences* 127 (1898), pp. 175–178.

[137] Frederick Soddy. "Intra-atomic Charge". In: *Nature* 92.2301 (Dec. 1913), pp. 399–400. DOI: 10.1038/092399c0.

[138] Frederick Soddy. *The Origins of the Conception of Isotopes*. 1923. DOI: 10.1038/112208a0.

[139] J. Kenneth Shultis and Richard E. Faw. *Fundamentals of nuclear science and engineering, second edition*. 2007.

[140] H. D. Smyth. "Atomic Energy for Military Purposes". In: *Reviews of Modern Physics* 17.4 (Oct. 1945), pp. 351–471. DOI: 10.1103/RevModPhys.17.351.

[141] Laura Harkness-Brennan. *An Introduction to the Physics of Nuclear Medicine*. IOP Publishing, 2018. DOI: 10.1088/978-1-6432-7034-0.

[142] I. Tanihata et al. "Measurements of interaction cross sections and radii of He isotopes". In: *Physics Letters B* 160.6 (1985), pp. 380–384. DOI: 10.1016/0370-2693(85)90005-X.

[143] O. Kofoed-Hansen and K. O. Nielsen. "Short-Lived Krypton Isotopes and Their Daughter Substances". In: *Physical Review* 82.1 (Apr. 1951), pp. 96–97. DOI: 10.1103/PhysRev.82.96.2.

[144] David J. Morrissey and Brad M. Sherrill. "In-Flight Separation of Projectile Fragments". In: *Springer Lecture Notes Phys* 651 (2004), pp. 113–135. DOI: 10.1007/978-3-540-44490-9{_}4.

[145] Y. Blumenfeld, T. Nilsson, and P. Van Duppen. "Facilities and methods for radioactive ion beam production". In: *Physica Scripta* T152 (2013). DOI: 10.1088/0031-8949/2013/T152/014023.

[146] M Lindroos. "Review of Isol-Type Radioactive Beam Facilities". In: *Proceedings of EPAC 2004, Lucerne, Switzerland REVIEW* (2004), pp. 45–49.

[147] David Leimbach. "Radioactive negative ions: Production and laser spectroscopy at ISOLDE". In: *Ph.D. Thesis* (2021).

[148] M. Lindroos et al. "HIE-ISOLDE". In: *Nucl Instrum Methods Phys Res B: Beam Interactions with Materials and Atoms* 266.19-20 (Oct. 2008), pp. 4687–4691. DOI: 10.1016/J.NIMB.2008.05.136.

[149] Antonio C.C. Villari. "First results at SPIRAL-GANIL". In: *Nuclear Instruments and Methods in Physics Research, Section B: Beam Interactions with Materials and Atoms* 204 (2003), pp. 31–41. DOI: 10.1016/S0168-583X(02)01887-6.

[150] P Van Duppen. *The Euroschool Lectures on Physics With Exotic Beams, Vol. II: Isotope Separation On Line and Post Acceleration*. Vol. 700. 2006, pp. 37–77. DOI: 10.1007/3-540-33787-3.

[151] CERN. *CERN Home Page*. 2022. DOI: https://home.cern/.

[152] Ewa Lopienska. "The CERN accelerator complex, layout in 2022. Complexe des accélérateurs du CERN en janvier 2022". In: (2022).

[153] R. Catherall et al. "An overview of the HIE-ISOLDE Design Study". In: *Nuclear Instruments and Methods in Physics Research Section B: Beam Interactions with Materials and Atoms* 317 (Dec. 2013), pp. 204–207. DOI: 10.1016/J.NIMB.2013.07.030.

[154] María J.G. Borge and Klaus Blaum. "Focus on Exotic Beams at ISOLDE: A Laboratory Portrait". In: *Journal of Physics G: Nuclear and Particle Physics* 45.1 (2018). DOI: 10.1088/1361-6471/aa990f.

[155] R. Kirchner and E. Roeckl. "A Novel ISOL Ion Source". In: *Nuclear Instruments and Methods* 139 (Dec. 1976), pp. 291–296. DOI: 10.1016/0029-554X(76)90687-X.

[156] T. Day Goodacre et al. "Blurring the boundaries between ion sources: The application of the RILIS inside a FEBIAD type ion source at ISOLDE". In: *Nuclear Instruments and Methods in Physics Research Section B: Beam Interactions with Materials and Atoms* 376 (June 2016), pp. 39–45. DOI: 10.1016/J.NIMB.2016.03.005.

[157] G.V. Samsonov and V.S. Fomenko. *Handbook of thermionic properties*. Springer New York, NY, 1966. DOI: https://doi.org/10.1007/978-1-4684-7293-6.

[158] J Pelletier and C Pomot. "Work function of sintered lanthanum hexaboride". In: *Applied Physics Letters* 34.4 (1979), pp. 249–251. DOI: 10.1063/1.90769.

[159] Jacques Lettry. "Off-Line Isotope Separator". In: (1994).

[160] A. Jokinen et al. "RFQ-cooler for low-energy radioactive ions at ISOLDE". In: *Nucl Instrum Methods Phys Res B: Beam Interactions with Materials and Atoms* 204.July (2003), pp. 86–89. DOI: 10.1016/S0168-583X(02)01894-3.

[161] Carla Babcock and Tim Giles. "Upgrade of the radio frequency quadrupole cooler and buncher for the HIE-ISOLDE project". In: *Nuclear Instruments and Methods in Physics Research, Section B: Beam Interactions with Materials and Atoms* 317.PART B (2013), pp. 484–487. DOI: 10.1016/j.nimb.2013.08.020.

[162] D. Hanstorp. "A secondary emission detector capable of preventing detection of the photoelectric effect induced by pulsed lasers". In: *Measurement Science and Technology* 3.5 (1992), pp. 523–527. DOI: 10.1088/0957-0233/3/5/013.

[163] F Bonaccorso et al. "Graphene photonics and optoelectronics". In: *Nature Photonics* 4.9 (2010), pp. 611–622. DOI: 10.1038/nphoton.2010.186.

[164] J. Warbinek et al. "A graphene-based neutral particle detector". In: *Applied Physics Letters* 114.6 (2019). DOI: 10.1063/1.5080517.

[165] Dag Hanstorp. "An ion beam apparatus for collinear photodetachment experiments". In: *Nuclear Inst. and Methods in Physics Research, B* 100.1 (1995), pp. 165–175. DOI: 10.1016/0168-583X(94)00656-3.

[166] C. Diehl et al. "Ion optical design of a collinear laser-negative ion beam apparatus". In: *Review of Scientific Instruments* 82.5 (2011). DOI: 10.1063/1.3587617.

[167] R. Middleton. "A versatile high intensity negative ion source". In: *Nuclear Instruments and Methods In Physics Research* 214.2-3 (1983), pp. 139–150. DOI: 10.1016/0167-5087(83)90580-X.

[168] Ming L. Yu. "Work-function dependence of negative-ion production during sputtering". In: *Phys. Rev. Lett.* 40.9 (1978), pp. 574–577. DOI: 10.1103/PhysRevLett.40.574.

[169] S. L. Kaufman. "High-resolution laser spectroscopy in fast beams". In: *Optics Communications* 17.3 (1976), pp. 309–312. DOI: 10.1016/0030-4018(76)90267-4.

[170] J. Welander et al. "A field ionizer for photodetachment studies of negative ions". In: *Review of Scientific Instruments* 93.6 (2022). DOI: 10.1063/5.0061736.

[171] R. D. Thomas et al. "The double electrostatic ion ring experiment: A unique cryogenic electrostatic storage ring for merged ion-beams studies". In: *Review of Scientific Instruments* 82.6 (June 2011). DOI: 10.1063/1.3602928.

[172] E Bäckström et al. "Storing keV Negative Ions for an Hour: The Lifetime of the Metastable P 2 1 /2o level in S 32 - The". In: *Physical Review Letters* 114.14 (2015), p. 143003. DOI: 10.1103/PhysRevLett.114.143003.

[173] Matthieu Génévriez and Xavier Urbain. "Animated-beam measurement of the photodetachment cross section of H". In: *Physical Review A - Atomic, Molecular, and Optical Physics* 91.3 (Mar. 2015), p. 033403. DOI: 10.1103/PhysRevA.91.033403.

[174] Matthieu Génévriez et al. "Absolute total, partial, and differential cross sections for photodetachment of O". In: *Physical Review A* 98.3 (Sept. 2018), p. 033410. DOI: 10.1103/PhysRevA.98.033410.

[175] P. Juncar et al. "New Method to Measure the Relativistic Doppler Shift: First Results and a Proposal". In: *Physical Review Letters* 54.1 (Jan. 1985), pp. 11–13. DOI: 10.1103/PhysRevLett.54.11.

[176] S Rothe et al. "A complementary laser system for ISOLDE RILIS". In: *Journal of Physics: Conference Series* 312.5 (Sept. 2011), p. 052020. DOI: 10.1088/1742-6596/312/5/052020.

[177] Valentin Fedosseev et al. "Ion beam production and study of radioactive isotopes with the laser ion source at ISOLDE". In: *Journal of Physics G: Nuclear and Particle Physics* 44.8 (Aug. 2017), p. 084006. DOI: 10.1088/1361-6471/aa78e0.

[178] D. E. Hull and Herman Seelig. "The half-life of iodine (128)". In: *Physical Review* 60.8 (1941), pp. 553–555. DOI: 10.1103/PhysRev.60.553.

[179] B Vosicki et al. "Intense beams of radioactive halogens produced by means of surface ionization". In: *Nuclear Instruments and Methods* 186.1-2 (1981), pp. 307–313. DOI: 10.1016/0029-554X(81)90918-6.

[180] A. Borschevsky et al. "Ionization potentials and electron affinities of the superheavy elements 115–117 and their sixth-row homologues Bi, Po, and At". In: *Physical Review A* 91.2 (Feb. 2015), p. 020501. DOI: 10.1103/PhysRevA.91.020501.

[181] S. Rothe et al. "Measurement of the first ionization potential of astatine by laser ionization spectroscopy". In: *Nature Communications* 4.May (2013), pp. 1–6. DOI: 10.1038/ncomms2819.

[182] Zhiwei Chang, Jiguang Li, and Chenzhong Dong. "Strengths , And Ionic Radii of Element Uus (Z) 117) and Astatine". In: *Potentials* (2010), pp. 13388–13394.

[183] Junqin Li et al. "Theoretical study for the electron affinities of negative ions with the MCDHF method". In: *Journal of Physics B: Atomic, Molecular and Optical Physics* 45.16 (Aug. 2012), p. 165004. DOI: 10.1088/0953-4075/45/16/165004.

[184] Dumitru Claudiu Sergentu et al. "Scrutinizing "invisible" astatine: A challenge for modern density functionals". In: *Journal of Computational Chemistry* 37.15 (2016), pp. 1345–1354. DOI: 10.1002/jcc.24326.

[185] R. Si and C. Froese Fischer. "Electron affinities of At and its homologous elements Cl, Br, and I". In: (June 2019). DOI: 10.1103/PhysRevA.98.052504.

[186] *DIRAC, a relativistic ab initio electronic structure program, Release DIRAC15 (2015), written by R. Bast, T. Saue, L. Visscher, and H. J. Aa. Jensen, with contributions from V. Bakken, K. G. Dyall, S. Dubillard, U. Ekstroem, E. Eliav, T. Enevoldsen, E. Fa.*

[187] T. A. Patterson et al. "Resonances in alkali negative-ion photodetachment and electron affinities of the corresponding neutrals". In: *Physical Review Letters* 32.5 (1974), pp. 189–192. DOI: 10.1103/PhysRevLett.32.189.

[188] J. Slater et al. "Alkali negative ions. III. Multichannel photodetachment study of Cs- and K-". In: *Physical Review A* 17.1 (Jan. 1978), pp. 201–213. DOI: 10.1103/PhysRevA.17.201.

[189] M. Scheer et al. "Experimental Evidence that the 6 s 6 p 3 P J States of Cs – Are Shape Resonances". In: *Physical Review Letters* 80.4 (Jan. 1998), pp. 684–687. DOI: 10.1103/PhysRevLett.80.684.

[190] P. Frey, F. Breyer, and H. Holop. "High resolution photodetachment from the rubidium negative ion around the Rb(5p1/2) threshold". In: *Journal of Physics B: Atomic and Molecular Physics* 11.19 (1978). DOI: 10.1088/0022-3700/11/19/005.

[191] Constantine E. Theodosiou. "Lifetimes of alkali-metalatom Rydberg states". In: *Physical Review A* 30.6 (Dec. 1984), pp. 2881–2909. DOI: 10.1103/PhysRevA.30.2881.

[192] C. S. Feigerle et al. "Binding energies and structure of transition metal negative ions". In: *The Journal of Chemical Physics* 74.3 (1980), pp. 1580–1598. DOI: 10.1063/1.441289.

[193] T. M. Mendonca et al. "Production and release of ISOL beams from molten fluoride salt targets". In: *Nuclear Instruments and Methods in Physics Research, Section B: Beam Interactions with Materials and Atoms* 329.2014 (2014), pp. 1–5. DOI: 10.1016/j.nimb.2014.03.003.

[194] R. R. Reddy and R. Viswanath. "Estimation of the dissociation energy of CO+from spectroscopic data". In: *Journal of Astrophysics and Astronomy* 11.1 (1990), pp. 67–72. DOI: 10.1007/BF02728023.

[195] K. P. Huber and G. Herzberg. *Molecular Spectra and Molecular Structure: IV Constants of Diatomic Molecules*. Van Nostrand Reinhold Company, New York, 1979.

[196] J. Pitters, M. Breitenfeldt, and F. Wenander. "Charge breeding of CO+ beams at REX-ISOLDE". In: 2018, p. 070012. DOI: 10.1063/1.5053354.

[197] Katerina Chrysalidis et al. "Continuously tunable diamond Raman laser for resonance ionization experiments at CERN". In: *Advanced Solid State Lasers - Proceedings Laser Congress 2019 (ASSL, LAC, LS and C)* 44.16 (2019), pp. 3924–3927.

[198] Eduardo Granados et al. "Continuously tunable diamond Raman laser for resonance ionization experiments at CERN". In: *Advanced Solid State Lasers - Proceedings Laser Congress 2019 (ASSL, LAC, LS and C)* 44.16 (2019), pp. 3924–3927.

[199] D. A. Fink et al. "On-line implementation and first operation of the Laser Ion Source and Trap at ISOLDE/CERN". In: *Nuclear Instruments and Methods in Physics Research, Section B: Beam Interactions with Materials and Atoms* 344 (2015), pp. 83–95. DOI: 10.1016/j.nimb.2014.12.007.

[200] R. Heinke et al. "High-resolution in-source laser spectroscopy in perpendicular geometry: Development and application of the PI-LIST". In: *Hyperfine Interactions* 238.1 (2017). DOI: 10.1007/s10751-016-1386-2.

[201] B Andel et al. "Investigation of octupole deformation in neutron-rich actinium using high-resolution in-source laser spectroscopy". In: CERN-INTC-2020-029. INTC-P-556 (2020), pp. 1–9.

[202] M Nichols et al. "Measuring the electron affinity of polonium". In: *CERN-INTC-2023-011, INTC-007* (2023), pp. 1–12.

[203] U. Berzinsh et al. "Isotope shift in the electron affinity of chlorine". In: *Physical Review A* 51.1 (1995), pp. 231–238. DOI: 10.1103/PhysRevA.51.231.

[204] Michel R. Godefroid and Charlotte Froese Fischer. "Isotope shift in the oxygen electron affinity". In: *Physical Review A - Atomic, Molecular, and Optical Physics* 60.4 (1999), R2637–R2640. DOI: 10.1103/PhysRevA.60.R2637.

[205] Sergiy Bubin et al. "Isotope shift in the electron affinity of lithium". In: *Journal of Chemical Physics* 131.23 (2009). DOI: 10.1063/1.3275804.

[206] Thomas Carette et al. "Isotope shift in the sulfur electron affinity: Observation and theory". In: *Physical Review A - Atomic, Molecular, and Optical Physics* 81.4 (2010), pp. 1–10. DOI: 10.1103/PhysRevA.81.042522.

[207] T. Carette and M. R. Godefroid. "Isotope shift on the chlorine electron affinity revisited by an MCHF/CI approach". In: *J Phys B - At Mol Opt.* 46.9 (2013). DOI: 10.1088/0953-4075/46/9/095003.

[208] T. Carette and M. R. Godefroid. "Theoretical study of the isotope effects on the detachment thresholds of Si-". In: *Physical Review A - Atomic, Molecular, and Optical Physics* 89.5 (2014), pp. 1–8. DOI: 10.1103/PhysRevA.89.052513.

[209] Ran Si et al. "Ab initio multiconfiguration Dirac-Hartree-Fock calculations of the In and Tl electron affinities and their isotope shifts". In: *Physical Review A* 104.1 (2021), pp. 1–8. DOI: 10.1103/PhysRevA.104.012802.

[210] Dag Hanstorp. *Measurement of shifts in the electron affinities of chlorine isotopes*. Tech. rep. CERN-INTC-2019-014, INTC-SR-073: - CERN, Geneva, 2019.

[211] S. V. Andreev, V. S. Letokhov, and V. I. Mishin. "Laser resonance photoionization spectroscopy of Rydberg levels in Fr". In: *Physical Review Letters* 59.12 (Sept. 1987), pp. 1274–1276. DOI: 10.1103/PhysRevLett.59.1274.

[212] M Nichols et al. "Investigating radioactive negative ion production via double electron capture". In: *Nuclear Instruments and Methods in Physics Research B* To be subm (2023).

[213] Arie Landau et al. "Benchmark calculations of electron affinities of the alkali atoms sodium to eka-francium (element 119)". In: *The Journal of Chemical Physics* 115.6 (Aug. 2001), pp. 2389–2392. DOI: 10.1063/1.1386413.